INVESTIGATION OF DIAGONAL-TENSION BEAMS WITH VERY THIN STIFFENED WEBS.

By

Alexander G. Tsongas
and
Robert T. Ratay

Structural Mechanics Section
GRUMMAN AEROSPACE CORPORATION
BETHPAGE, NEW YORK 11714

RECEIVED
NASA STI FACILITY
INPUT BRANCH
AUG 1969

July 1969

Prepared for

NATIONAL AERONAUTICS AND SPACE ADMINISTRATION
Manned Spacecraft Center

Contract No. NAS 9-8284

FACILITY FORM 602

N69-32379
(ACCESSION NUMBER)
(THRU)
118
(PAGES)
1
(CODE)
CR-101854
(NASA CR OR TMX OR AD NUMBER)
32
(CATEGORY)

NASA CR 101854

INVESTIGATION OF DIAGONAL-TENSION BEAMS WITH VERY THIN STIFFENED WEBS

By

Alexander G. Tsongas

and

Robert T. Ratay

Structural Mechanics Section

GRUMMAN AEROSPACE CORPORATION

BETHPAGE, NEW YORK 11714

July 1969

Prepared for

NATIONAL AERONAUTICS AND SPACE ADMINISTRATION
Manned Spacecraft Center

Contract No. NAS 9-8284

Grumman

FOREWORD

The work reported herein was performed under Contract NAS 9-8284 that Grumman Aerospace Corporation (formerly Grumman Aircraft Engineering Corporation) was awarded by NASA. The project was procured by NASA Manned Spacecraft Center, R&D Procurement Branch, Houston, Texas. NASA's Technical Monitor was Thomas J. Dunn of NASA-MSC. Period of performance was June 24, 1968 through July 24, 1969.

Other Grumman technical personnel, in addition to the authors, who significantly and actively contributed to the project were the following: Alexander Gomza, Assistant Chief, Structural Mechanics Section, directed the preparation of the Proposal, reviewed and contrituted to this report; James M. Barnes, Methods Engineering Improvement Group Leader, supervised the chem-milling, fabrication and assembly of the test specimens; John Inge, Structural Test Lead Engineer, directed the design and construction of the test rig and the testing of all the specimens; Robert D. Torczyner, Structural Mechanics Engineer, worked with the authors on the design of the specimens and evaluation of the test data.

The efforts of these colleagues and the assistance of Dr. Warner Lansing, Chief, Structural Mechanics Section, are much appreciated. The suggestions and cooperation of Mr. Thomas J. Dunn were most helpful.

ABSTRACT

An experimental and analytical program has been carried out to ascertain the applicability to current spacecraft construction of the semi-empirical diagonal-tension beam analysis methods developed for aircraft construction and summarized in 1952 by Kuhn, Peterson and Levin in NACA TN 2661, "Summary of Diagonal-Tension, Part I."

Full-scale diagonal-tension beams, representative of current spacecraft construction, with very thin chem-milled 7075-T6 aluminum alloy web sheets and formed stiffeners of the same material were designed, constructed, instrumented and tested. Fourteen specimens were static-tested, four were fatigue tested. Description and results of the experimental program and analyses of the data are presented. Conclusions and recommendations are made that extend the range of applicability of the method of stress analysis given in NACA TN 2661.

TABLE OF CONTENTS

	Page
FOREWORD	ii
ABSTRACT	iii
1. INTRODUCTION	1
2. LIST OF SYMBOLS	3
3. TEST PROGRAM	8
3.1 General	8
3.2.1 Static Test Specimens	8
3.2.2 Fatigue Test Specimens	10
3.3.1 Testing and Recording Apparatus	11
3.3.2 Testing Procedure	12
3.4.1 Static Test Data	13
3.4.2 Fatigue Test Data	15
4. ANALYSIS OF STATIC TEST RESULTS	16
4.1 General	16
4.2 Modifications to NACA Method	16
4.3 Ultimate Loads and Failure Modes	18
4.4 Evaluation of Instrumentation Data	24
4.4.1 General	24
4.4.2 Stiffener Data	24
4.4.3 Web Data	28
4.4.4 Panel Deflections	30
4.5 Additional On-Site Observations	31

Continued

TABLE OF CONTENTS (Cont'd)

	Page
5. ANALYSIS OF FATIGUE TEST RESULTS	34
6. CONCLUSIONS AND RECOMMENDATIONS	37
REFERENCES	41
TABLES	43
FIGURES	51
PHOTOGRAPHS	81
APPENDIX A (Illustrative Analysis)	A1
APPENDIX B (Shop Assembly Drawings)	B1

1. INTRODUCTION

Diagonal-tension shear beams, in applications where the web buckles well before the ultimate load is reached, have long proven to be efficient forms of construction. Although the basic behavior of diagonal-tension beams is well understood, neither the complex stress distributions that result after the web has buckled nor the ultimate strength of these beams may be predicted accurately by pure theory. Tension-field beam design in aircraft and, more recently, in spacecraft has been largely guided by semi-empirically derived design criteria, summarized in 1952 by Kuhn, Peterson and Levin in NACA TN 2661 and 2662, "Summary of Diagonal Tension" (References 1 and 2). The information in those references was obtained by analysis of tests on shear beams representative of those used in aircraft at that time. However, beams in some current aerospace structures have been designed to largely different geometries and with different manufacturing techniques from those described in TN 2661 and 2662. The development of the chemical etching method of reducing material thickness has made feasible the use of extremely thin web panels. For example, deep beams with very thin chem-milled webs were used in order to achieve minimum-weight structures for both the Orbiting Astronomical Observatory (OAO) and the Lunar Module (LM) spacecraft. There seems to be, however, no published material, either experimental or analytical, which could be used to verify whether the analysis methods presented in TN 2661 apply to beams with such large depth-to-thickness ratios, or which provides sufficient information to allow these methods to be corrected if necessary. An experimental and analytical program has been needed to supply this information.

The work under this project consisted of an experimental investigation of the buckling and failure of 14 statically loaded and 4 fatigue-loaded full-scale specimens, specifically designed to be representative of beams of the type currently used in aircraft and spacecraft, supplemented by analytical evaluations for the purpose of facilitating the analysis and

design of such structures. The primary objective of the project, as set forth by NASA-MSC, was to extend the range of applicability of the NACA method to include 7075-T6 aluminum alloy incomplete-tension-field beams having very thin and deep chem-milled webs. Specimens of this type of construction and in this extended range of geometry were designed, manufactured and tested to determine their post-buckling behavior and failing strengths. The experimental data were correlated with predictions made with the NACA analysis method.

The range of concern was within the following limitations:

$$1500 < \frac{h}{t} < 15{,}000; \; 0.15 = \frac{d}{h}; \; 45 < \frac{f_s}{f_{scr}} < 2200$$

where h = height of web sheet

t = thickness of web sheet

d = stiffener spacing

f_s = applied shear stress

f_{scr} = initial buckling stress

The secondary objective was to obtain data on the fatigue life of this type of tension-field beam.

2. LIST OF SYMBOLS

$A_{f\ell}$	cross-sectional area of beam flange
A_ℓ	cross-sectional area of land: $t_\ell \cdot d_\ell$
A_{st}	cross-sectional area of stiffener
A'_{st}	$A_{st} + A_\ell$ = cross-sectional area of stiffener with land
A_{ste}	$\dfrac{A_{st}}{1 + (e/\rho_{st})^2}$ = effective cross-sectional area of stiffener
A'_{ste}	$\dfrac{A'_{st}}{1 + (e'/\rho'_{st})^2}$ = effective cross-sectional area of stiffener with land
b_{f1}, b_{f2}	widths of stiffener flanges
b_{p1}, b_{p2}	widths of stiffener lips
b_w	height of stiffener web
d	c.c. stiffener spacing
d_c	width of chem-milled bay
d_ℓ	width of land at stiffener
D	$\dfrac{Et^3}{12\,(1 - \nu^2)}$ web sheet bending stiffness
e	distance from c.g. of stiffener to median plane of web sheet for single stiffener
e'	distance from c.g. of combined stiffener and land to median plane of web sheet
E	modulus of elasticity of beam material
f_1, f_2, f_3	first and second principal stresses and maximum shear stress at a point in the web sheet

$f_{f\ell}$	compressive stress in beam flange
f_s	average shear stress in web of beam parallel to stiffeners
f_{scr}	initial shear buckling stress of web
$f_{s\ max}$	maximum shear stress in web of beam
f_{st}	stiffener compressive stress at median plane of sheet; average along length of stiffener
f_{st*}	longitudinal stress in outstanding flange of stiffener
$f_{st\ avg}$	stiffener compressive stress; average over cross-section and average along length of stiffener
$f_{st\ max}$	stiffener compressive stress at median plane of sheet; at mid-length of stiffener
f_α	average diagonal tension stress in web of beam
F_{cy}	compressive yield stress of material
$F_{c\ all}$	allowable column stress of stiffener
$F_{fc\ all}$	allowable stiffener stress to guard against local failure (referred to as "forced crippling" in NACA TN 2661, 2662)
$F_{f\ell\ all}$	allowable compressive stress in beam flange
$F_{p\ell}$	proportional limit of material
$F_{s\ all}$	allowable shear stress in web of beam
F_{su}	ultimate shear stress of material
F_{sy}	allowable shear yield stress of material
F_{tu}	ultimate tensile stress of material
F_{ty}	tensile yield stress of material

$F_{\alpha\ all}$	allowable diagonal tensile stress in web
G	shear modulus of beam material
G_{IDT}	equivalent shear modulus of incomplete diagonal-tension
h_c	depth of chem-milled bay
h_e	effective depth of beam measured between centroids of flanges
h_ℓ	width of land at beam flange
h_{st}	length of stiffener measured between centroids of stiffener to flange rivet patterns
$I_{f\ell}$	moment of inertia of each beam flange
I_{st}	moment of inertia of stiffener cross-section about its c.g. axis parallel to the web
I'_{st}	moment of inertia of stiffener and land about c.g. of this combined section
I_{ste}	moment of inertia of single stiffener about inner face of sheet
J_{st}	torsional constant of stiffener ($= 1/3\ st_{st}^3$ for thin-walled open cross-section)
K_T	theoretical elastic stress concentration factor in a notched fatigue specimen
k	diagonal-tension factor
k_s	shear buckling stress coefficient
k_{ss}	$k_s \cdot \dfrac{\pi^2}{12\ (1 - \nu^2)}$
$M_{f\ell}$	flange bending moment near stiffeners
M.S.	margin of safety
P	total shear load

$P_{all\ c}$, $P_{all\ fc}$, $P_{all\ w}$	"NACA predicted allowable" loads for stiffener column failure, stiffner local failure and web sheet failure, respectively.
$P_{f\ell}$	shear load carried by flanges
P_s	shear load carried by web sheet
P_{ult}	ultimate shear load
r	bend radius in formed stiffener cross-section
R_h, R_d	empirical restraint coefficients
s	developed length of stiffener cross-section
S_{max}	amplitude of cyclic diagonal-tension stress under fatigue loading, and cyclic stress amplitude in a notched fatigue specimen
t	beam web thickness
$t_{f\ell}$	thickness of flange leg attached to web
t_ℓ	thickness of land
t_{st}	thickness of stiffener leg directly attached to the web
α_{IDT}	angle of incomplete diagonal-tension
α_{PDT}	angle of pure diagonal-tension
γ_{IDT}	f_s/G_{IDT} = shear strain of panel with buckled web
ϵ	normal strain
ν	Poisson's ratio of material (= .33)
ωd	$\sin \alpha_{IDT} \cdot d_c \sqrt[4]{\frac{t}{2I_{f\ell}h_c}}$

ρ_{st}	$\sqrt{I_{st}/A_{st}}$
ρ'_{st}	$\sqrt{I'_{st}/A'_{st}}$

Superscripts:

ct	computed from test data
d	design prediction for test
m	measured in test
p	predicted by NACA TN 2661 method

Symbols appearing on curves:

—⊙— measured in test

—△— computed from test data

— — — — — predicted by NACA TN 2661 method

3. TEST PROGRAM

3.1 General

The test program consisted of fourteen static tests and four fatigue tests of specimens specifically designed to be representative of chem-milled 7075-T6 aluminum alloy stiffened webs presently being used in spacecraft construction.

In the static tests measurements were taken towards the establishment of the following test data:

Initial sheet buckling stress,
Stresses induced in the sheet and in the stiffeners,
Angle of folds in the buckled sheet,
Deflection of beam versus loading,
Loads carried by "portal frame effect",
Initial sheet yielding stress,
Failing loads of the beam, whether by sheet rupture or failure of the stiffeners.

The four fatigue specimens were fatigue-tested to observe the behavior and determine the fatigue-life of the panels under cyclic loading. The effects of two different land configurations on web fatigue, including crack initiation, were also examined. An overall view of the test setup is shown in Photo 1 and schematically in Figure 4.

3.2.1 Static Test Specimens

The static test beams had thin chem-milled 7075-T6 aluminum alloy webs with lands to which stiffeners and flanges of the same material were riveted on one side. Figures 1, 2 and 3 show the geometry and some details of the test specimens; the shop assembly drawing in Appendix B shows all the details of construction. The nominal dimensions of the test panels were:

$t = .028"$, $.009"$ and $.005"$; $h_c = 56.0"$; $d_c = 8.4"$; $d_\ell = .75"$

Geometric properties of each test panel are listed in Table 1.

The average, minimum and maximum web sheet thicknesses measured after failure are listed in Table 7.

All specimens were designed and built so as to be efficient and realistic structural members while being suitable for obtaining the desired test data. The configuration and loading were established in such manner that the middle bay of the panel would simulate a typical interior bay of a multi-bay beam under pure shear loading; the end bays were designed to transmit and distribute evenly the applied load and to minimize the effects of edge restraints on the interior. The flanges were designed to have sufficient strength and stability to prevent premature failure.

The NACA method (NACA TN 2661 and 2662) was relied upon for the design of these specimens. The calculations were performed by a computerized version (Reference 4) of the procedure in Reference 3. Since the aim was to verify the NACA method for different modes of failure, the beams were designed to fail in predetermined modes and the allowable load prediction methods of NACA TN 2661 were modified to suit this purpose. Based on known analytical and experimental data, past experience and "engineering judgement," the following strength criteria were adopted in the design of the test specimens:

a) Web sheet strength - 10% higher than allowables in Figure 19b of NACA TN 2661, adjusted for the actual material properties by a formula developed at Grumman and shown on Figure 5 of this report.

b) Stiffener local failure strength - same as allowable value in Figure 23 of NACA TN 2662, adjusted for the actual material properties by a formula used at Grumman and shown on Figure 6 in this report; except that the maximum value shall not exceed the value obtained at

$$k^{2/3}(t_{st}/t)^{1/3} = 1.3$$

c) Lipped stiffeners - values in b above increased by 30%.

d) Stiffener column failure - same as in Section 4.11(b) of NACA TN 2661.

e) The land was not considered as an integral part of the stiffener (Reference 3). Note that this is different from recommendations made in Sections 4 and 6.

Land dimensions, stiffener lip sizes, sizes and spacing of rivets and other dimensions not covered by NACA TN 2661 criteria were established by Grumman Company practice. Failure loads predicted by the above criteria are not listed in this report.

The first three specimens (Panels A, B, C) were designed to be "most efficient and balanced designs," i.e., to have zero margins of safety for all principal modes of failure. A large number of stiffener sections for each panel were analyzed to this end. Following the testing of these three panels, subsequent ones were designed to provide some primary failures in the web sheet and some in the stiffeners.

Table 1 summarizes the geometric properties of the static test specimens. Material properties of the web sheets were determined from test coupons cut from each specimen sheet prior to chem-milling; these are listed in Table 2.

3.2.2 Fatigue Test Specimens

The four fatigue test specimens were designed to be representative of the most efficient types determined from the static tests of the .009" web series. Two of these were identical to Panel E, the two others were identical to Panel N. These Panels E and N were nominally identical to each other, except that Panel N had double lands, i.e., the change from sheet to land thickness was made in two steps (see Figure 3). Previous experience indicated that fatigue failures in chem-milled panels were likely to originate in the fillet between the web and the land. It was therefore decided to investigate whether the less abrupt changes in thickness provided by a double land (two steps) would reduce stress concentrations and improve the fatigue life of chem-milled panels.

3.3.1 Testing and Recording Apparatus

A schematic drawing of the test setup is shown in Figure 4; details of the test rig are shown on the shop drawing in Appendix B. The same rig was used for both the static and fatigue tests. The load was applied to the top of the specimen by the fixture which transmitted both known shear and moment. The fixture was designed so as to introduce an essentially pure shear load, with no bending moment, in the middle bay of the test specimen. The loading arm and the mid-points of the specimen flanges were restrained against lateral motion to maintain stability of the set-up under load. The weight of the upper fixture was counterbalanced.

The load was applied by a double-acting hydraulic ram. Loads were monitored by a calibrated, electric strain-gaged link. Hydraulic pressure was supplied by a pump and controlled by an electro-hydro servo valve. A servo feed-back control system was used to operate both the static and the fatigue tests. For the static tests, the signal to the servo valve was controlled by adjusting a potentiometer by hand and monitoring calibrated link loads and hydraulic ram pressures. For the fatigue tests the operating limits were set into a service control error accompanying detector. The control point was the calibrated link. The cycling signal was derived from a sine-wave generator.

The output from the strain-gaged load link was recorded on an oscillograph and monitored periodically during the fatigue cycles.

The resistance strain gages used on the webs, stiffeners and flanges of the panels were BHL Electronics, Inc. 350 ohm resistance, temperature-compensated SR-4 foil gages, using constant grid and polyimide backing material. The gage length was 0.25 inches. The gage designations were:

Single axis gages: FAE - 25 - 35 - S13EL
Rosette gages: FAER - 25R - 35 - S13EL

The gages were bonded to the web and stringer surfaces with BHL Electronics, Inc. Epoxy cement, EPY - 150. Gage-to-instrument lead wires were Type B vinyl color-coded 24 gage copper wire.

The strain gages for the first six static test panels were read out on B & F strain plotting instruments. The strain gages on the remaining eight static test panels were traced using C.E.C. oscillograph recorders. Gage locations are shown in Figure 8a and 8b.

3.3.2 Testing Procedure

A general description of the testing procedure is given here; specific information pertaining to each test was recorded on Test Logs.

Each specimen was loaded so as to apply pure shear along the center of the middle bay parallel to the stiffeners. A small base load was applied to take up slack in the assembly and zero readings were established at this load. The load was increased to a predetermined fraction of the anticipated failure load ("test reference load"); it was held there (generally for 1-3 minutes) while dial and strain gage readings were taken and visual observations were made; the load was then decreased back to the base value and held (generally for 1-3 minutes) for taking gage readings and making other observations. The load was again increased to a higher level and the foregoing procedure repeated several times; each time to a higher load level. (In static tests #9 through #13 and #16, 17, 18 continuous, rather than intermittent, strain gage readings were recorded.) After the 90±% of anticipated failure load level the load was increased until complete collapse of the panel. The time duration of load increase was, in general, about 1 to 2 minutes for each 10% of anticipated ultimate load; the rate of load decrease was about twice as fast. Still photographs and high speed motion pictures (the latter during failure) were taken during most of the tests. The same test engineer directed all the tests.

The fatigue test specimens were installed in the same testing unit as the static test specimens and subjected to completely reversed cyclic loading. One Type E specimen and one Type N specimen were cycled at approximately seven tenths of the previously tested ultimate static load of Panel E. A second Type E specimen and second Type N specimen were cycled at approximately four tenths of the above ultimate static load. The number of cycles at initiation of crack and the number of cycles at complete failure were observed. Photographic records were made of portions of these tests.

3.4.1 Static Test Data

During the 14 static tests the following information was obtained:

- Initial sheet buckling stress - The measuring of the applied load at initial buckling of the web sheets was attempted without success. Due to the extreme thinness of the sheets their instability loads were so low that the actual test buckling load could not be determined either by measurements, by listening or by watching. It appeared that even minute imperfections in the planeness of the sheets were enough to eliminate any distinct initial buckling phenomenon.
- Strains in the sheet - These were measured in eight of the tests by strain gages in the middle bay. In tests #1, 2, 3, 5, and 6 the gages were read at incremental load levels, in tests #16, 17, 18, they were recorded continuously (see Table 5).
- Axial strain in the stiffener - These were measured by strain gages in all tests at three cross-sections along the height of one stiffener. In tests #1 through #6 the gages were read at incremental load levels, in tests #9 through #18 (except #14 and #15) they were recorded continuously (see Table 5).

- Shear strains in the flanges - These were measured by strain gages on the leg of the flange in the first three tests in an attempt to determine the portion of the applied shear load carried across the flanges. However, because of apparent torsion in the flanges the strain gage readings could not be meaningfully interpreted in terms of "portal frame" shear loads, so that these measurements were abandoned in subsequent tests.
- Panel deflections - These were measured in all tests by dial gages parallel to the stiffeners at incremental load levels.
- Angle of diagonal tension folds in the web - These were measured from photographs.
- Number of diagonal tension folds - These were counted at incremental load levels during several tests.
- Approximate initial sheet yielding - This was determined by recording the incremental load level after which permanent buckles were observed under base load.
- Still photographs - These were taken at all incremental load levels in the first three tests and at intermittent load levels and after failure in most other tests.
- High-speed motion pictures - These were taken in twelve tests for the purpose of recording the events of failure.
- Visual and aural observations throughout each test.

The above data have been reduced and converted to convenient forms for examination and evaluation and are presented in those forms and discussed in Section 4.

Original Test Logs, strain gage, recordings and tabulations of reduced data are on file in the Structural Mechanics Section, Grumman Aerospace Corporation. All pertinent photographs are reproduced in this report.

The high-speed motion pictures, taken during static test failures and during portions of fatigue tests, have been edited and put on one reel. The film is entitled:

"GRUMMAN AEROSPACE CORPORATION

DIAGONAL-TENSION

BEAM TESTS

NASA Contract NAS 9-8284

June 1968 - July 1969"

The film is on file in the Structural Mechanics Section, Grumman Aerospace Corporation.

3.4.2 Fatigue Test Data

The following information was obtained from the four fatigue tests:

- Number of load-cycles at which the initiation of a fatigue crack was noticed (except in Test #7).
- Location of fatigue crack initiation (not observed in Test #7) and crack propagation.
- Number of load cycles at total fatigue failure.
- A number of photographs during crack propagation and after failure; also normal and high-speed motion pictures.

These data are discussed in Section 5.

4. ANALYSIS OF STATIC TEST RESULTS

4.1 General

The most significant test data, as far as the objectives of this project were concerned, were the ultimate loads and modes of failure of the specimens. Data were obtained on these in the form of ultimate load measurements, high-speed movies, still photos and on-site observations. These data and their comparisons with the predictions of NACA TN 2661 and 2662 are discussed in Section 4.3. Evaluations of all other data, pertaining to the behavior of the various components of the test panels prior to failure, are given in Section 4.4.

4.2 Modifications to NACA Method

Some modifications were made to the NACA method of analysis to make it suitable for strength predictions for panels made of materials of different properties from those considered in NACA TN 2661 and 2662, and also to allow for the presence of a land on the web sheet behind the sitffener. Based on the findings in this project as well as on previous experience, these modifications are also offered as recommended additions to the NACA method.

- The sheet allowable stresses were established by a formula developed at Grumman (Reference 3):

$$\frac{F_{s\ all}}{F_{ty}} = 0.9\left[1 + \frac{1}{2}\left(\frac{F_{tu}}{F_{ty}} - 1\right)^2\right]\left[\frac{1}{2} + (1 - k)^3\left(\frac{F_{su}}{F_{tu}} - \frac{1}{2}\right)\right]$$

  The formula satisfies shear failure in pure shear (at $k = 0$) and tensile failure in pure diagonal-tension ($k = 1$). Compared to the NACA allowable sheet stress curves (Figures 19a and 19b of NACA TN 2661), the formula is about 2% too low for 2024-T3 bare aluminum alloy sheets and about 2% too high for 7075-T6 alcald sheets. The formula is plotted in Figure 5 for typical properties of 7075-T6 bare sheet material.

- The stiffener allowable stresses to guard against local failure of stiffeners were established by a formula used at Grumman (Reference 3):

$$\frac{F_{fc\ all}}{F_{cy}} = 26.0\left[k^{2/3}\left(\frac{t_{st}}{t}\right)^{\frac{1}{3}}\right]\frac{.00182}{\sqrt{F_{cy}/E_c + .002}}$$

  The formula is based on Figure C11.38 of Reference 5 and matches the "forced crippling" allowable stress curves for 2024-T3 and 7075-T6 alclad aluminum alloys in Figures 21 and 23 of NACA TN 2662. It compares well with test data from C-110M titanium stiffeners. The formula is plotted in Figure 6 for typical properties of 7075-T6 bare material. An arbitrary upper limit was imposed on the allowable stress curve which is the value it reaches at $k^{2/3}(t_{st}/t)^{1/3} = 1.3$. The highest value of this parameter represented by test points in NACA TN 2662 is approximately 1.2. Considering this and the trend indicated by those test points, it was felt that extrapolating the NACA curves for values of the abscissa beyond 1.3± was of questionable validity.

- The stiffener column strength calculations of NACA TN 2661, using half of the stiffener length in the Euler-column formula, was not modified.

- For the calculations of stiffener area and stiffener moment-of-inertia the land was taken as an integral part of the stiffener (see Illustrative Analysis). The reasons for this procedure were that

  - o strain gage readings on the land and on the attachment leg of the stiffener indicated that the land tended to work with the stiffener (see Section 4.4.2);
  - o better correlation was obtained between actual and predicted stiffener failure loads in this manner than with other schemes that were tried.

Other than the above modifications, the analysis method was that of NACA TN 2661. The calculations were performed by a modified version of the computer program of Reference 4.

4.3 Ultimate Loads and Failure Modes

Failure modes are defined in three categories:

a) Sheet failure - the rupturing of the sheet prior to any noticeable instability of the stiffeners. (The sheets eventually ruptured in all tests but in some cases this happened after stiffener failure.)

b) Stiffener local failure - the localized buckling of one or more stiffeners causing an immediate and significant drop in the sustained applied load. In some cases this occurrence was followed almost instantaneously be sheet rupture and panel collapse; in other cases the applied load could be increased again, but never more than 3-4% above that just before the drop, and sheet rupture and complete collapse occurred seconds later.

c) Stiffener column failure - the long-wave, Euler-type buckling of the stiffeners out of the plane of the panel. Although noticeable bowing of the stiffeners was observed in every test during loading, none failed in this mode. The reason for this is believed to be partly that the "infinitely" stiff mounting edges of the panel (the floor and the loading arm) acted as unyielding edge-supports of a stiffened plate and thus enabled the diagonally stretched sheet to provide more lateral support to the stiffeners then if the panel had many more bays. In addition, the highly developed diagonal-tension in these tests could provide more lateral support than the less-developed diagonal-tension in the NACA tests (NACA TN 2662). While this lateral support allowed bowing, it prevented overall instability of the stiffeners.

Ultimate Load, P^m_{ult}, is defined here as the highest applied load.

The "NACA predicted allowable" load is defined here as $P^p_{all} = f^p_{s\ all}\ h_c t$, where $f^p_{s\ all}$ is the average shear stress in the sheet at which the lowest margin of safety is zero as calculated by the method of analysis of NACA TN 2661, modified as per Section 4.2.

A summary of the ultimate loads, modes of failure and the comparisons with the NACA predicted allowable loads are given in Tables 3 and 4.

In every test the measured ultimate load, P^m_{ult}, was greater than the NACA predicted allowable load, P^p_{all}. In all but two tests (Tests #6 and #12) the actual modes of failure corresponded to those predicted by the NACA analyses for allowable loads, i.e. either sheet failure or stiffener local failure; column failure predictions were ignored for reasons discussed earlier in this section.

A detailed discussion of sheet and stiffener failures follows.

Sheet failures - The rupturing of the sheet, whether as an initial failure or after stiffener failure, always began either along the fillet at the edge of the stiffener land or along a relatively straight line between two stiffeners, running at approximately right angles across the buckles. The former type will be referred to as shear failure, the latter as tensile failure of the sheet. This initial rupture line then progressed "instantaneously" along the chem-milled edge and precipitated collapse. Occasional sheet rupture spreading into a neighboring bay is attributed to the extremely large deformations during collapse. In Panels C, E and I, the failure of the sheet initiated in an area where the thickness of the sheet, as measured after failure, was the smallest; this was not the case in Panels N and M.

Panel I was different from the others in that the stiffeners were attached to the land side rather than to the flat side of the sheet. (This was an error in the assembly.) The exceptionally good performance of this panel ($P^m_{ult}/P^p_{all\ w} = 1.30$) is noted. Except for the stiffener being on the other side and being slightly thinner, and having two rivets to the flanges at each end, this panel was identical to Panel C which tested some 11% weaker.

There is indication, based on sounds of rivet "popping" and a visible flying rivet on the high-speed movie, that the failure of Panel M was precipitated by premature rivet failure.

Panel N had a slightly different configuration in that the land was made in two steps rather than in one step, as shown in Figures 1 and 3; in comparison to Panel E, to which it was identical in all respects except that Panel E had a single land and slightly greater average sheet thickness, it performed the same way within test scatter.

The tabulated results in Tables 3 and 4 and the plot in Figure 7a indicate approximately 16% average conservatism of the NACA predicted allowable loads for sheet failures, with the individual conservatisms ranging from 7% to 30%.

Stiffener local failures - Stiffener failure consisted of a series of local failures at various locations along the stiffeners in rapid succession. This rapid succession could not be distinguished by eye (except in Tests #10 and 13) but could be seen on the high-speed movies. The location of the first local instability in the stiffener was generally at the point where a diagonal tensile fold originating from the outside corner of one of the side bays intersected the stiffeners (see Photos 8a and 9a). Local failures in the stiffeners appeared to be combinations of local buckling, torsional buckling and forced crippling (see Photo 8b). (This complex failure was defined as "forced crippling" in NACA TN 2661 and 2662.) The deformations in the stiffeners were very extensive, even immediately after their occurrence and prior to collapse of the panel, (see Photo 11c). It could not be determined in each case which portion(s) of the stiffener cross-section became unstable first, i.e. whether a web, flange or lip initiated the failure.

There were indications, such as the sound of rivets "popping" before failure and broken rivets afterwards, that in Tests #1 and #2 the ultimate strengths were adversely affected by premature failure of the stiffener-to-flange single rivets. (In Test #4 and above, two rivets were used. See Shop Drawing in Appendix B.)

Nine panels failed in their stiffeners, of which seven were predicted to fail in the stiffeners, and two were predicted to fail in the sheet. As seen from the tabulated results in Tables 3 and 4 and in Figure 7b, the measured ultimate loads in stiffener failures were, on the average, approximately 19% higher than the NACA predicted allowable loads for the seven panels that were predicted to fail in the stiffeners. The conservatisms for these panels ranged from 8% to 28%. In general, the unlipped stiffeners showed lower margins than the lipped stiffeners.

Panels F and L (Tests #6 and #12) failed in the stiffeners, although they were predicted to fail in the web. The actual ultimate loads for these two panels were lower than predicted for stiffener failures, but were higher than predicted for web failures. After failure in these two panels the stiffeners appeared to have greater local buckling and twisting deformations than the stiffeners in the other panels. It is noted that of the panels which failed in their stiffeners, Panels F and L had the highest values of $k^{2/3}(t_{st}/t)^{1/3}$, which is a critical parameter for the NACA "forced crippling" allowable stress curves (Figures 21, 22, 23 of NACA TN 2662 or Figure 6 here). This parameter places these panels so far away from the original NACA tests that the erroneous failure predictions for these two panels are not surprising. (The NACA test points on Figures 21, 22, 23 of NACA TN 2662 were at values of $k^{2/3}(t_{st}/t)^{1/3} <$ 1.2; for Panels F and L this parameter is 1.5 and 1.35, respectively). This may indicate that, especially with the presence of the land on the sheet, the NACA parameter for predicting forced crippling of stiffeners is of limited applicability and a more generally valid parameter is desirable.

<u>For all of the tests</u> the approximate average conservatism of the modified (as per Section 4.2) NACA method of analysis is 16%. It is emphasized that numbers such as these can be misleading because the conservatism obtained from the tests can vary with certain parameters. Figures 7a and 7b show such variations. There may well be other parameters that affect the line-up of these numbers.

There are three factors inherent in the configuration of the test panels which are believed to contribute in part to the conservatism of the NACA predictions.

1. As the panel deforms under load, a fraction of this load is carried by the flanges in "restrained beam action," i.e. in a combination of flexure and shear restrained by the membrane stiffness of the attached web sheet. (This is referred to as "portal frame effect" in NACA TN 2661). Some of the applied shear load was apparently carried by the flanges. Hence the shear stress in the web sheet is somewhat less than $f_s = P/h_c t$ and consequently the load on the stiffeners (which is a component of the diagonal tension in the sheet) is also lower than that computed from f_s.

2. When the applied load is several times the initial sheet buckling load, the sheet is stretched diagonally to such an extent that by virtue of "tension-strap" action it provides the stiffeners with considerable lateral support against bending out of the plane of the panel. The effect of this support is to reduce the bending moment and curvature, due to eccentric loading, of the stiffener. Thus in the attachment flange of the stiffener the compressive stress, which is the sum of axial and flexural compressive stresses, is not as high as computed for an eccentrically loaded cross-section by an expression such as Equation 30.a. of NACA TN 2661 or Equation A.4 in the Illustrative Analysis in this report. Apparently, in the NACA test data (NACA TN 2662) this phenomenon was not as pronounced because the degree of diagonal-tension was lower. A stiffener of Panel B was idealized as an eccentrically loaded pin-ended column with continuous lateral

elastic support. Calculations with its mathematical model (from Reference 6) at 80% of panel ultimate load showed that the out-of-plane component (created by the lateral deflection of the stiffener) of the sheet diagonal-tensile stress was a sufficient lateral supporting force to enforce a reverse curvature along the middle portion of the stiffener. This was also apparent from strain gage measurements at mid-length of that stiffener, which showed greater compressive strain in the outstanding flange than in the attachment flange of the stiffener.

3. The expression for stiffener load, $P_{st} = kf_s \tan \alpha \, d \, t$, in Equation 30.a of NACA TN 2661 and Equation A.4 in the Illustrative Analysis here) is derived from the assumption that the flange is a multi-span beam of many spans continuously loaded by the tension in the sheet and supported by the stiffeners as unyielding supports. In the panels tested, however, the flange was more like a three-span beam clamped at its two ends (near stiffeners #1 and #4) with two intermediate supports (stiffeners #2 and #3). Because of the stiff loading arm and floor-mounting the clamped end supports of the flange were unyielding; the intermediate supports, however, did have the flexibility of the stiffeners. Thus the intermediate reactions, i.e. the axial forces in stiffeners #2 and #3, were less than the above load per span, P_{st}. Calculations based on measured strain data indicated that in panels of 0.028", 0.009" and 0.005" sheet thicknesses the stiffeners #2 and #3 might have been loaded only to 95%±, 90%± and 85%±, respectively, of the load per span P_{st}.

4.4 Evaluation of Instrumentation Data

4.4.1 General

In this section the pertinent information obtained from strain gage and dial gage recordings is analyzed and compared with predictions of the "Engineering Theory of Incomplete Diagonal Tension" (NACA TN 2661 and 2662). The number and location of strain gages were established so as to provide the most essential data within the budgetary limits of the project. The instrumentation was not complete enough, in terms of the number of strain gages, for a thorough and indisputable evaluation of the distribution and magnitudes of stresses and strains in diagonal-tension beams of the types tested. However, the gathered data exposed and clarified some very important and interesting phenomena which are believed to be of considerable value for the understanding of the post-buckling behavior and for the design of such panels.

Strain gages were installed on the test panels at the locations shown on Figures 8a and 8b. Because of symmetry in the test panels and in loading, only half of each panel was instrumented. (The symmetry was ascertained in the first five tests by the identical readings of gages #54 and 55; see Figure 8a). All the rectangular strain gage rosettes on the web sheet were back-to-back on both sides of the sheet and were monitored so as to cancel flexural strains and record only the strains in the median plane of the sheet. In the first six tests, the gages were monitored at increments of loading; in all the other static tests they were monitored continuously (see Table 5).

Dial gages were read at increments of loading in every test.

4.4.2 Stiffener Data

Longitudinal strains in a stiffener adjacent to the middle bay in each test were measured at locations shown on Figures 8a and 8b.

In the analysis of these data and in their comparisons with the NACA TN 2661 predictions, the following sources of uncertainty should be kept in mind:

1. Gages were installed at only three locations along the length of the stiffener, thus continuous variations, if any, in longitudinal stresses could not be accurately determined.

2. Local deformations in the stiffener, caused by the waving of the buckled sheet, could give rise to erratic readings.

3. Rivet holes in the land and stiffener attachment flange probably affected the readings.

Despite these adverse conditions much useful information was gathered.

The curves of Figure 9 show plots of measured longitudinal strains on the attachment leg of the stiffeners and on the sheet lands at three locations along the stiffeners. The measured strains are connected by straight lines. While individual readings could be affected by local deformations, the collection of diagrams do reflect the valid picture. The plots do not show a consistent trend of increase of longitudinal strains or stresses from the ends to half-heights of the stiffeners, as suggested in Section 3.5 of NACA TN 2661. In Panels A, D, G, J, K the plots do show an increase in stress from end to middle of stiffener; in Panels B, C, E, F, H, I, L, M, and N the stresses are either roughly uniform or decreasing, rather than increasing from end to middle. The former group of panels were of 0.028" sheet thickness, the latter were of 0.009" and 0.005" sheet thicknesses.

The curves of Figure 10 show plots of measured longitudinal stiffener stresses, at mid-height of the stiffeners, based on stresses measured by strain gages on the land (gage #41), on the free surface of the attachment flange (gage #42), and on the outer surface of the outstanding

flange (gage #43). Measured values are connected by straight lines. Also shown on these figures are analytically determined stiffener stresses, f^p_{st}, $f^p_{st\ max}$, $f^p_{st\ avg}$, and f^p_{st*}, computed from the expressions of NACA TN 2661, with the land considered an integral part of the stiffener. Details are given in the Illustrative Analysis of this report.

In comparing calculated stiffener stresses with the test data it should be noted that f^p_{st} and $f^p_{st\ max}$ are the calculated average and maximum (average and maximum along the length) values of the stiffener stress at the web line, a position roughly midway between the locations of gages #41 and #42. Therefore, f^p_{st} and $f^p_{st\ max}$ can be compared with the average of the values recorded by gages #41 and #42. Although, according to NACA TN 2661, only $f^p_{st\ max}$ and not f^p_{st}, need be considered at the mid-height of the stiffener, both values are plotted in Figure 10 because the test data (see Figure 9) did not show the consistent variation of stiffener stress along the stiffener length as predicted by NACA TN 2661.

The information from gage #43 should be compared with f^p_{st*}. Because of the very large discrepancy between test and prediction in this case, the value of f^p_{st*} is plotted only at $P^m/P^m_{ult} = 1.0$. In all the panels the analysis methods of TN 2661 would have predicted a tensile stress in the outstanding flange of the stiffeners, whereas gage #43 generally recorded a compressive stress. (In order to make the graphs more compact, the negative value of f^p_{st*} was plotted in Figure 10).

An examination of the curves in Figure 10 indicates the following:

a) The measured stresses in the land and in the attached leg of the stiffener are considerably less than predicted and are, in fact, closer to the predicted values of the average stresses in the stiffeners.

b) The measured stress in the outstanding flange of the stiffener is greatly different from what would be predicted by the methods of NACA TN 2661. Instead of showing a tensile stress, gage #43 generally indicated a compressive stress of the same order of magnitude as did gages #41 and #42.

c) There are sharp changes in slope in the test curves, possibly due to local buckles and other local effects which could significantly affect the strain gage readings.

The most important conclusion that can be drawn from the above observations is that the bending moment in single-upright stiffeners of the proportions used in these test panels is much smaller in magnitude and may even be opposite in direction from what would be predicted by TN 2661. Consequently, the stress distribution across the stiffeners is much more uniform than that predicted by TN 2661, resulting in a maximum compression stress in the stiffener that is considerably less than predicted. An explanation of this behavior, in terms of the elastic support given to the eccentrically loaded stiffener by the sheet in diagonal-tension, was given in Section 4.3.

That the measured average stiffener stress was somewhat lower than predicted can also be explained in part by the comments in Section 4.3. Some of the test data, however, such as the low stiffener stresses measured in Panel F, have not been explained.

The fact that the band of three gage readings (#41, 42, 43) correlates reasonably well with $f^{p}_{st\ avg}$, indicates that the "Engineering Stress Theory for Incomplete Diagonal-Tension" is basically applicable in predicting the load on the stiffeners but not the distribution of stresses in the stiffeners.

The plots in Figure 11 show computed stiffener stresses at local failure, compared with the "NACA allowable" line. This line is the same as Curve B on Figure 6 and represents computed, not actual, stiffener stresses (see Section 2.5 of NACA TN 2662). The triangles represent the stiffener compressive stresses at the median plane of the sheet, at mid-length of the stiffeners, computed by equation for $f_{st\ max}$ shown on the Figure with $f_{s\ ult} = P^m_{ult}/h_c t$.

The group of points from Panels D, A, G, K, J, B, and H fall well in line with the points on Figures 21, 22, 23, of NACA TN 2662. The significantly different behavior indicated by the points for Panels L and F was discussed in Section 4.3.

4.4.3 Web Data

Strains in the web sheet were measured in eight tests by rectangular strain gage rosettes placed back-to-back on both sides of the sheet at locations shown on Figures 8a and 8b. Principal and other strains and stresses in the mid-plane of the sheet where computed from the data. In some tests there were possible errors in instrumentation that resulted in data which were incomplete or could not be evaluated with full confidence. These data were made use of in qualitative rather than quantitative analyses. (As discussed later in this Section, the strain gage readings on Panels E, F, J and N appear to be too high.)

Figure 12 gives "computed-from-test" plots of principal stresses, f_1^{ct} and f_2^{ct}, and maximum shear stress, f_3^{ct}, in the median plane of the sheet at the strain gage locations. These stresses were computed with $E = 10.5 \times 10^3$ ksi and $\nu = 0.33$. Although some of the strain gage data are questionable, the curves indicate an approximately linear variation of the principal tensile stress along the buckles and of the maximum shear stress with increasing load, within the range of recording. The second principal stress (i.e., across the buckles) is compressive at

initial sheet buckling but becomes tensile when the web undergoes large deflections at loads well beyond initial buckling. This tensile stress, however, is much smaller than the diagonal tensile stress along the buckles.*

Figure 12 shows plots of the angle of major principal stress, α^{ct}, measured from the flange line, computed from the gage readings. The figures which refer to gage W1 also show the angle of folds, or buckles α^{m}_{fold}, at the middle of the web sheet as measured from photographs. Also plotted on these figures are the angles of diagonal tension, α^{p}_{IDT}, computed by the NACA method. The direction of the folds and the angle of major principal stress correlate very well on these plots, indicating that in highly developed diagonal-tension the direction of the buckles follow the direction of the major principal stress. The above curves indicate that the angles of incomplete diagonal-tension, α^{p}_{IDT} are considerably different from the observed angles. Theoretically, α^{p}_{PDT} is the angle of major principal stress in pure diagonal-tension (Reference 7), but in incomplete diagonal-tension α^{p}_{IDT} is the angle that the major principal tensile stress would follow if the sheet were not carrying part of the applied load in pure shear. It is believed that the differences between the observed angles and α^{p}_{IDT} may be somewhat greater than they would be in the same panel with many more bays. The reason is that the angles increase with increasing axial stiffness of stiffeners and since the thicker edge bays and rigid mounting edges of the panels probably produced this same effect, this may have increased the values at α^{ct} and α^{m}_{fold}.

---

* A theoretical analysis of the post-buckling state of stress in stiffened plates under shear loads is being conducted at Grumman, based on the work of D.M.A. Leggett (Reference 8). The results will be published in a Grumman Advanced Development Report. Some initial results, for a few particular cases, indicate that at loads exceeding approximately 20 times the initial sheet buckling load, a portion of the sheet away from the support lines goes into tension stress in both principal in-plane directions. The known published papers on post-buckled plates in shear (References 9, 10, 11, 12, etc.) do not carry the analyses sufficiently far into the post-buckled region to show a tensile stress in the direction across the buckles.

The strain gage data were used in an attempt to determine what portion of the applied shear load was carried by the sheet, P_s, and by the flanges, $P_{f\ell}$, ("portal frame effect"). From the recordings of gages along the web sheet the shear stresses parallel with the stiffeners, $f^{ct}_{s,i}$, at each gage location, i, were computed at various load levels. These stresses were then multiplied by the contributing sheet areas, $(\Delta h_i)t$, (half-way to the neighboring gage location on both sides). These forces were then summed along the sheet height, giving the total shear force, $P_s = \Sigma f^{ct}_{s,i}(\Delta h_i)t$, carried by the sheet. The shear force carried across the flanges was computed as the difference $P_{f\ell} = P - P_s$. The results are shown on Figure 13. Some of these results are very questionable. In particular, the results from Panels E, F, J and N show $P_s > P$ and $P_{f\ell} < 0$. There is no obvious explanation of this discrepancy. No error was found in the instrumentation. Because of these questionable test results, the results from Panels A, B, and C, which appear reasonable, are suspect.

The approximate load to cause yielding of the web sheet, P^m_y, was determined by noting the applied load which, when dropped to base load, left the sheet with visible residual diagonal buckles. It was not always clear just when initial permanent set was reached. From tests 2, 3, 4 and 5 it was observed that P^m_y(14, 7.8, 42, and 14 kips, respectively) was reached when the principal tensile stress, f^{ct}_1, at the middle of the sheet was about 55 to 60 ksi, which is approximately the proportional limit $F_{p\ell}$, of the sheet material. For design purposes a reasonable estimate of P_y appears to be the value which makes the principal tensile stress, f_1, computed from the equations of NACA TN 2661 (Equation A.13 in the Illustrative Analysis) equal to $F_{p\ell}$.

4.4.4 Panel Deflections

Overall deflections of the panels were measured by dial gages at the locations shown on Figures 8a and 8b. Of these, the data obtained from dial gages #3 and #4 were evaluated in detail. Figure 14 gives

plots of equivalent shear stiffness G^p_{IDT} (computed by equations 31.a and b. of NACA TN 2661) and G^{ct}_{IDT}($G^{ct}_{IDT} = P^m/h_c t\ \gamma_{IDT}$, where $\gamma_{IDT} = \frac{\text{Gage 3 - Gage 4}}{d}$).

The curves show that G^p_{IDT}/G^{ct}_{IDT} is greater than 1.0 for panels with 0.028" thick webs and less than 1.0 for panels with 0.005" and 0.009" thick webs. The differences between G^p_{IDT} and G^{ct}_{IDT} decrease with increasing load. Near failure the correlation is very good and modification of the NACA equations is not warranted.

It was noted that when the applied load was held for a few seconds at a constant value near failure, the deflections increased rapidly.

4.5 Additional On-site Observations

The following is a list of miscellaneous observations made before and during the tests:

In general, it was found that working with panels of this relatively large size and such extremely thin sheets was difficult; it required precision and care in every step.

In almost all of the panels the sheets were "buckled" before load was applied to them. This was the result of necessarily tight fitting into the test fixture. These original buckles prevented the observation of initial sheet buckling under applied shear load but are believed to have had no effect on the post-buckling behavior.

The formation of a new buckle under increased load was followed by 2-3 seconds of clearly visible out-of-plane vibration of the sheet but not of the stiffeners. The dial gages did not jump visibly when a new buckle formed.

In several tests the number of buckles in the sheet were counted at incremental load levels; this information appears in the Test Logs (not included in this report).

The event of failure in each static test is briefly described below. The descriptions represent observations made during the tests and from the high-speed movies. In referring to left and right side, the panel is viewed from the stiffener side, the shear load being applied at the top to the left and at the bottom to the right, parallel with the stiffeners.

Test #1, Panel A. Stiffener-to-flange rivets failed; Stiffeners #3 and #2 failed; web ruptured in tension in Bay #1.

Test #2, Panel B. Stiffener-to-flange rivet failed at left end of Stiffener #2; Stiffener #3 failed at 0.4 h_{st} from left end; Stiffener #2 failed at 0.25 h_{st} from left end; web ruptured in tension in Bay #3 near right side.

Test #3, Panel C. Web ruptured in tension in Bay #3 near right side; then progressed to the left along Stiffener #4.

Test #4, Panel D. Stiffeners #2 and #3 failed at locations diagonally from lower right corner of Bay #3; web ruptured in tension in Bay #1.

Test #5, Panel E. Web failed in shear in Bay #1 along Stiffener #1.

Test #6, Panel F. Stiffeners #2 and #3 failed at an intersection with a diagonal tension fold from the upper left corner of Bay #1; web ruptured in tension in Bay #3 on left and right side at the same time.

Test #9, Panel G. Stiffeners #2 and #3 failed at intersections with a diagonal tension fold from the lower right corner of Bay #3; collapse of panel not recorded.

Test #10, Panel H. Stiffeners #2 and #3 buckled at intersections with a diagonal tension fold from the lower right corner of Bay #3 (at 1550 lbs. load); Stiffeners #2 and #3 failed at intersections with a diagonal tension fold from the upper left corner of Bay #1 (at 1850 lbs. load); web ruptured in Bay #3.

Test #11, Panel I. Web failed in shear in Bay #1 along Stiffener #1 and in Bay #2 along Stiffener #2.

Test #12, Panel L. Stiffeners #2 and #3 failed at intersections with a diagonal tension fold from the upper left corner of Bay #1; web ruptured in tension near left end of Bay #2 and near right end of Bay #3.

Test #13, Panel K. Stiffener #3 buckled at intersection with a diagonal tension fold from the upper left corner of Bay #2, then at intersection with a diagonal tension fold from the lower right corner at Bay #3; web failed in shear in Bay #3 along Stiffener #4; left flange broke completely at Stiffener #4.

Test #16, Panel N. Web failed in tension near left end of Bay #2.

Test #17, Panel J. Stiffeners #2 and #3 failed at intersections with a diagonal tension fold from the lower right corner of Bay #3; web failed in shear in Bay #3 along Stiffener #4; left flange broke completely at Stiffener #4.

Test #18, Panel M. Stiffener-to-flange rivets failed at right end of Stiffener #3; web failed in tension at left end of Bay #2.

Photographs of the failed panels are given elsewhere in this report.

5. ANALYSIS OF FATIGUE TEST RESULTS

The basic information obtained from the four fatigue tests is tabulated in Table 6. The panels were essentially identical except that the type E panels had a one-step land, while the type N panels had two-step lands. The panels were subjected to completely reversed cyclic loading.

In all the tests the fatigue crack initiated at a corner of the panel, at the edge of a chem-milled land, and then progressed along the chem-mill line, indicating the effect of the stress concentration at the edge of a chem-milled land.

In Test #7 initiation of the crack was not noticed prior to failure. A metallurgical examination of the failed region indicated that the crack initiated at the upper right corner of Bay #1 (looking from the stiffener side of the panel) at the edge of the chem-milling and then propagated around the land edge (see Photo 16a and 16b).

In Test #8 a 1/8 inch long fatigue crack was noticed at 4169 cycles at the upper left corner of Bay #1 at the edge of the chem-milling at a point half-way around the corner curve. The crack then propagated along the chem-mill line in both directions from the starting point until it reached the straight portions of the chem-milled edge. At this time the web "instantaneously" ruptured along the flange and stiffener and the panel collapsed.

In Test #14 a pin-point crack was observed at the lower left corner of Bay #3 at the root of the step between the two lands at a point half-way around the corner curve. It then progressed along the chem-mill line between the two lands similarly to Test #8 (see Photo 17a and 17b).

In Test #15 the same thing was observed as in Test #14 above, except the crack initiated in the upper right corner of Bay #1 (see Photo 18).

After the cracks were noticed in Tests #8, 14 and 15, close-up still photographs of the critical area were taken at every 5 cycles of loading to document the crack propagation to failure. A few minutes of normal-speed and high-speed motion pictures were taken during Tests #7 and 14 showing the changing buckle patterns in the webs.

A close observation of the corners of all four fatigue panels where fatigue cracks initiated disclosed that a web buckle crest ran through the point where the crack initiated. The buckle crest line was at an angle of approximately 45° to the stiffener and started in the land at the intersection of the stiffener and flange rivet lines. The depth of the buckle increased for approximately two inches away from the chem-milled step and then stayed constant until it reached the proximity of the next stringer. The slope of the buckle in the web was steepest at the edge of the land but then quickly decreased within the land. The sharp curvature in the web at the edge of the land indicated the presence of significant bending moment in the web at this section.

The fatigue lives from the four tests were plotted in Figure 15 against the calculated approximate values of diagonal tensile stresses in the web at maximum cyclic load. The calculated values of diagonal tensile stress did not include the effects of stress concentrations at the land edge. Also plotted on this figure is an S-N curve, interpolated from Figure 9 of Reference 13 for notched 7075-T6 specimens ($K_T = 4$) under constant amplitude cyclic loading with a zero minimum stress. This data was chosen for comparison because it was believed to be reasonably representative of the variation of the basic membrane stress in a diagonal direction in the web under complete load reversal (the membrane stress in any given direction in the buckled web does not undergo complete reversal when the applied load is completely reversed). The test results indicate that, for a given value of cyclic membrane stress in the basic web, the fatigue lives of the Type N panels were somewhat

better than the lives of the Type E panels. However, the actual failure locations were different. (The type E panels failed in the web at the edge of the land, whereas the type N panels failed at the root of the step between the two lands.) Comparison with the S-N curve in Figure 15 indicates that the effects of the lands, together with the effect of the local curvature in the web at the lands, resulted in an effective stress concentration factor of approximately 4, applied to the basic web membrane stress.

6. CONCLUSIONS AND RECOMMENDATIONS

Static Tests

The parameters affecting the behavior and strength of diagonal-tension beams are numerous. Considering the extent of this project, some of the quantitative conclusions and recommendations can be tentative only. In comparison with the "Engineering Theory of Incomplete Diagonal-Tension," as presented in NACA TN 2661 and herein referred to as the NACA method, the following conclusions and recommendations are offered for the type of stiffened shear panels tested.

- The NACA method must be modified to allow for the inclusion of a land on a chem-milled sheet. Strain gage measurements indicated that the land tends to work with the stiffener in supporting the compressive load in the stiffener. Computations correlated best with test data when the land cross-sectional area was included as part of an effective stiffener area, A'_{st}, defined in the list of symbols. Therefore, it is recommended that A'_{st} be used for the stiffener area when using the NACA method to analyze stiffened chem-milled shear panels.

- In twelve of the fourteen static tests the NACA method correctly predicted the mode of failure (stiffener or sheet). Predictions of column failure were disregarded for reasons discussed in the report. The measured ultimate loads of all fourteen static test panels exceeded the lowest allowable loads computed by the NACA method (using the land as recommended), regardless of whether or not the actual failure mode was the same as the mode corresponding to the lowest predicted allowable load. When the test ultimate loads were compared with the NACA allowable loads for the actual modes of failure, an average conservatism of 16% was obtained for sheet failures and 13% for stiffener failures; in the

latter group the lipped stiffeners performed somewhat better than the unlipped ones. The conservatism in stiffener failures decreased with the parameter $k^{2/3}(t_{st}/t)^{1/3}$, while in sheet failures it increased with k.

Based on this information and on the criteria of providing at least 10% margin of safety in sheet failure and at least 15% margin of safety in stiffener local failure (satisfied by all but the lowest test in each of the two failure modes in the project) the following recommendations are made for the calculation of allowable loads:

a) The allowable shear load based on sheet failure should be as computed with the NACA method, using the expression (or curve) for allowable sheet stress as given in this report.

b) The allowable shear load based on stiffener local failure should be as computed with the NACA method, using the expression (or curve) for allowable stiffener stress as given in this report for values $k^{2/3}(t_{st}/t)^{1/3} < 1.3$; for values greater than 1.3 the NACA method is seen to be unconservative but there were not enough tests in this range to support specific recommendations.

c) The NACA allowables to guard against column-type failure of stiffeners appear to be conservative, but lack of sufficient data prevents specific conclusions.

- The "amplification of stiffener stresses" from end to middle of stiffeners as indicated in NACA TN 2661 is substantiated by the stiffener strain measurements on the panels with .028" sheet thickness but not on panels with .009" and .005" sheets. The data, however, are insufficient to permit specific quantitative conclusions.

- The longitudinal strains measured at the mid-length section of the stiffeners lead to two significant conclusions:

  a) The stresses are relatively uniform across the cross-section, showing little or none of the bending predicted by the NACA method for single-upright stiffeners, thereby indicating that the sheet provides considerable elastic restraint against bending of the stiffener.

  b) The measured stresses in the stiffener are, on the average, a little lower than the average stress $f^{p}_{st\ avg}$, computed by the NACA method; the measured stress in the stiffener attachment flange is, therefore, at the mid-lenght 30% to 50% less than predicted by the NACA method. However, as indicated above, the stiffener local failure load is reasonably well predicted by the NACA method.

- A number of observations were made regarding the magnitude and distribution of stresses and strains in the web sheet. These are discussed in Section 4.4.3. The data is not complete enough to support recommendation which would affect the NACA method.

- Overall, the NACA method of static analysis with the recommended modifications was satisfactory for the prediction of ultimate load capacity of the type of stiffened shear panels tested in this project. The method's predictions of the distribution and magnitude of stresses and strains, however, were generally inaccurate.

More static test data as well as analytical work are needed for a more reliable method of analysis. Specimens similar to those in this project but with more extensive instrumentation should be tested. As indicated in the discussion of measured upright stresses in TN 2662, "correlation with any kind of theory can be expected only if a large number of gages is used to permit local stress effects to be averaged out." Analytical work should concentrate on deriving expressions for the actual induced stresses in the various parts of the panel.

Fatigue Tests

The behavior of structures, such as the specimens tested, under fatigue loading is very complex; hence data from as few as four tests should be considered preliminary only. The measured fatigue life and other observations from the tests are valuable in providing information where none existed before. In every fatigue test the crack initiated at the corner of a chem-milled bay of the web at the edge of the chem-milling at a point half-way around the corner curve. The crack then propagated along the edge of the land. In case of a two-step land the crack initiated and progressed along the root of the step between the two lands. The two specimens with two-step lands (which in effect provided gussetting of the corner of the web) had slightly longer fatigue lives than the two specimens with single lands. Since fatigue behavior may prevent the achievement of a minimum-weight design for static strength, knowledge of that behavior is very much desired. Many more fatigue tests on stiffened webs are needed for parametric studies that would lead to the establishment of design criteria.

REFERENCES

1. P. Kuhn, J. P. Peterson, L. R. Levin, "Summary of Diagonal-Tension, Part I.," NACA TN 2661, May, 1952.

2. P. Kuhn, J. P. Peterson, L. R. Levin, "Summary of Diagonal-Tension, Part II.," NACA TN 2662, May, 1952.

3. R. T. Ratay, "Instability and Failure Analysis of Flat Stiffened Plates Under Shear (Modified NACA Method)," GAEC Structural Mechanics Note #14, November 1968.

4. R. D. Torczyner, "Program DITEN - An IBM 1130 Program for Post-Buckling Analysis of Stiffened Flat Plates Under Applied Shear," GAEC Structural Mechanics Note #17, December, 1968.

5. E. F. Bruhn, Analysis and Design of Flight Vehicle Structures, Tri-State Offset Co., 1965.

6. M. Hetényi, Beams On Elastic Foundation, University of Michigan Press, 1964.

7. Herbert Wagner, "Flat Sheet Metal Girder with Very Thin Metal Web, Part I," NACA TN 604, February, 1931.

8. D. M. A. Leggett, "The Stresses in a Flat Panel Under Shear when the Buckling Load has been Exceeded," R.A.E. Rep. & Memo. No. 2430, September, 1940.

9. S. Levy, K. L. Fienup, R. M. Wooley, "Analysis of Square Web Above Buckling Load," NACA TN 962, February, 1945.

10. S. Levy, R. M. Wooley, J. M. Corrick, "Analysis of Deep Rectangular Shear Web Above Buckling Load," NACA TN 1009, March, 1946.

11. M. Skaloud, "Design of Webplates of Steel Girders with Regard to the Postbuckling Behavior (Analytical Solution)," The Structural Engineer, December, 1962.

REFERENCES (Cont'd)

12. Noboru Yamaki, "Postbuckling Behavior of a Clamped Infinite Strip Under the Action of Shearing Forces," Zeitschrift Für Angewandte Mathematik und Mechanik, 46, 3/4, 1966.

13. Walter Illg, "Fatigue Tests on Notched and Unnotched Sheet Specimens of 2024-T3 and 7075-T6 Aluminum Alloys and of SAE 4130 Steel With Special Consideration of the Life Range From 2 to 10,000 Cycles," NACA TN 3866, December, 1956.

TABLES

Grumman

Table 1. Geometric properties of test

PANEL	TEST #	STIFFENER SECTION	h_c (in.)	h_e (in.)	d_c (in.)	d (in.)	t^* (in.)	t_ℓ (in.)	d_ℓ (in.)	h_ℓ (in.)	t^*_{st} (in.)	b_{pl} (in.)	b_{fl} (in.)	b_w (in.)	b_{f2} (in.)
A	1		56.0	58.2	8.4	9.15	.0288	.063	.75	1.0	.0648	.312	.625	1.125	.312
B	2		"	"	"	"	.0103	.025	"	"	.0250	.250	.625	1.125	.375
C	3		"	"	"	"	.0046	.020	"	"	.0204	.220	.500	.875	.500
D	4		"	"	"	"	.0289	.063	"	"	.0640	.312	.625	1.125	.312
E	5		"	"	"	"	.0096	.025	"	"	.0320	.250	.625	1.125	.375
F	6		"	"	"	"	.0048	.020	"	"	.0194	-	.500	.875	.500
G	9		"	"	"	"	.0280	.063	"	"	.0650	-	.625	1.125	.312
H	10		"	"	"	"	.0100	.025	"	"	.0255	-	.625	1.125	.375
I	11		"	"	"	"	.0046	.020	"	"	.0198	.220	.500	.875	.500
J	17		"	"	"	"	.0280	.063	"	"	.0820	.312	.625	1.125	.312
K	13		"	"	"	"	.0290	.063	"	"	.0820	-	.625	1.125	.312
L	12		"	"	"	"	.0090	.025	"	"	.0302	-	.625	1.125	.375
M	18		"	"	"	"	.0096	.025	"	"	.0410	-	.625	1.125	.375
N	16		"	"	"	"	.0090	.013 .025	"	"	.0320	.250	.625	1.125	.375

* Average of several measurements. All other dimensions are nominal.

FOLDOUT FRAME 1

ble 1. Geometric properties of test panels

d_ℓ (in.)	h_i (in.)	t^*_{st} (in.)	b_{p1} (in.)	b_{f1} (in.)	b_w (in.)	b_{f2} (in.)	b_{p2} (in.)	r (in.)	A_{st} (in.^{2})	I_{st} (in.^{4})	e (in.)	A'_{st} (in.^{2})	I'_{st} (in.^{4})	e' (in.)	FLANGE TYPE	$A_{f\ell}$ (in.^{2})	$I_{f\ell}$ (in.^{4})
.75	1.0	.0648	.312	.625	1.125	.312	-	.125	.1281	.01905	.465	.1754	.02714	.335	T1	.715	.120
"	"	.0250	.250	.625	1.125	.375	-	.0625	.0551	.00990	.470	.0738	.01309	.349	T2	.422	.084
"	"	.0204	.220	.500	.875	.500	.220	.0625	.0430	.00506	.440	.0580	.00729	.324	T2	.422	.084
"	"	.0640	.312	.625	1.125	.312	-	.125	.1267	.01888	.465	.1740	.02694	.334	T1	.715	.120
"	"	.0320	.250	.625	1.125	.375	-	.0625	.0697	.01235	.471	.0884	.01574	.370	T2	.422	.084
"	"	.0194	-	.500	.875	.500	-	.0625	.0344	.00426	.440	.0494	.00635	.304	T2	.422	.084
"	"	.0650	-	.625	1.125	.312	-	.125	.1168	.01874	.484	.1640	.02725	.340	T1	.715	.120
"	"	.0255	-	.625	1.125	.375	-	.0625	.0512	.00957	.499	.0700	.01310	.363	T2	.422	.084
"	"	.0198	.220	.500	.875	.500	.220	.0625	.0418	.00493	.440	.0568	.00714	.322	T2	.422	.084
"	"	.0820	.312	.625	1.125	.312	-	.1563	.1537	.02143	.470	.2009	.03006	.355	T1	.715	.120
"	"	.0820	-	.625	1.125	.312	-	.1563	.1417	.02150	.483	.1890	.03036	.358	T1	.715	.120
"	"	.0302	-	.625	1.125	.375	-	.0625	.0603	.01117	.499	.0791	.01484	.378	T2	.422	.084
"	"	.0410	-	.625	1.125	.375	-	.0938	.0797	.01427	.497	.0985	.01815	.401	T2	.422	.084
"	"	.0320	.250	.625	1.125	.375	-	.0625	.0697	.01235	.471	.0884	.01573	.369	T2	.422	.084

FOLDOUT FRAME 2

Grumman

Table 2. Material properties of coupons cut from web sheet material of test panels.

Panel	Test No.	F_{ty}	F_{tu}	F_{cy} *	F_{su} *	$F_{p\ell}$	$E/10^3$
		ksi					
A	1	71.9	78.2	70.0	47.0	54	10.06
B	2	74.0	80.4	70.0	48.0	58	10.06
C	3	72.7	79.7	70.0	48.0	58	9.80
D	4	71.3	77.0	70.0	46.0	59	10.09
E	5	74.2	80.4	70.0	48.0	59	10.17
F	6	72.9	79.7	70.0	48.0	57	9.88
G	9	73.3	79.2	70.0	48.0	52	10.19
H	10	73.5	80.9	70.0	48.0	54	10.19
I	11	73.6	80.4	70.0	48.0	--	----
J	17	73.3	78.85	70.0	48.0	52	10.19
K	13	73.3	79.2	70.0	48.0	52	10.19
L	12	73.6	80.4	70.0	48.0	54	10.19
M	18	73.6	80.4	70.0	48.0	54	10.19
N	16	76.4	81.3	70.0	48.0	52	10.09

* Nominal values.

Table 3. Summary of measured ultimate loads and NACA predicted allowable loads.

Test No.	Panel	Stiffener section	$f^p_{s\,cr}$ (ksi)	$f^{ct}_{s\,ult} = \frac{P^m_{ult}}{h_c t}$ (ksi)	$\frac{f^{ct}_{s\,ult}}{f^p_{s\,cr}}$	k (Fig. 13 NACA TN 2661)	NACA predicted allowables $P^p_{all} = f^p_{s\,all}\ h_c\ t$ (kips): web $P^p_{all\,w}$	stiffener: local $P^p_{all\,fc}$	stiffener: column $P^p_{all\,c}$	Measured failure P^m_{ult} (kips): web	stiffener: local	stiffener: column	$\frac{P^m_{ult}}{P^p_{all\,w}}$	$\frac{P^m_{ult}}{P^p_{all\,fc}}$	$\frac{P^m_{ult}}{P^p_{all\,c}}$
3	C		.020	38.60	1930	.93	8.44		[8.1] ⓒ	9.96			1.18		See Section 4.3 for discussion of column failures.
5	E		.090	37.92	421	.87	17.99			20.4			1.13		
11	I ⓐ		.020	43.02	2151	.93	8.51		[7.9] ⓒ	11.1			1.30		
16	N ⓑ		.078	38.29	491	.87	17.39			19.3			1.11		
18	M		.089	35.32	397	.86	17.81			19.0 R			1.07 R		
6	F		.022	36.06	1639	.92	8.80	11.1	[7.3] ⓒ		9.7		(1.12+) ⓓ	0.87	
9	G		.728	33.61	46	.68		43.12			52.7			1.22	
10	H		.094	34.46	367	.86		16.69			19.3			1.16	
12	L		.078	35.71	458	.87	16.63	18.3			18.0		(1.08+) ⓓ	0.98	
13	K		.804	35.41	44	.67		49.21			57.5			1.17	
1	A		.767	34.53	45	.68		44.52			55.7 R			1.25 R	
2	B		.099	34.83	352	.86		17.31	[16.8] ⓒ		20.06 R			1.16 R	
4	D		.771	35.10	46	.68		44.33			56.8			1.28	
17	J		.753	34.44	46	.68		50.02			54.0			1.08	

NOTE: All computed stresses and forces are based on actual material properties as per Table 3-2.

R Rivet-initiated failure; see Section 4.3

ⓐ Stiffeners attached directly to land.

ⓑ Double land

ⓒ $P^p_{all\,c}$ for column failure when lower than $P^p_{all\,w}$ and $P^p_{all\,fc}$.

ⓓ Not included in averages of Table 4

Table 4.

Ratios of Ultimate Test Loads to NACA Allowable Loads: P^{m}_{ult}/P^{p}_{all} +	
Avg. for all tests:	1.14
Avg. for all tests; excl. Panel F & L: *	1.18
Avg. for 5 sheet failures:	1.16
Avg. for 4 sheet failures; excl. Panel M: **	1.18
Avg. for 9 stiffener failures:	1.13
Avg. for 7 stiffener failures; excl. Panel F & L: *	1.19
Avg. for 5 unlipped stiffener failures:	1.08
Avg. for 3 unlipped stiffener failures; excl. Panel F & L: *	1.18
Avg. for 4 lipped stiffener failures: ***	1.19

+ Allowable loads used in the comparisons are those which correspond to the actual failure modes.
For Panels F & L the ratios of 0.87 and 0.98, respectively, are used from Table 3.

* See Discussion in Section 4.3.

** Strength of Panel M was possibly affected by premature rivet failures.

*** Strengths of Panels A and B were probably affected by premature rivet failures.

Table 5. Instrumentation.

Panel	Test#	Strain gage layout on Figure No.	Strain gages used on			Strain gage monitoring	Dial gages used
			Web	Stiffr.	Flange		
A	1	8a.	x	x	x	Intermittent	x
B	2	"	x	x	x	"	x
C	3	"	x	x	x	"	x
D	4	"		x		"	x
E	5	8b.	x	x		"	x
F	6	"	x	x		"	x
G	9	"		x		Continuous	x
H	10	"		x		"	x
I	11	"		x		"	x
L	12	"		x		"	x
K	13	"		x		"	x
N	16	"	x	x		"	x
J	17	"	x	x		"	x
M	18	"	x	x		"	x

Table 6. Fatigue test data

Test #	Panel type	Cyclic Shear Load Amplitude		Crack first observed	Total failure
		kips	% of ultimate static load	@ number of cycles	
7	E	14.00	68.6	not observed	611
8	E	8.46	41.5	4169	4715
14	N	13.65	70.8	1070	1136
15	N	8.34	43.2	4478	5450

Frequency of loading in all tests was 30 cycles/minute.

Table 7.

Web Sheet Thicknesses Measured After Failure.

Panel	Test #	Average	Minimum	Maximum
		(inches)		
A	1	.0288	.0260	.0301
B	2	.0103	.0100	.0108
C	3	.0046	.0030	.0052
D	4	.0289	.0281	.0290
E	5	.0096	.0084	.0104
F	6	.0048	--	--
G	9	.0280	.0272	.0292
H	10	.0100	.0090	.0108
I	11	.0046	.0040	.0051
J	17	.0280	.0260	.0291
K	13	.0290	.0260	.0295
L	12	.0090	.0081	.0100
M	18	.0096	.0080	.0103
N	16	.0090	.0085	.0101
E	7	.0106	.0100	.0109
E	8	.0105	.0098	.0110
N	14	.0100	.0090	.0108
N	15	.0091	.0090	.0100

FIGURES

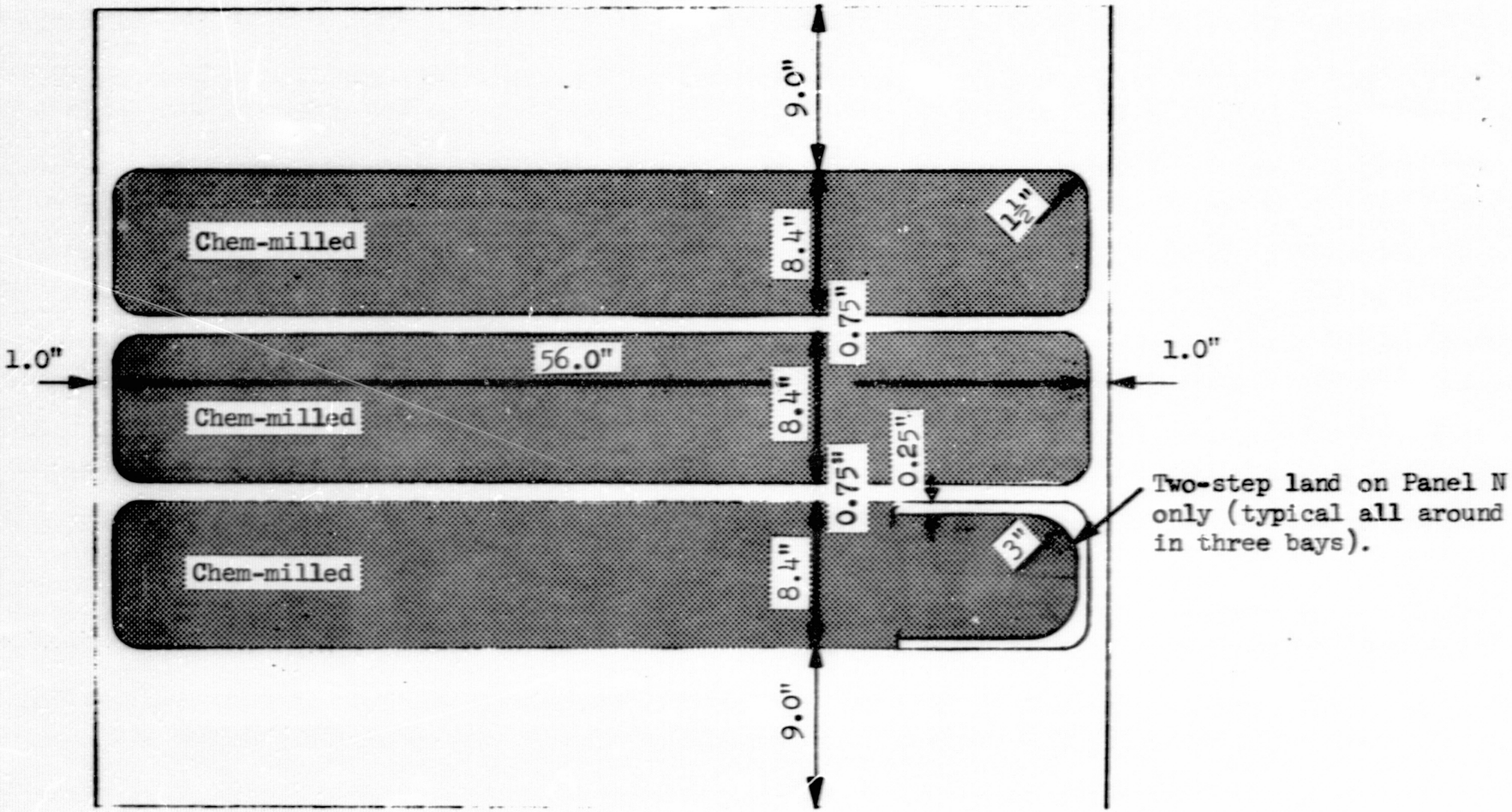

Figure 1. Chem-milled web sheet.

Grumman

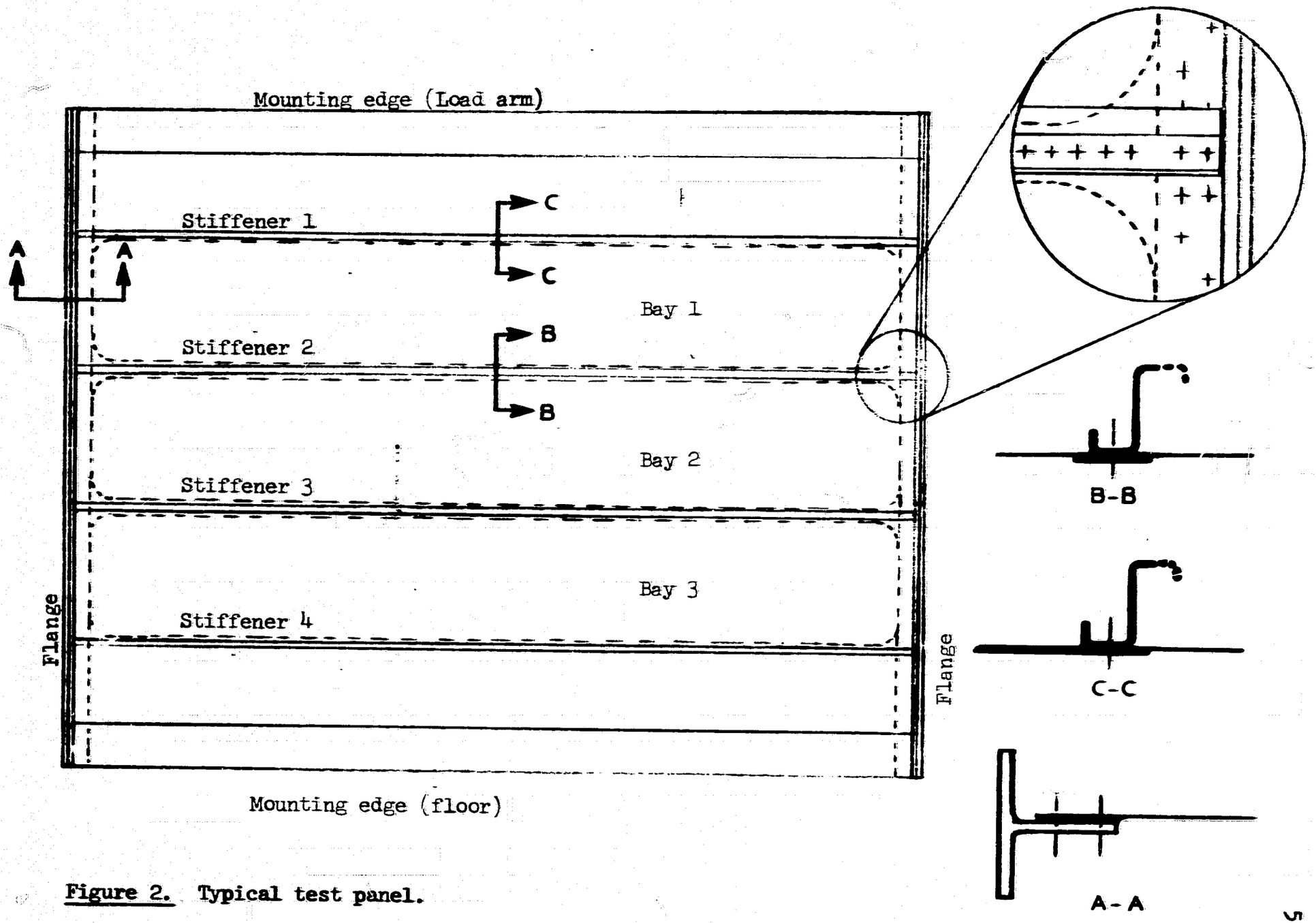

Figure 2. Typical test panel.

Grumman

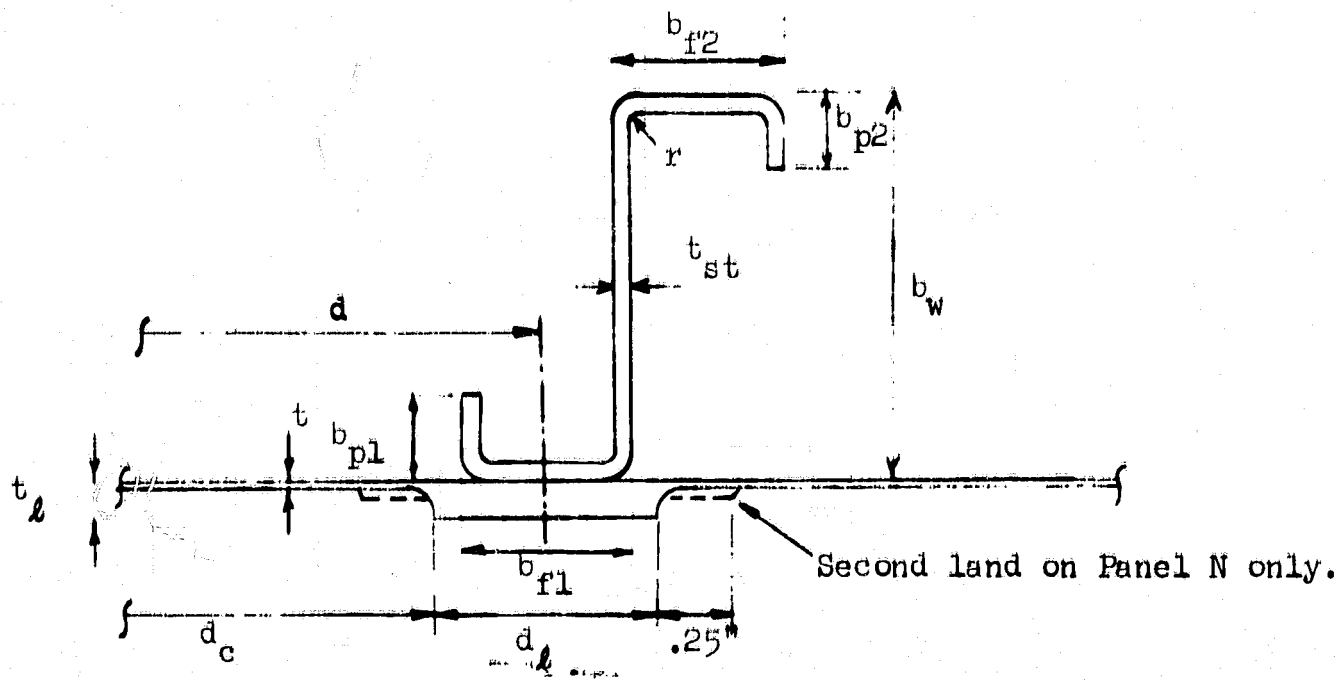

a.) Stiffener dimensions

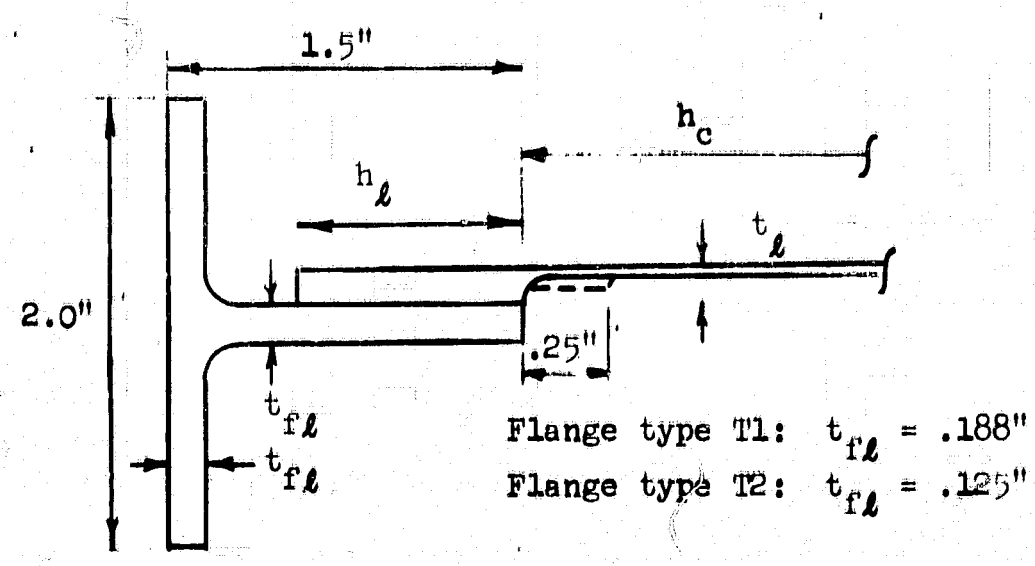

b.) Flange dimensions.

Figure 3. Dimension symbols for stiffener and flange sections.

1. Test panel
2. Tie-down to floor
3. Loading arm
4. Counter weight for loading arm
5. Lateral support for loading arm
6. Lateral supports for test panel

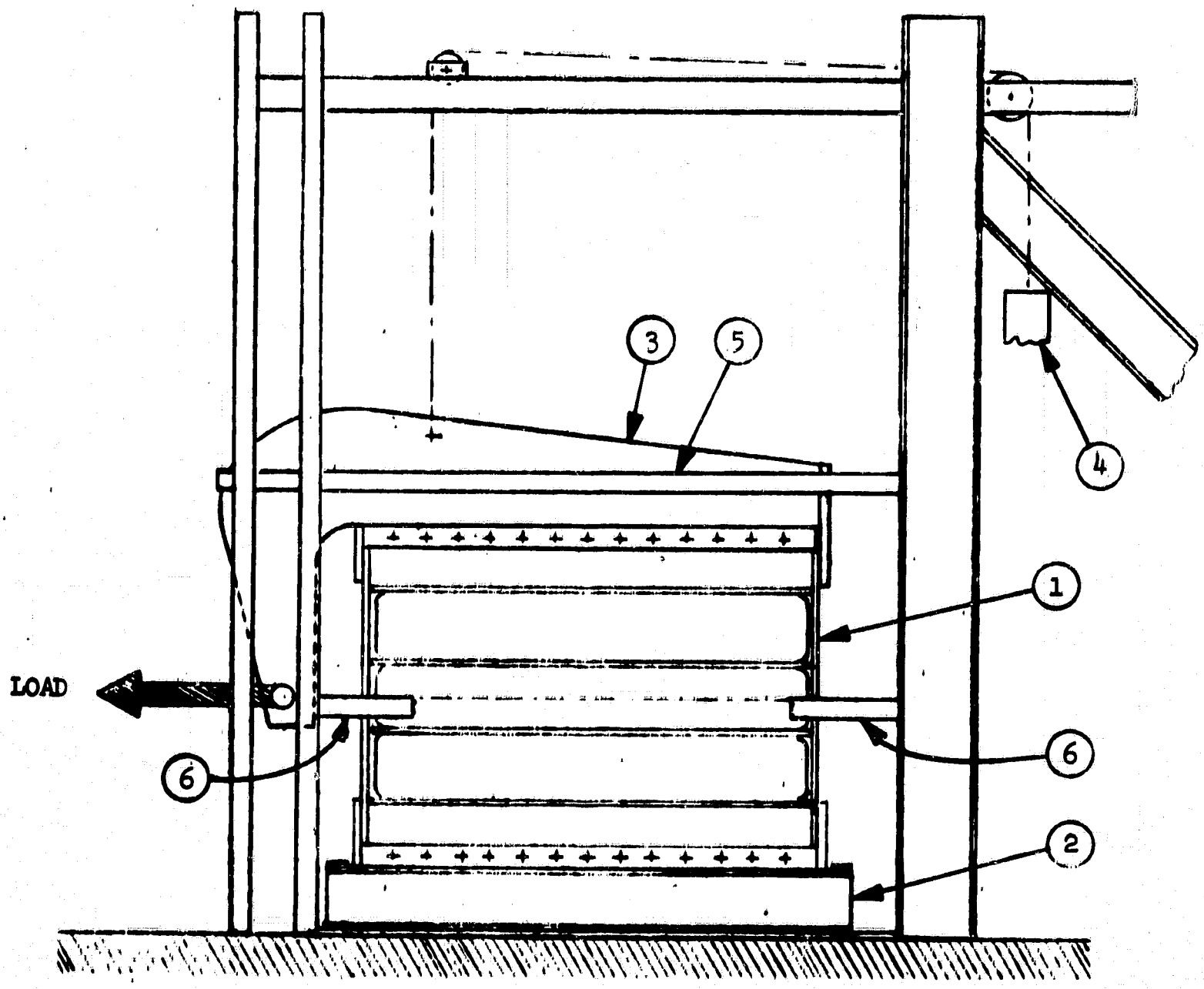

Figure 4. Schematic drawing of test setup.

$$\frac{F_{s\ all}}{F_{ty}} = 0.9\left[1 + \frac{1}{2}\left(\frac{F_{tu}}{F_{ty}} - 1\right)^2\right]\cdot\left[\frac{1}{2} + (1 - k)^3\left(\frac{F_{su}}{F_{tu}} - \frac{1}{2}\right)\right]$$

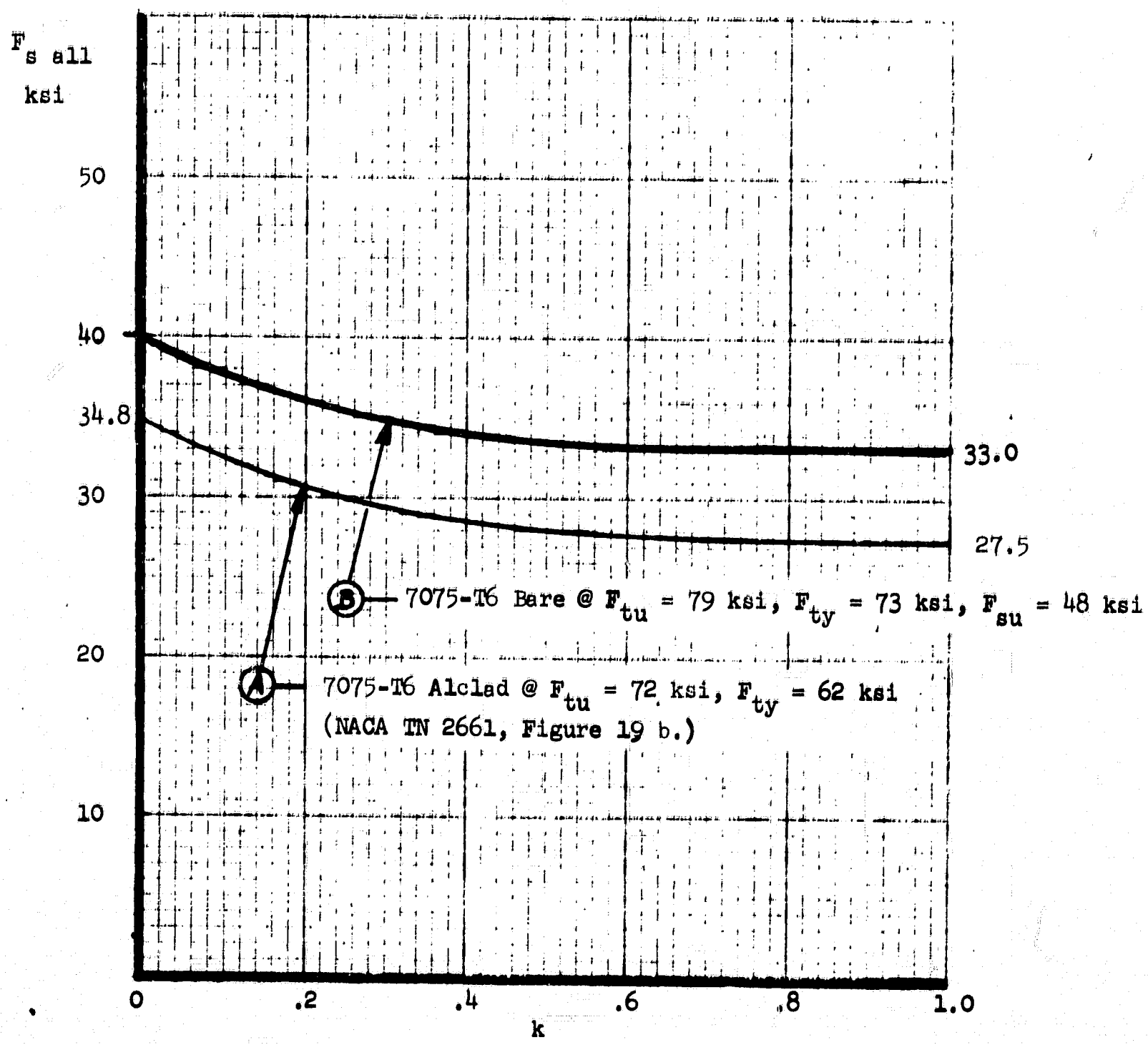

Figure 5. Allowable stress curve for web sheet failure. (Recommended.)

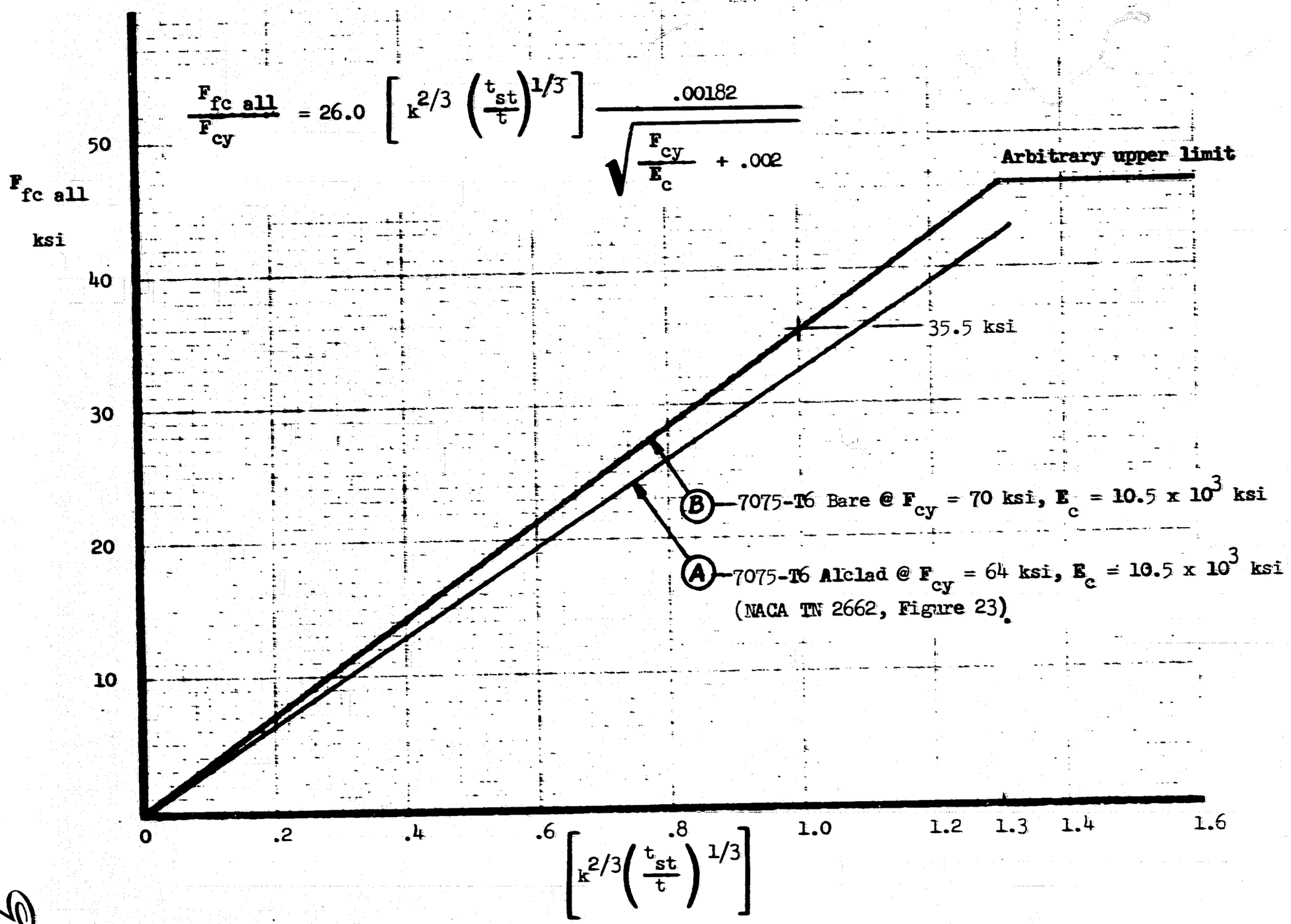

Figure 6. Allowable stress curve for stiffener local failure.

Grumman

NOTE: ⊗ = Predicted to fail in the sheet but actually failed locally in the stiffener.

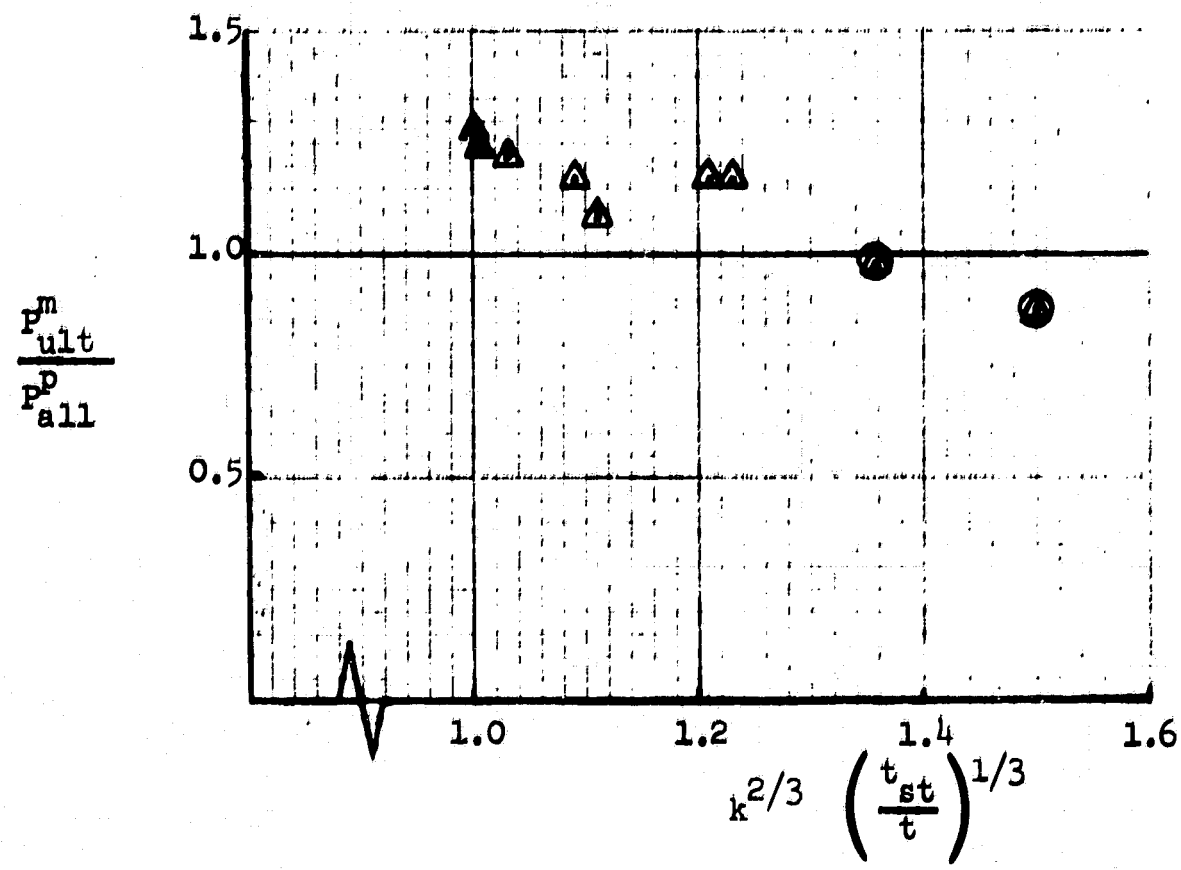

b) Stiffener local failures.

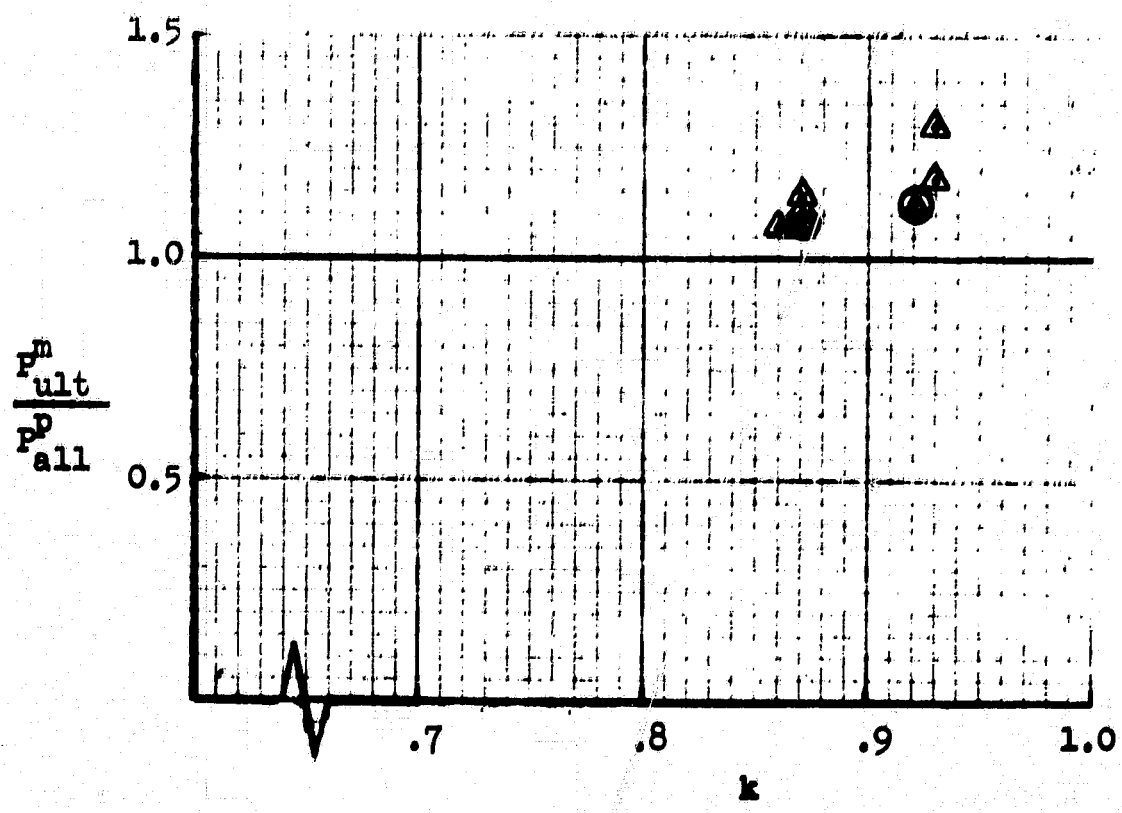

a) Sheet failures.

Figure 7. Conservatism of NACA allowables.

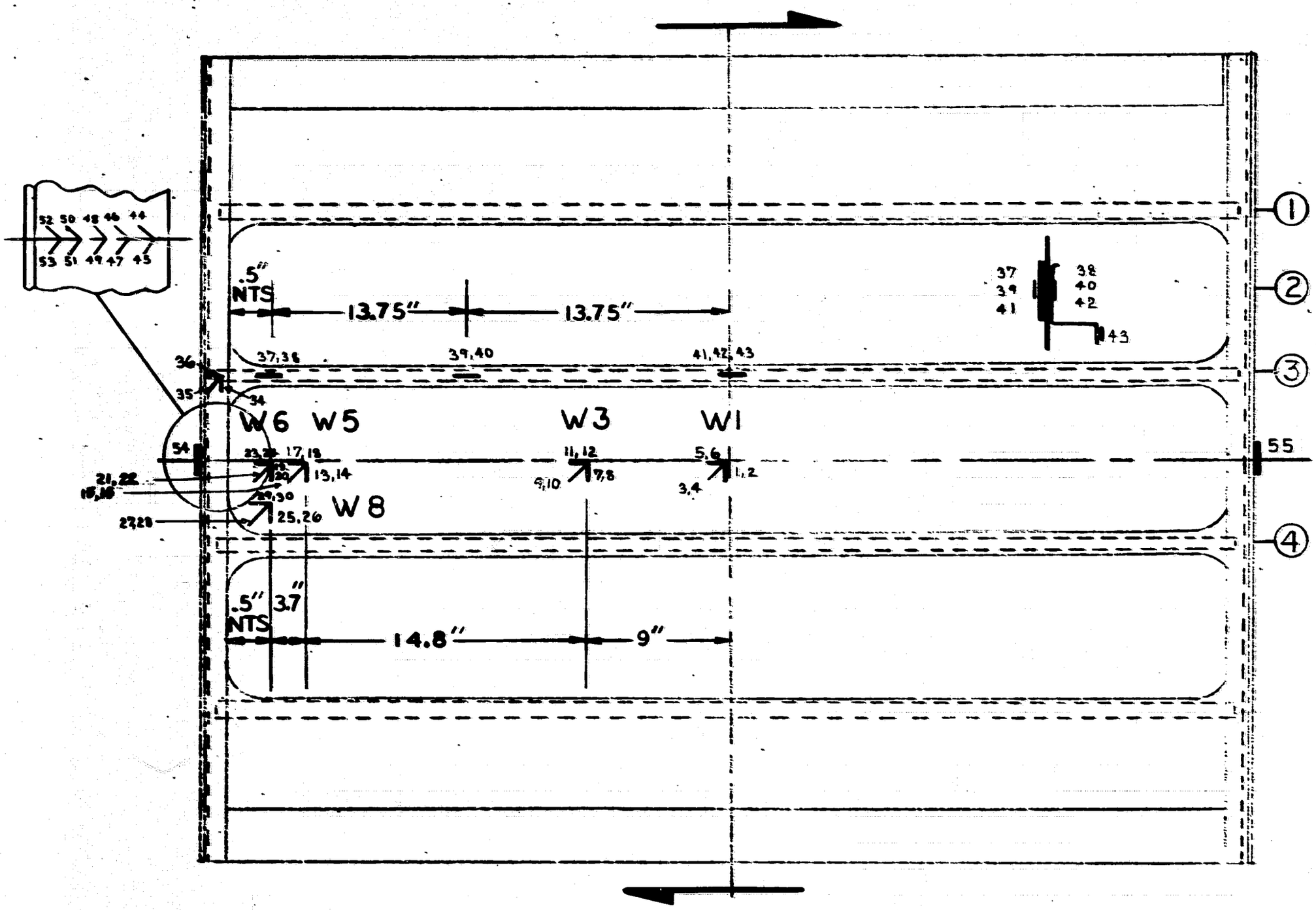

Figure 8a. Strain and dial gage numbers in Tests 1 through 5.
(Gages #54 and 55 not used in Test #5)

Grumman

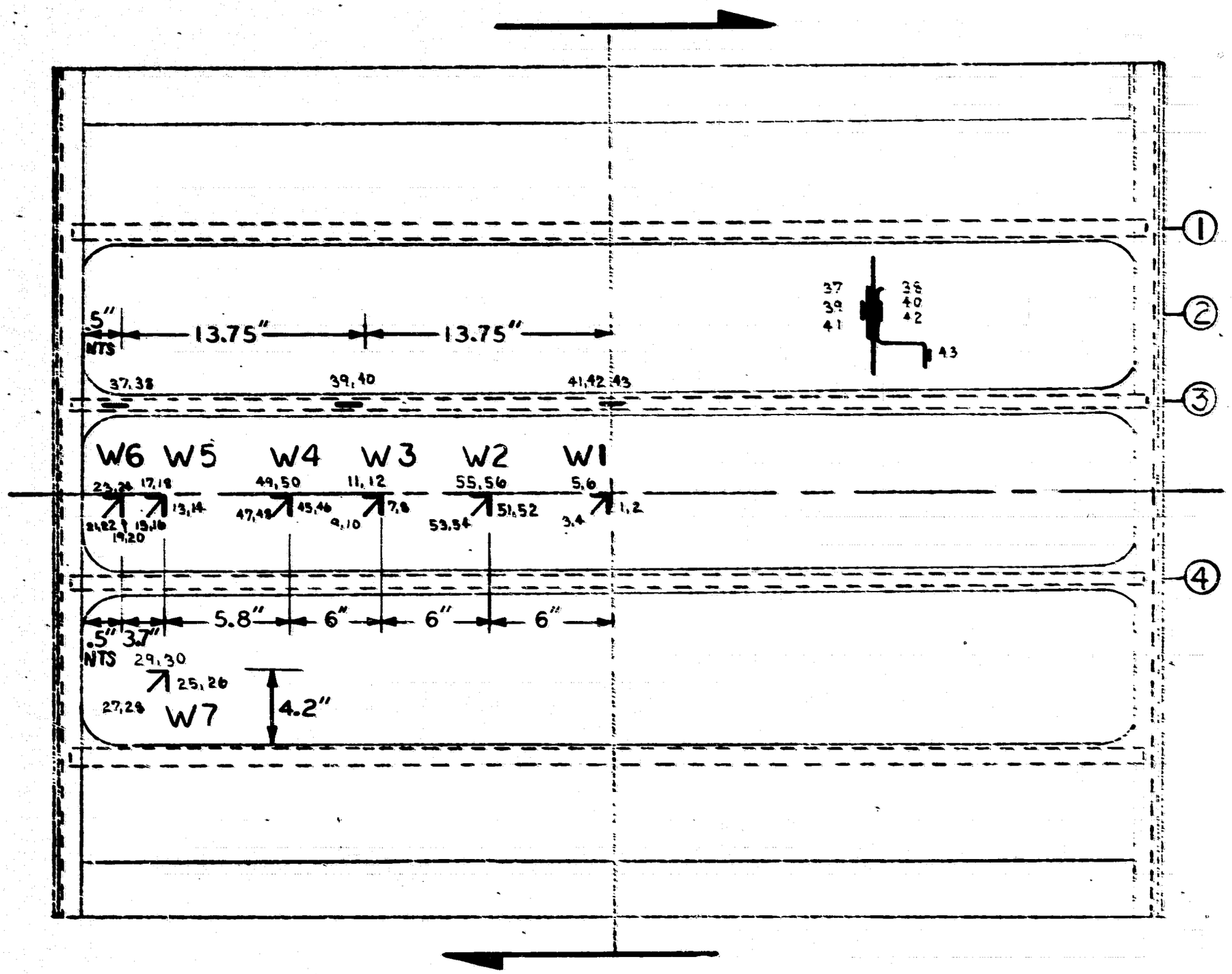

Figure 8b. Strain and dial gage numbers in static Tests #6 and up.

Grumman

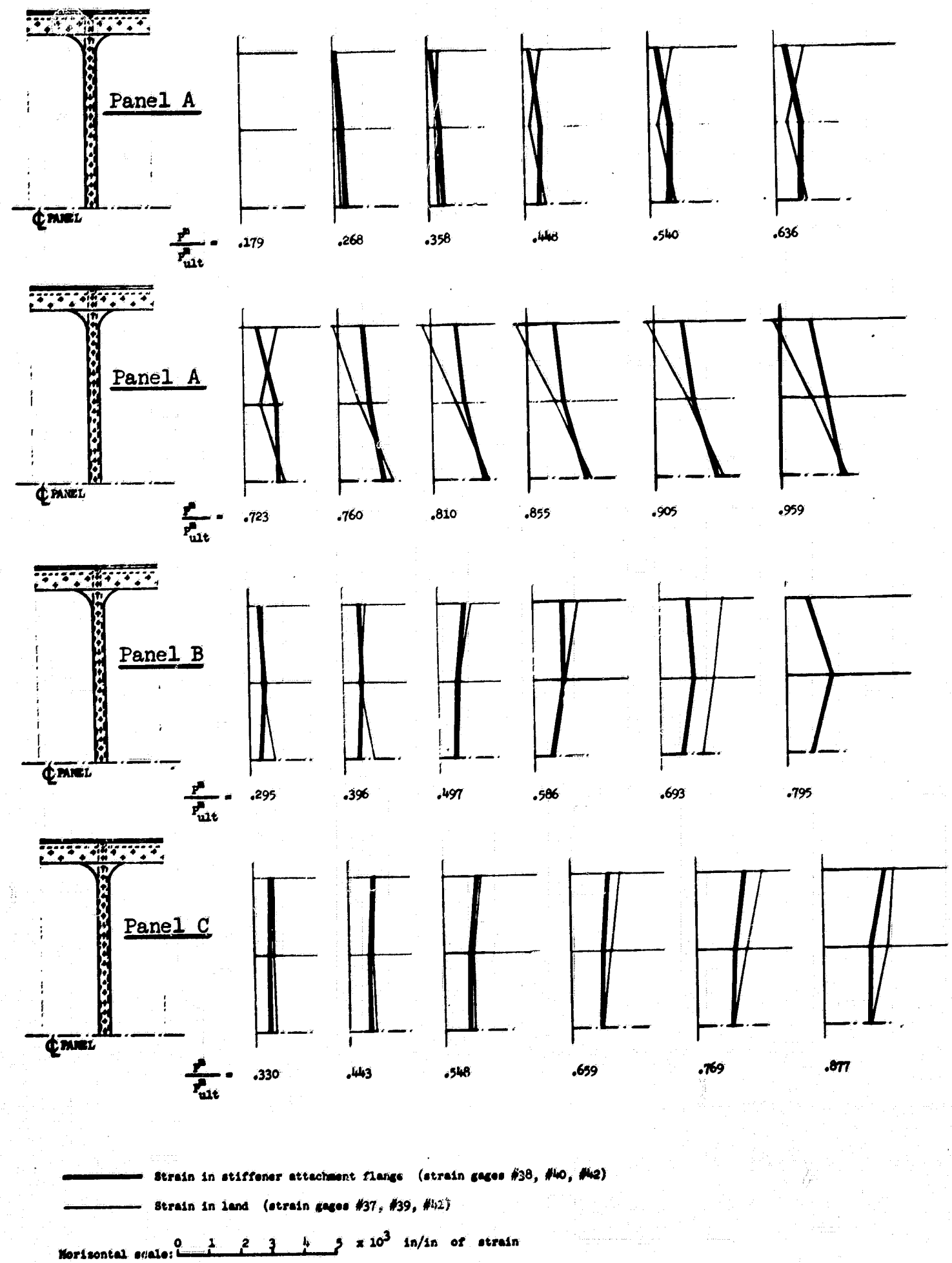

Figure 9. Measured compressive strain along the length of stiffeners.

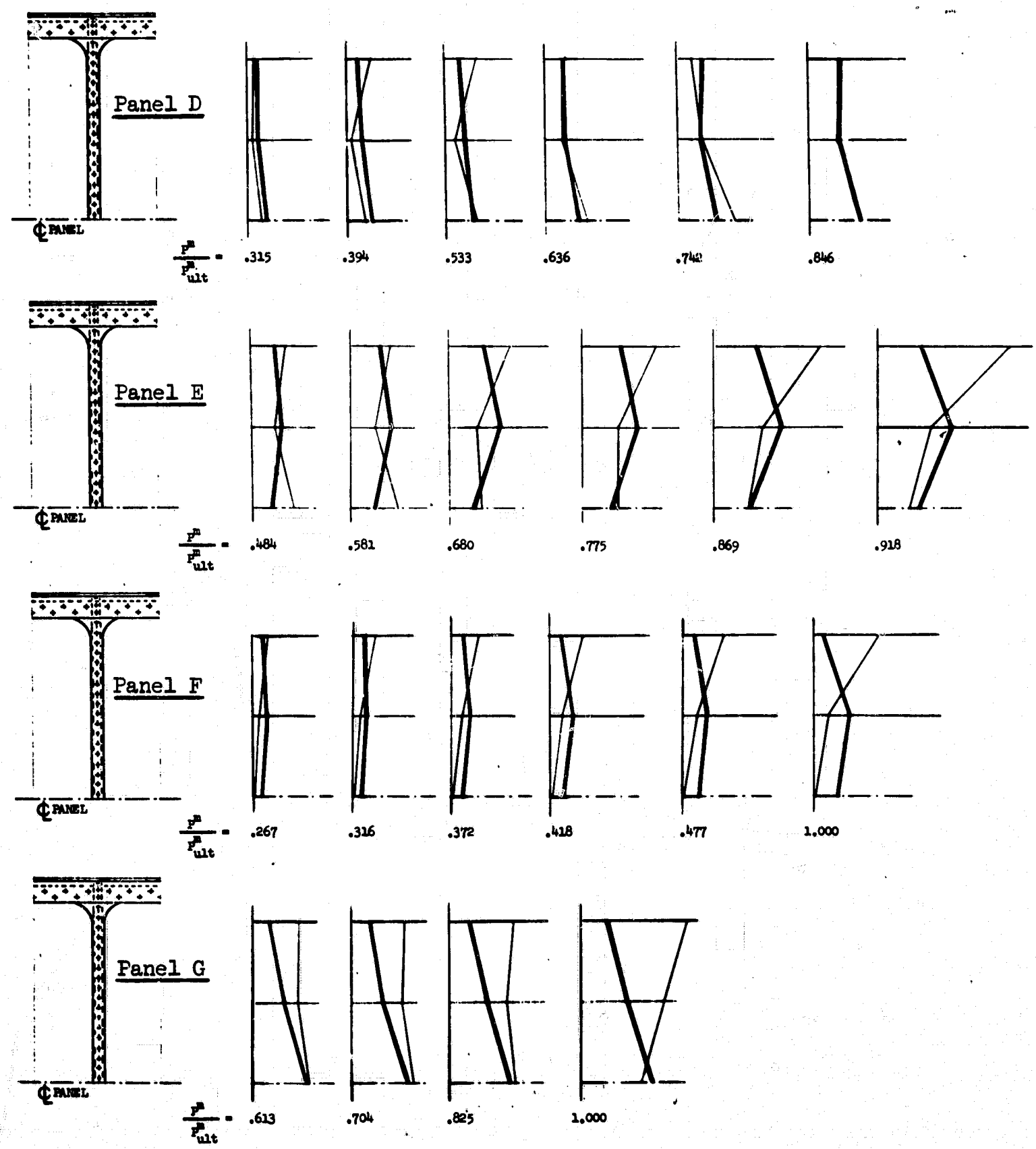

Figure 9. Continued

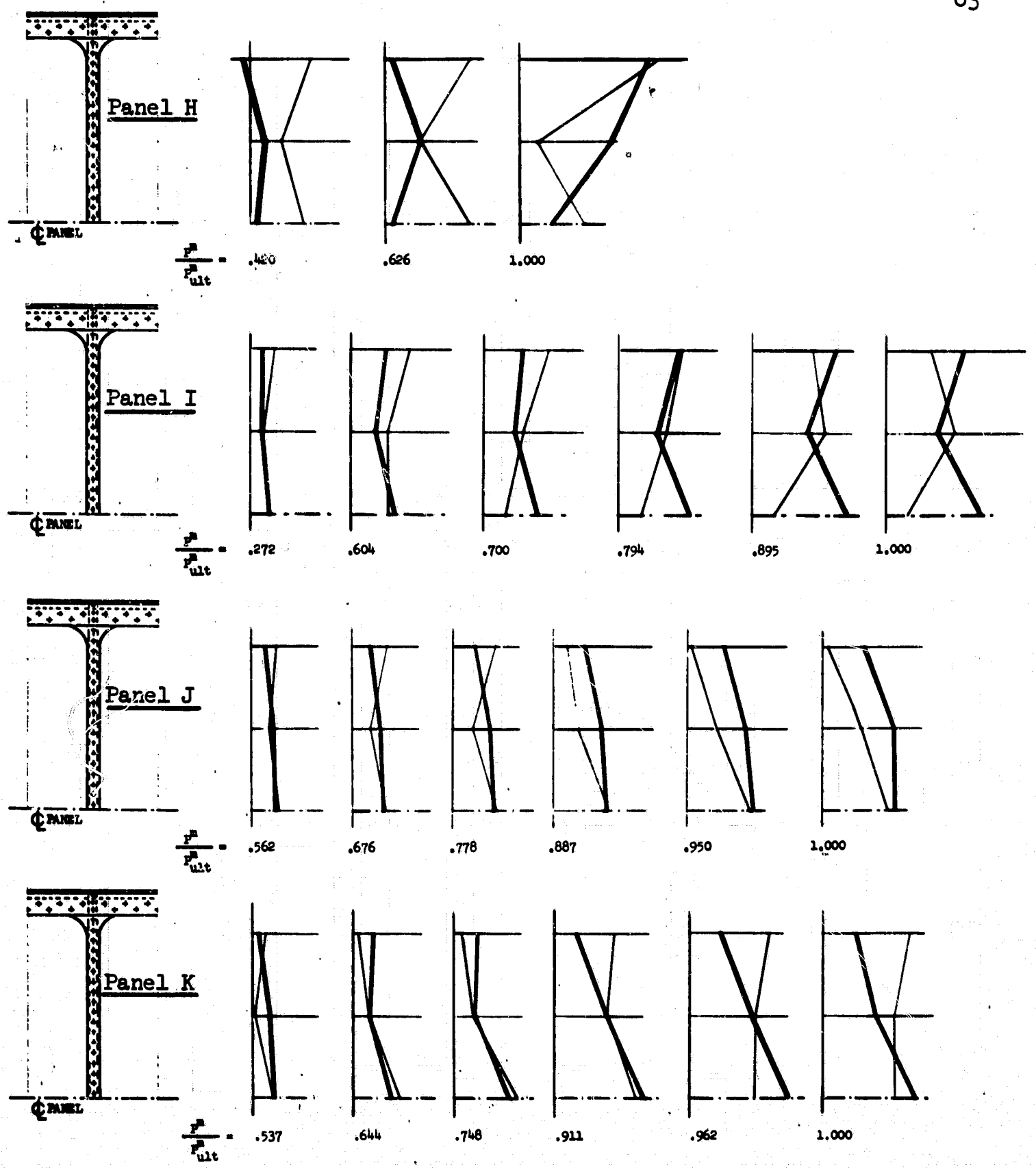

Figure 9. Continued

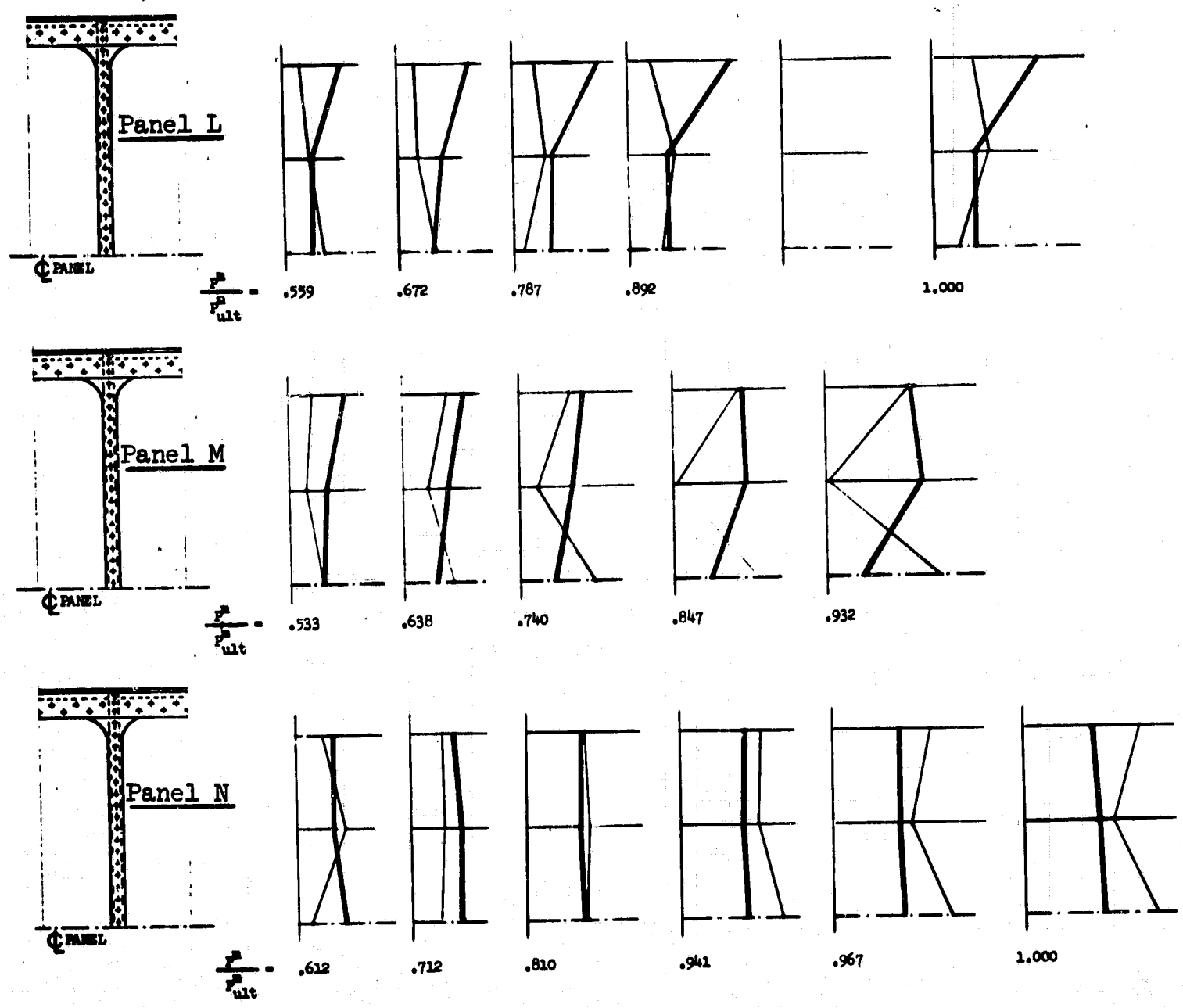

Strain in stiffener attachment flange (strain gages #38, #40, #42)

Strain in land (strain gages #37, #39, #41)

Horizontal scale: 0 1 2 3 4 5 x 10^3 in/in of strain

Figure 9. Continued

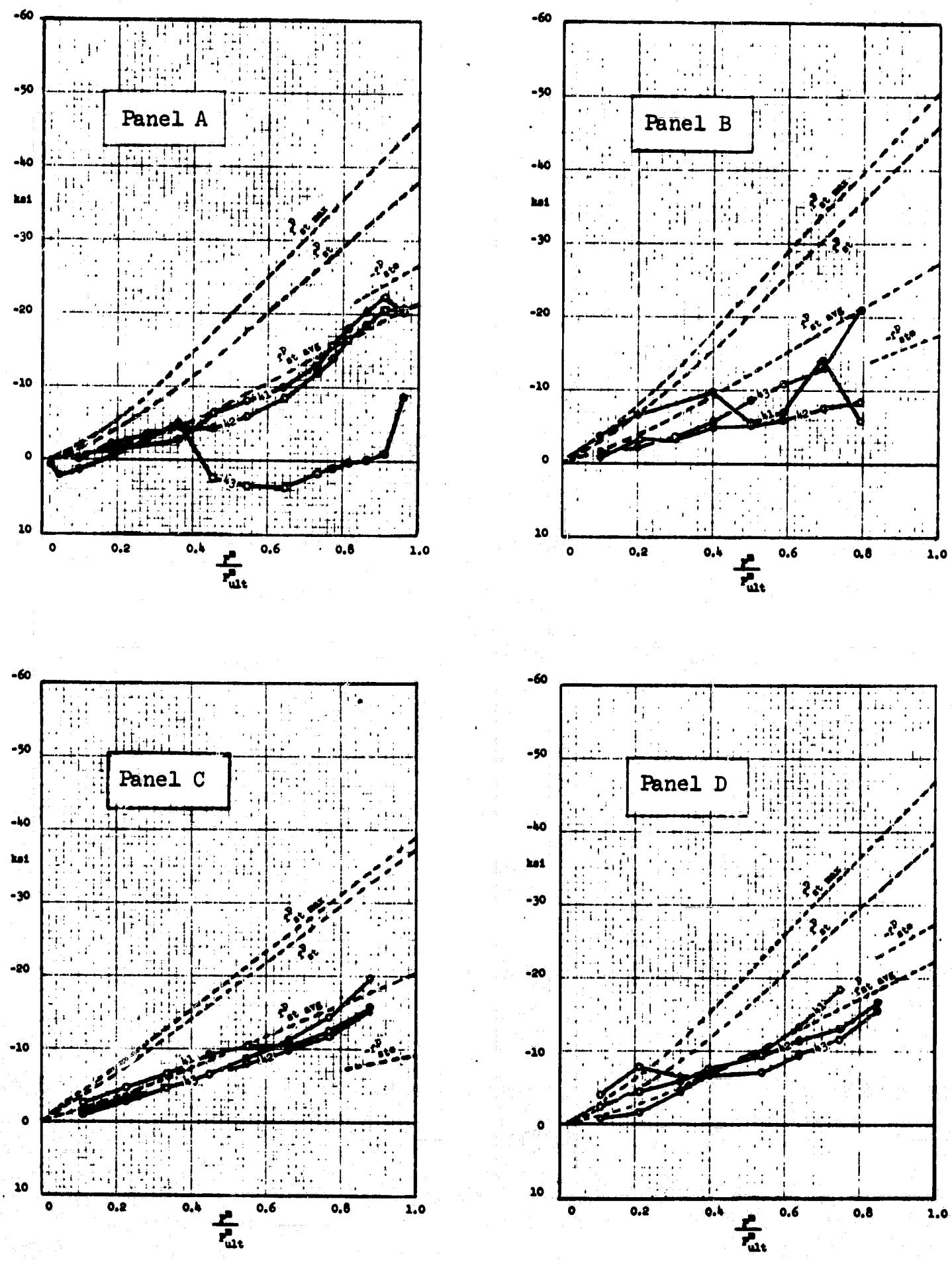

Figure 10. Measured and computed longitudinal stresses at mid-length of stiffener.

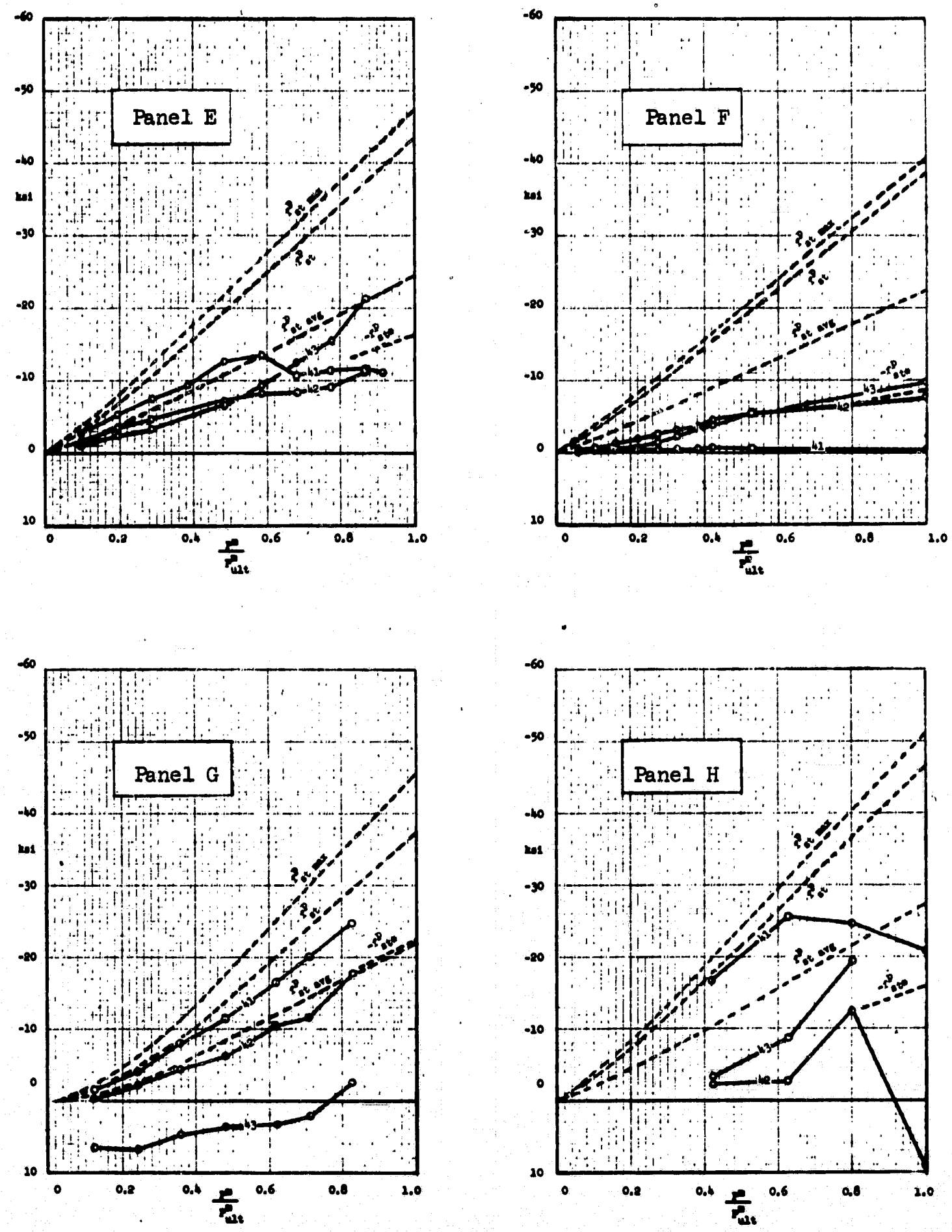

Figure 10. Continued.

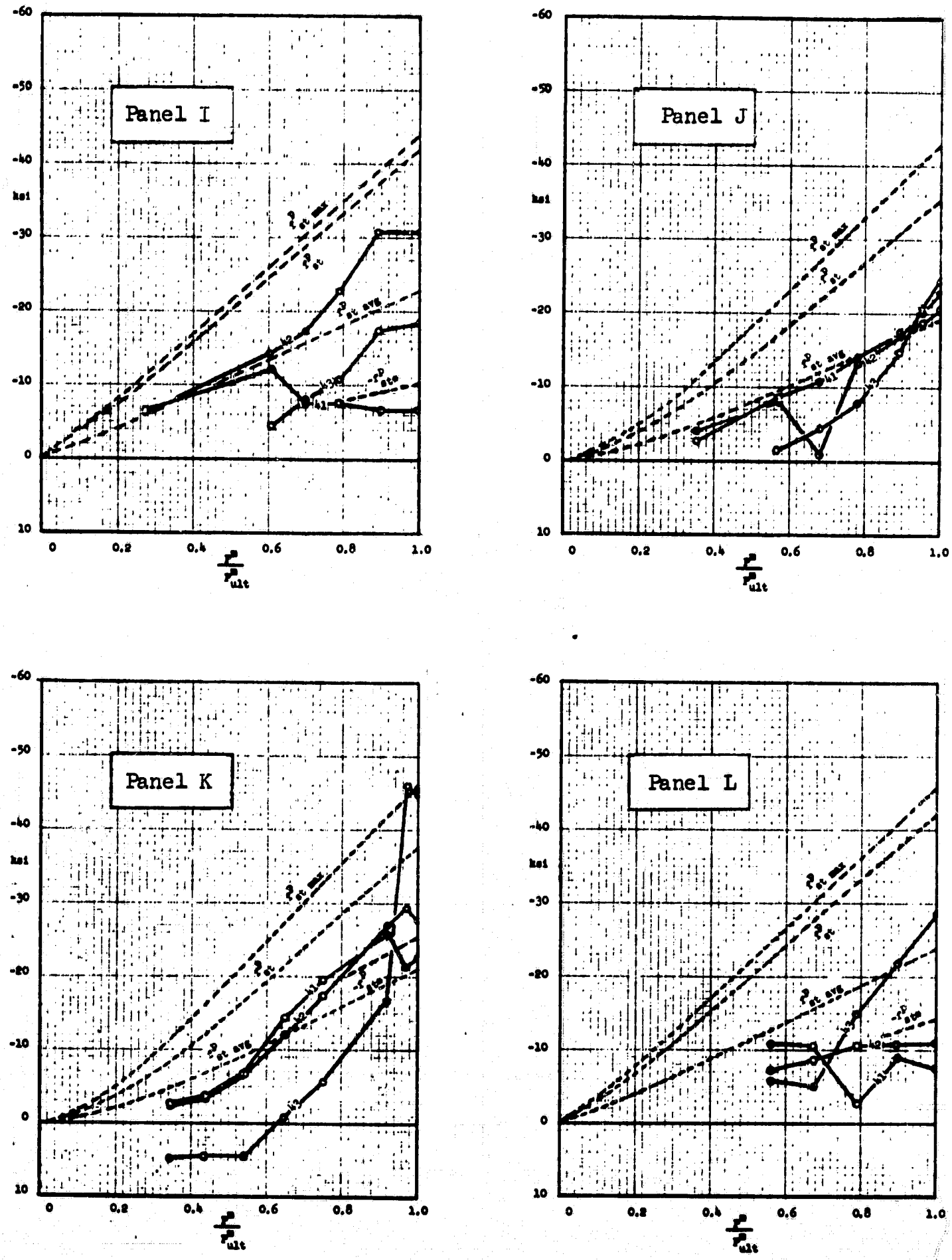

Figure 10. Continued.

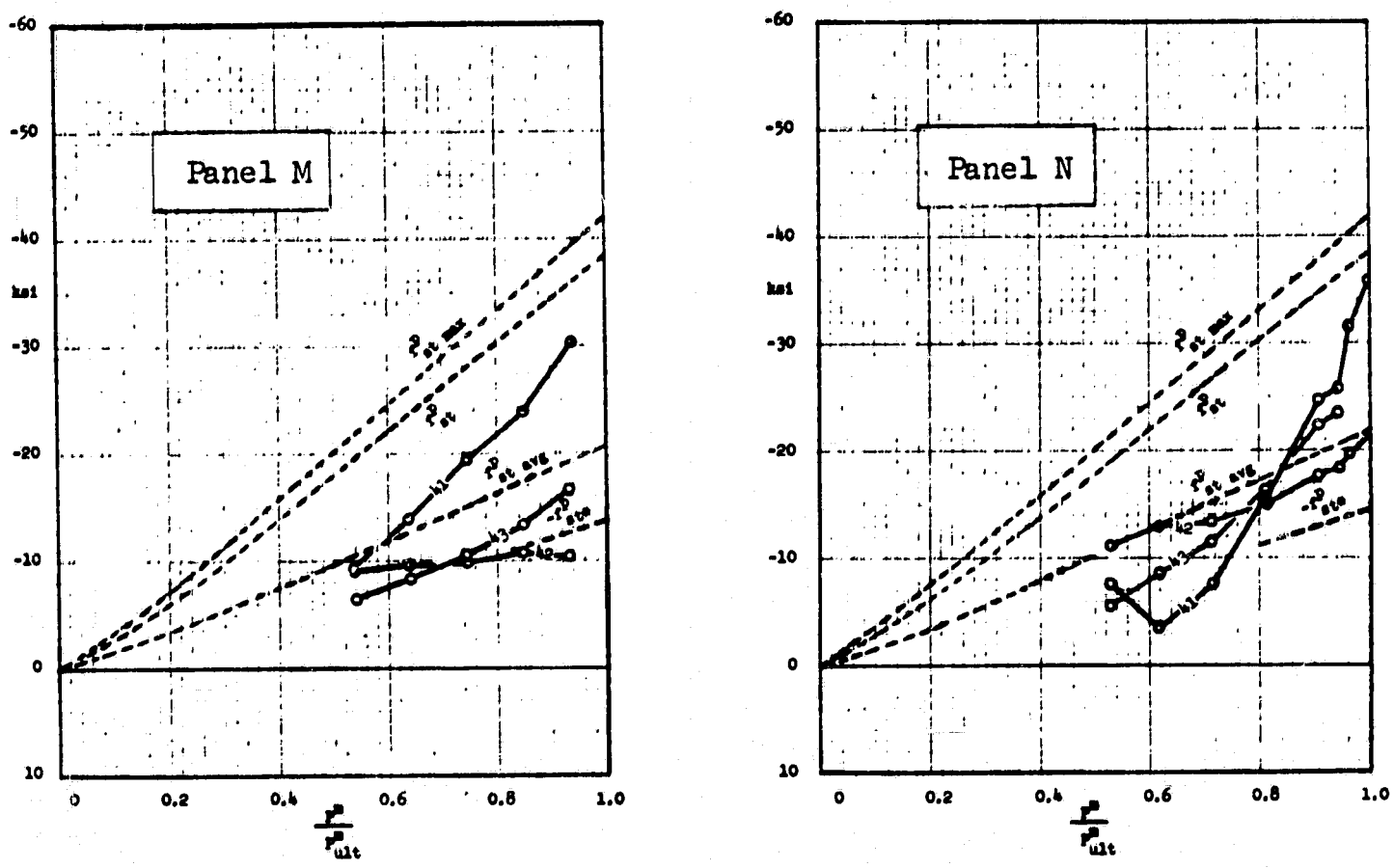

Figure 10. Continued.

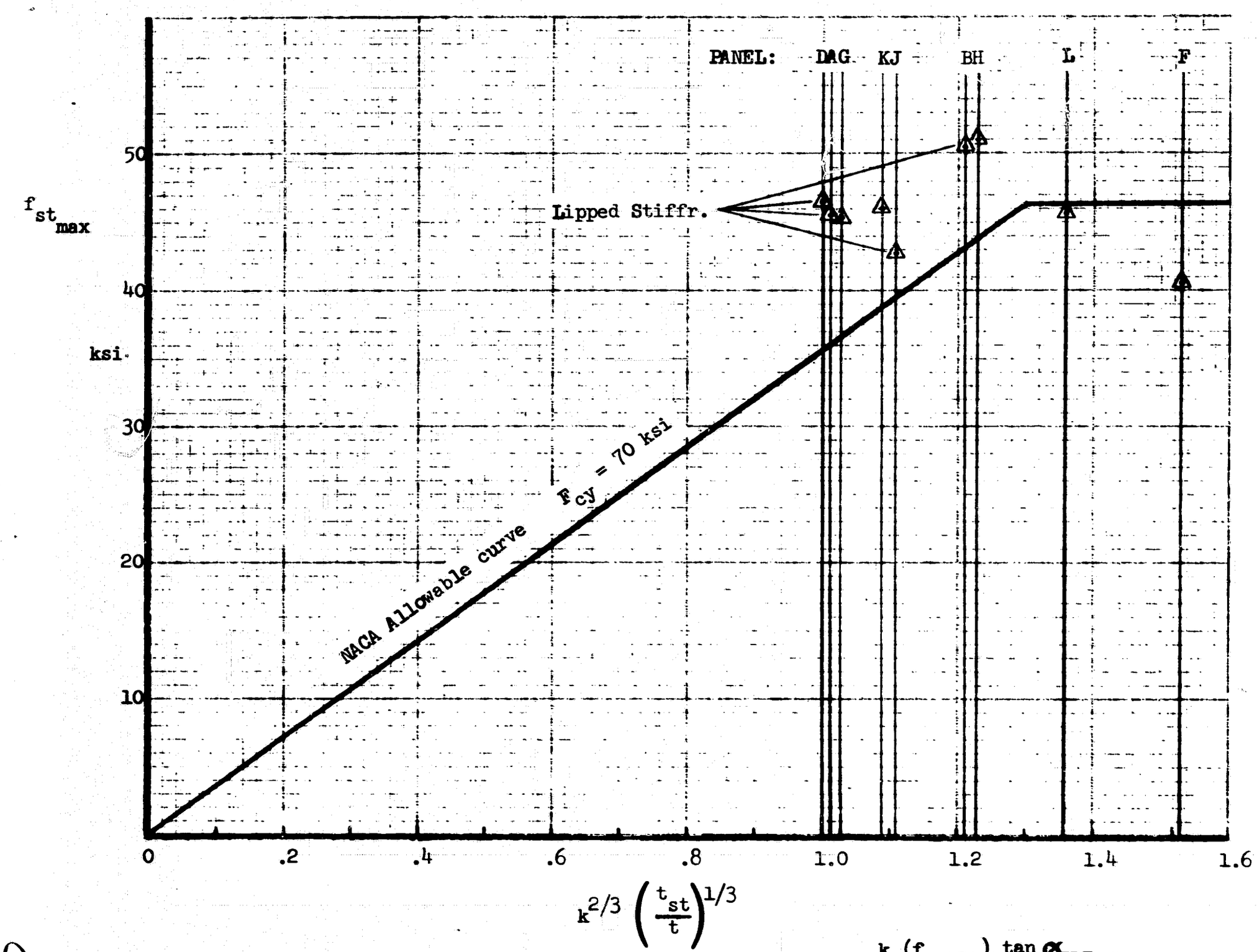

Figure 11. Computed stiffener stress at local failure: $f^{ct}_{st\ max} = \dfrac{k\,(f_{s\ ult})\tan\alpha_{IDT}}{\dfrac{A'_{st\ e}}{d_c t} + 0.5(1-k)}$

Grumman

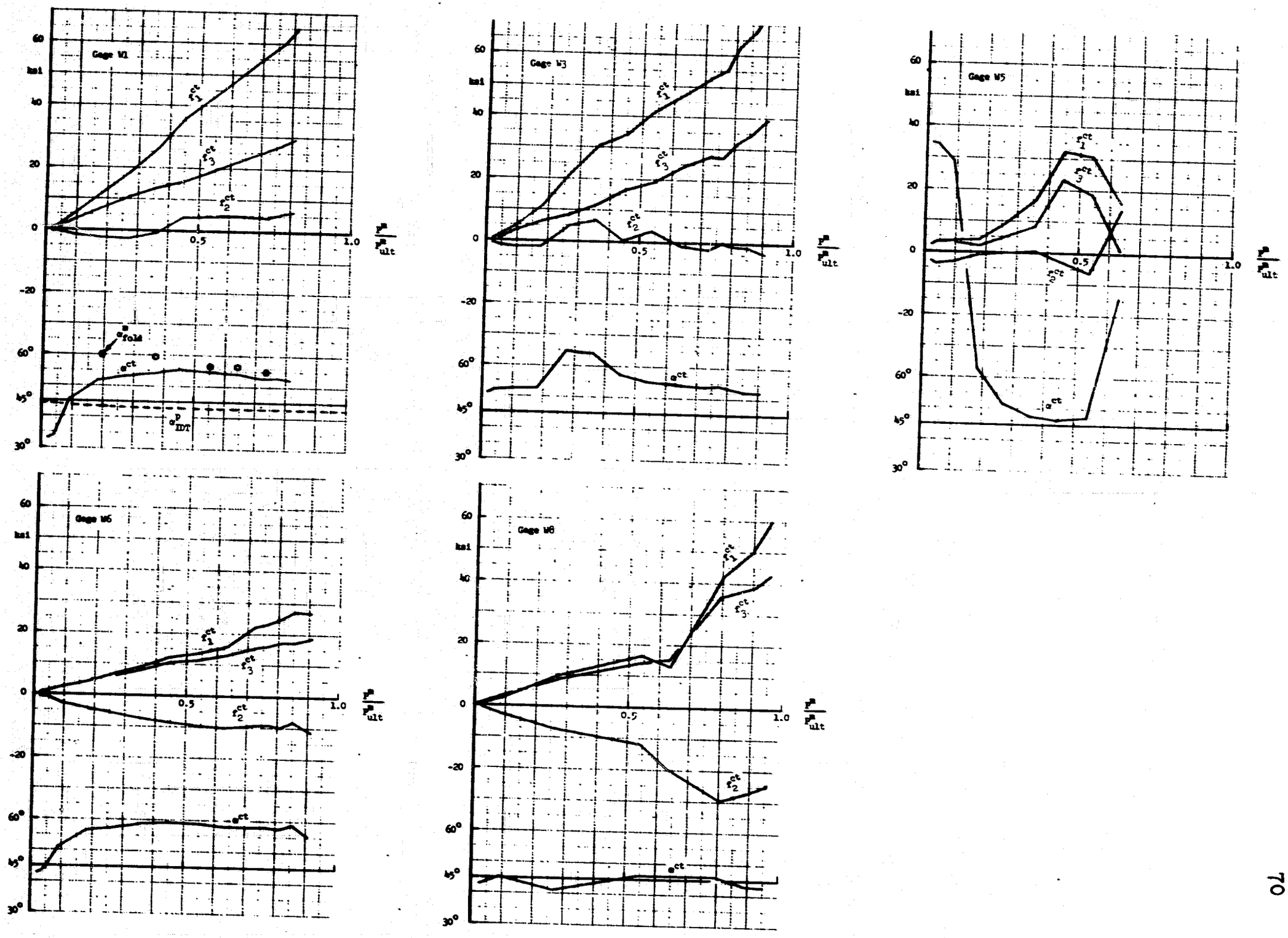

Figure 12. Magnitude and direction of principal stresses in the web sheet computed from strain gage measurements.

Panel A

Grumman

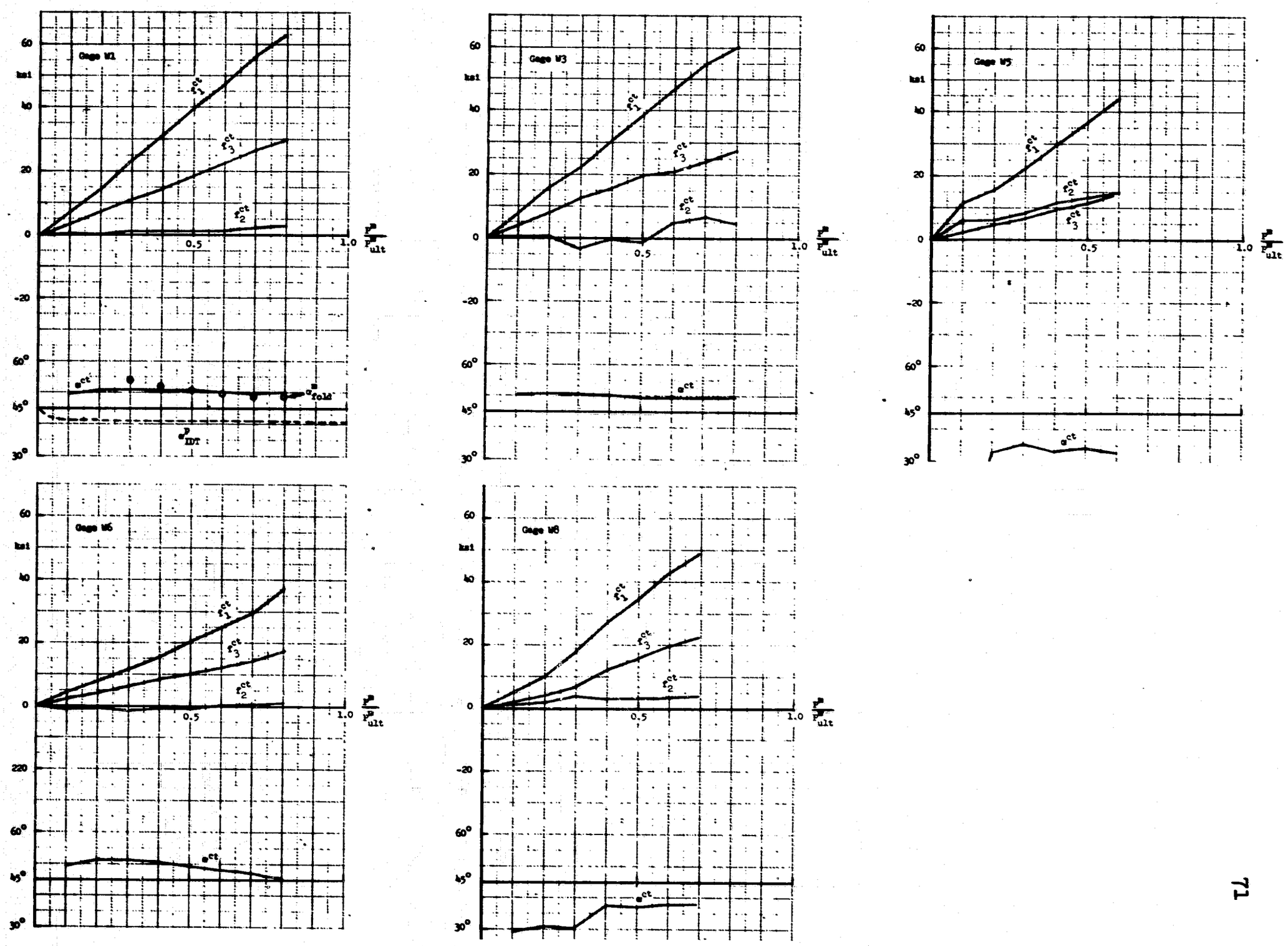

Figure 12. Continued.

Panel B

Grumman

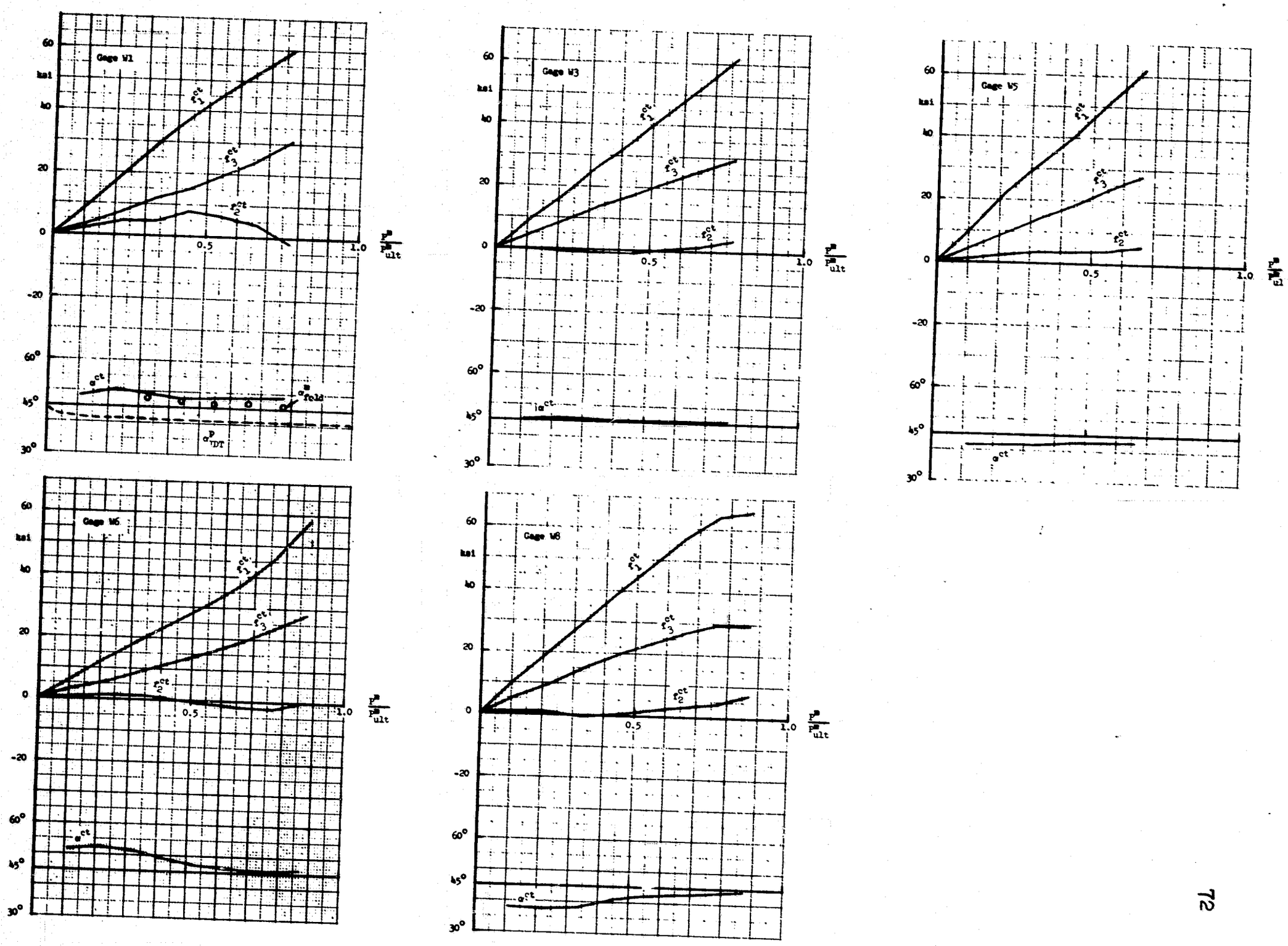

Figure 12. Continued.

Panel C.

Grumman

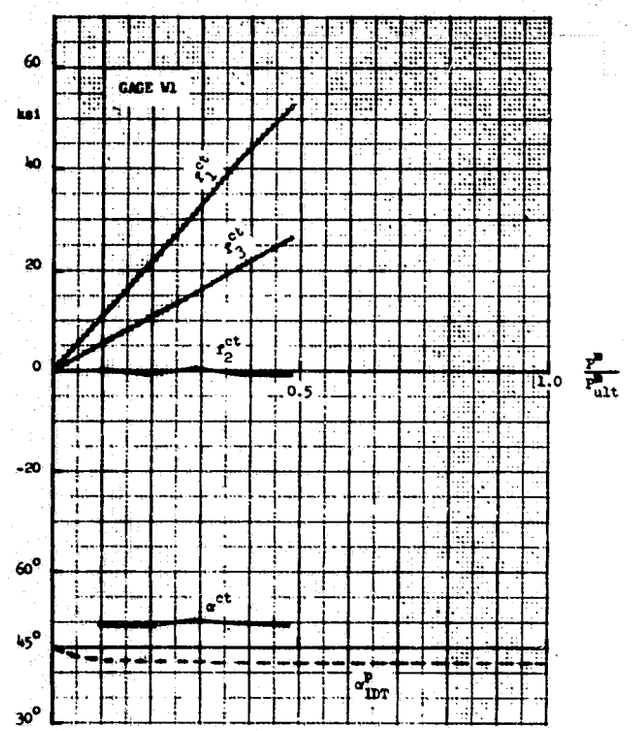

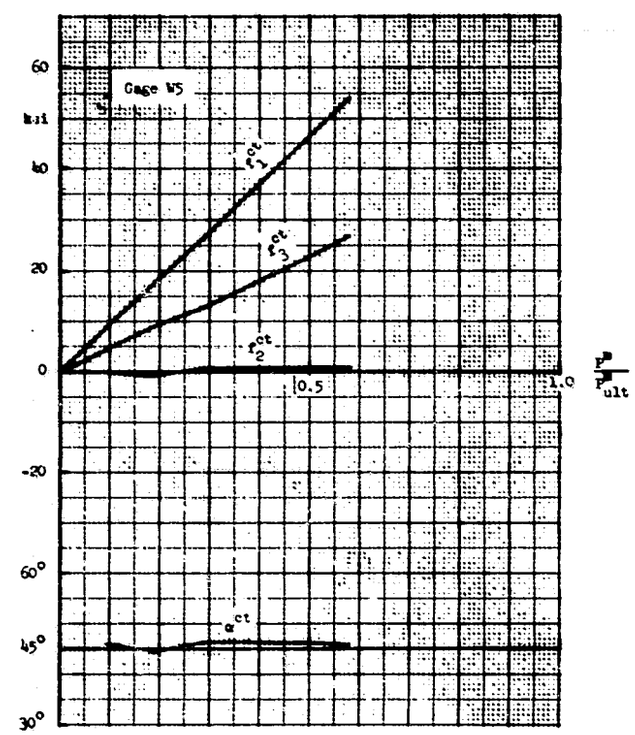

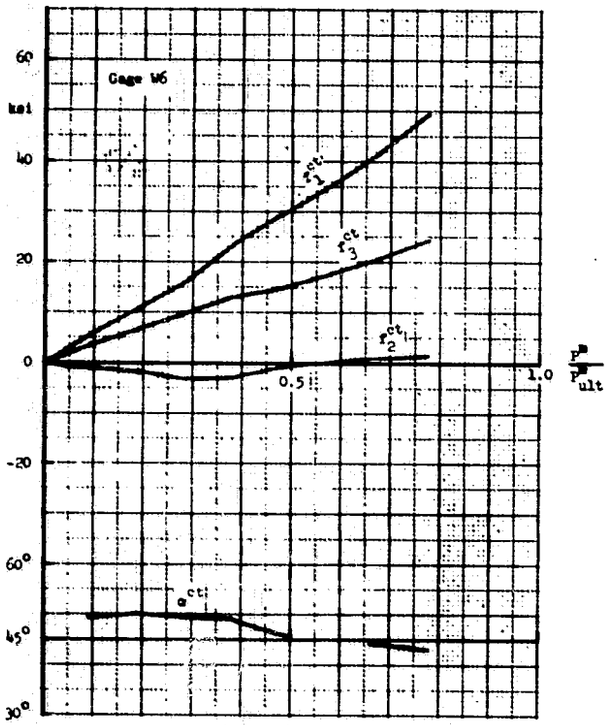

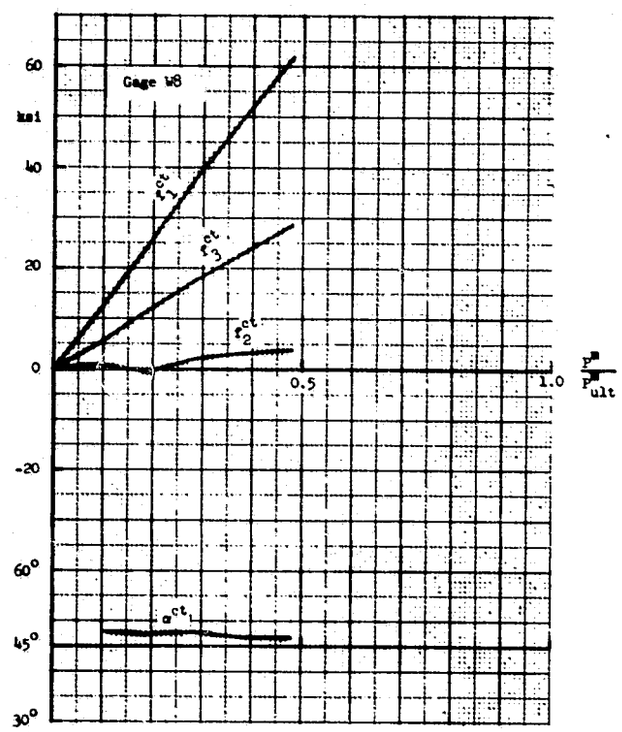

Figure 12. Continued.

Panel E

Grumman

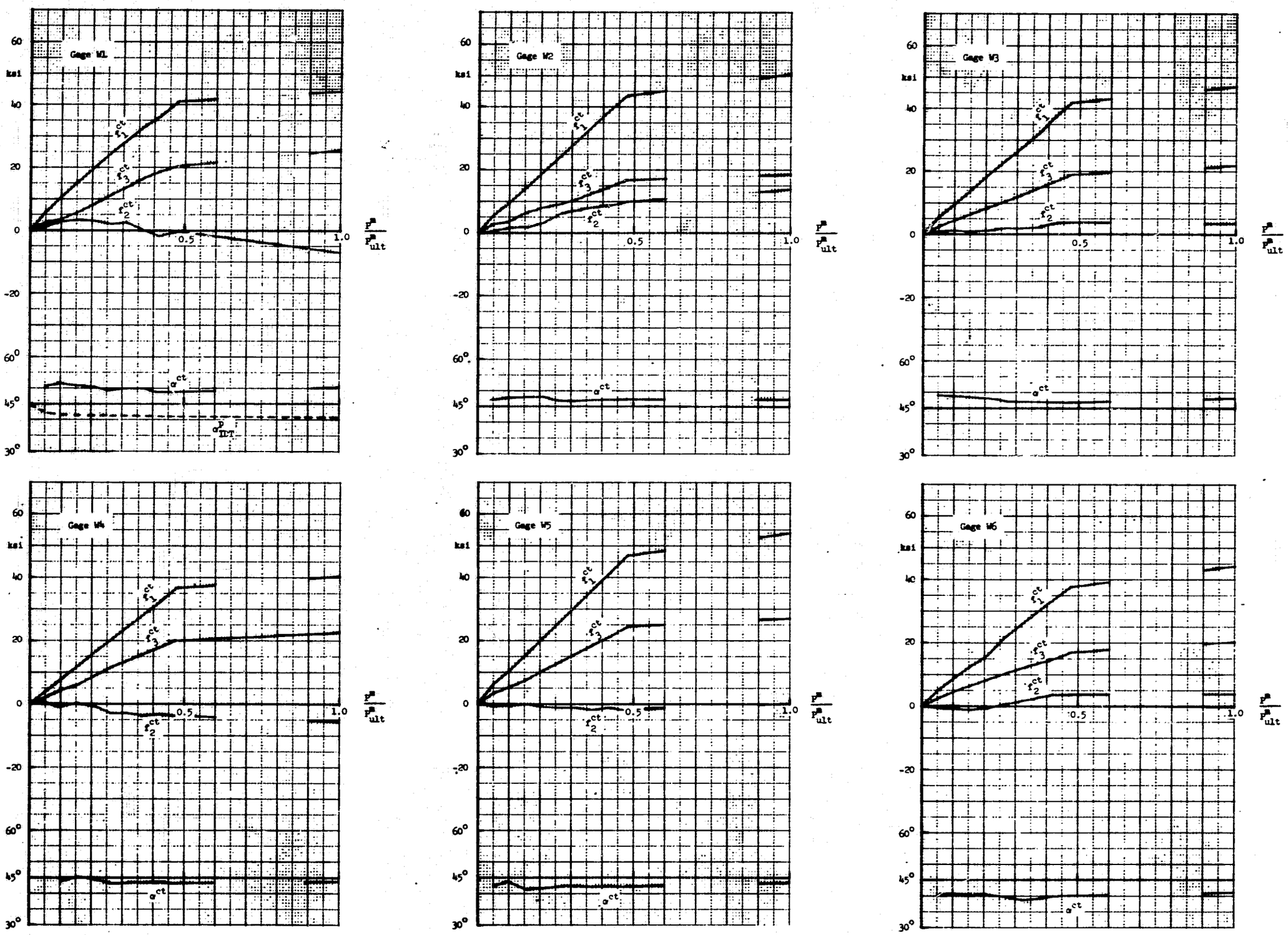

Figure 12. Continued.

Panel F

Grumman

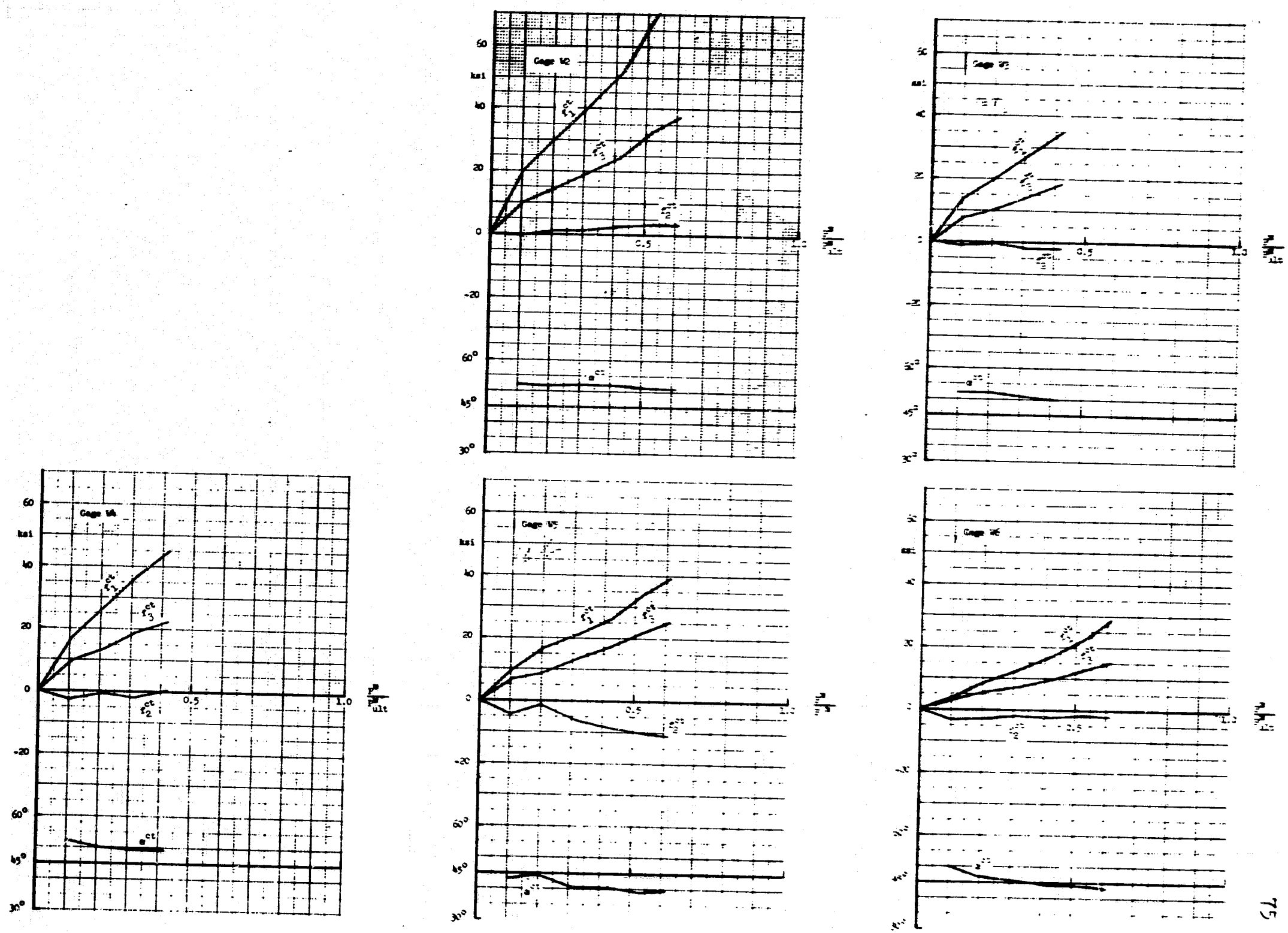

Figure 12. Continued.

Panel N

Grumman

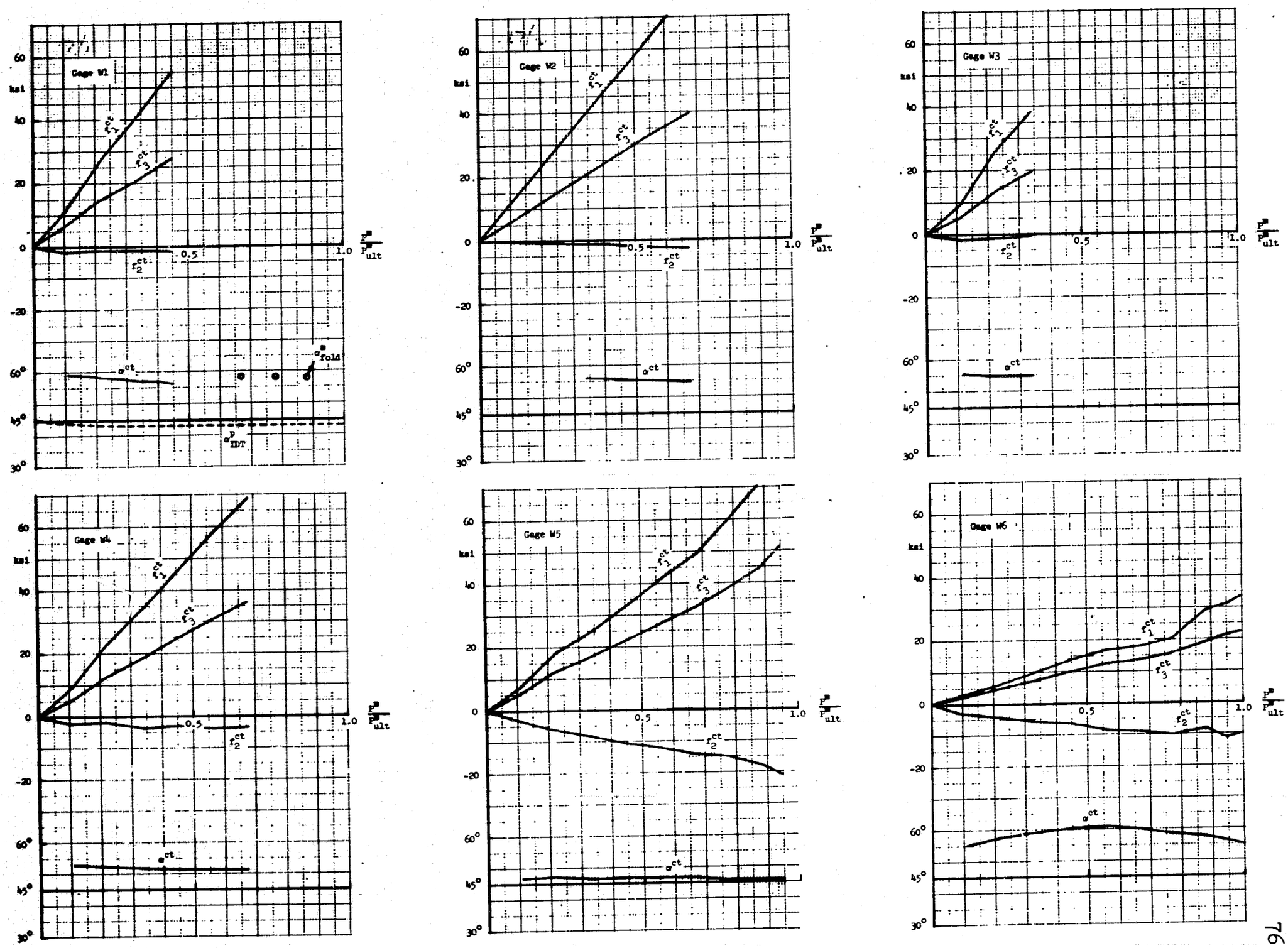

Figure 12. Continued.

Panel J

Grumman

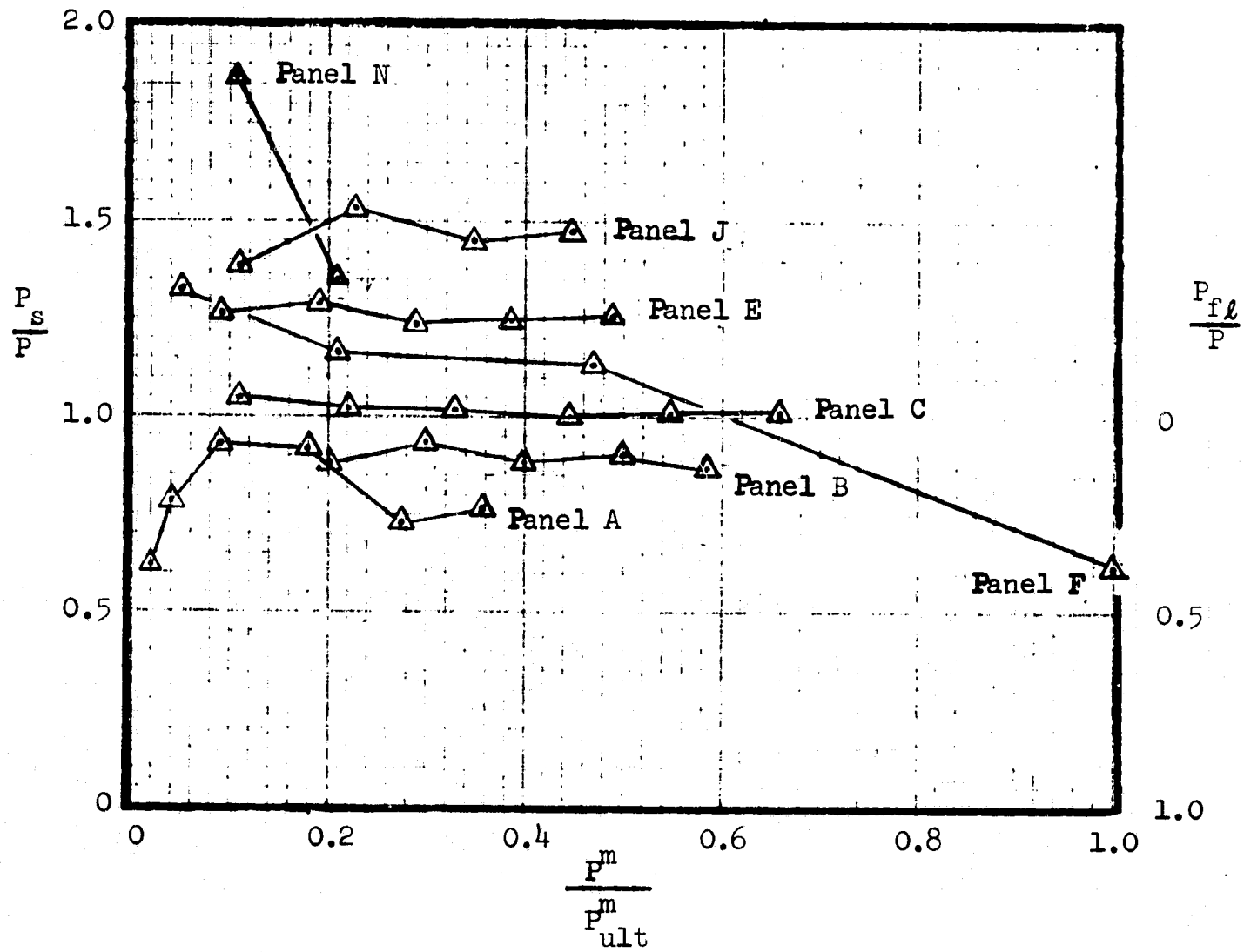

Figure 13. Portions of applied load carried by web sheet, P_s, and flanges, $P_{f\ell}$; computed from strain gage measurements.

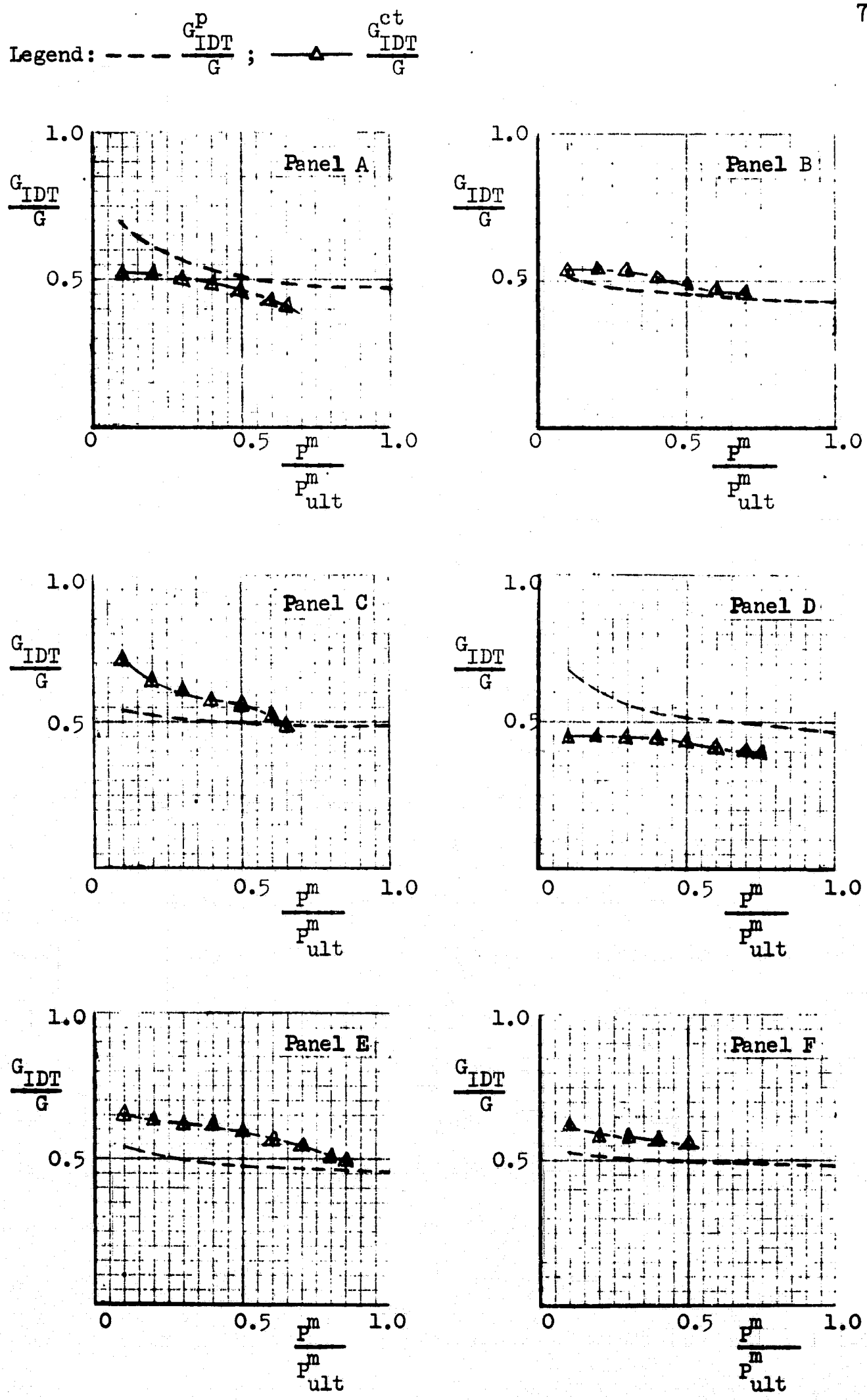

Figure 14. Equivalent shear modulus.

Legend: - - - - $\frac{G^{p}_{IDT}}{G}$; —△— $\frac{G^{ct}_{IDT}}{G}$

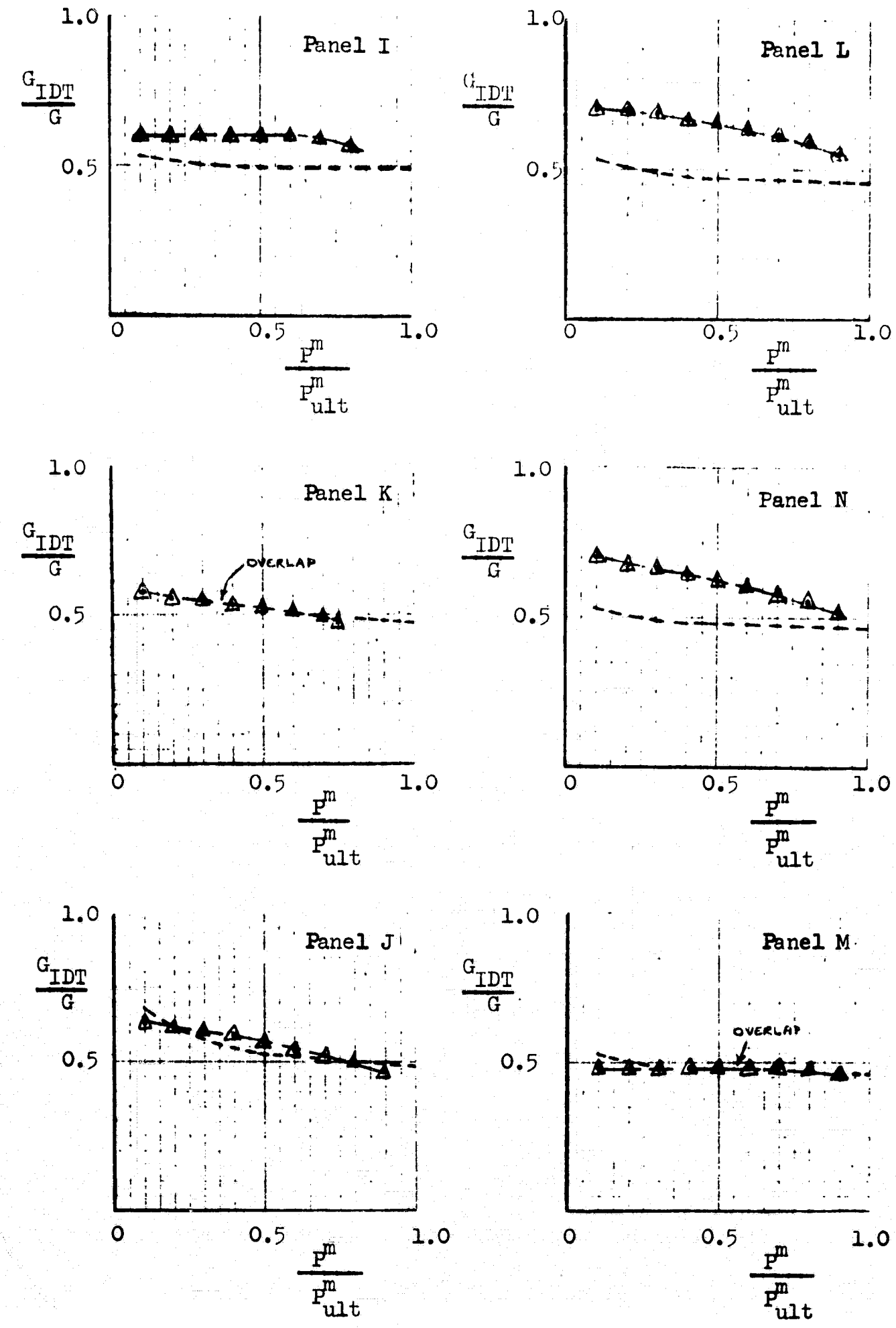

Figure 14. Continued.

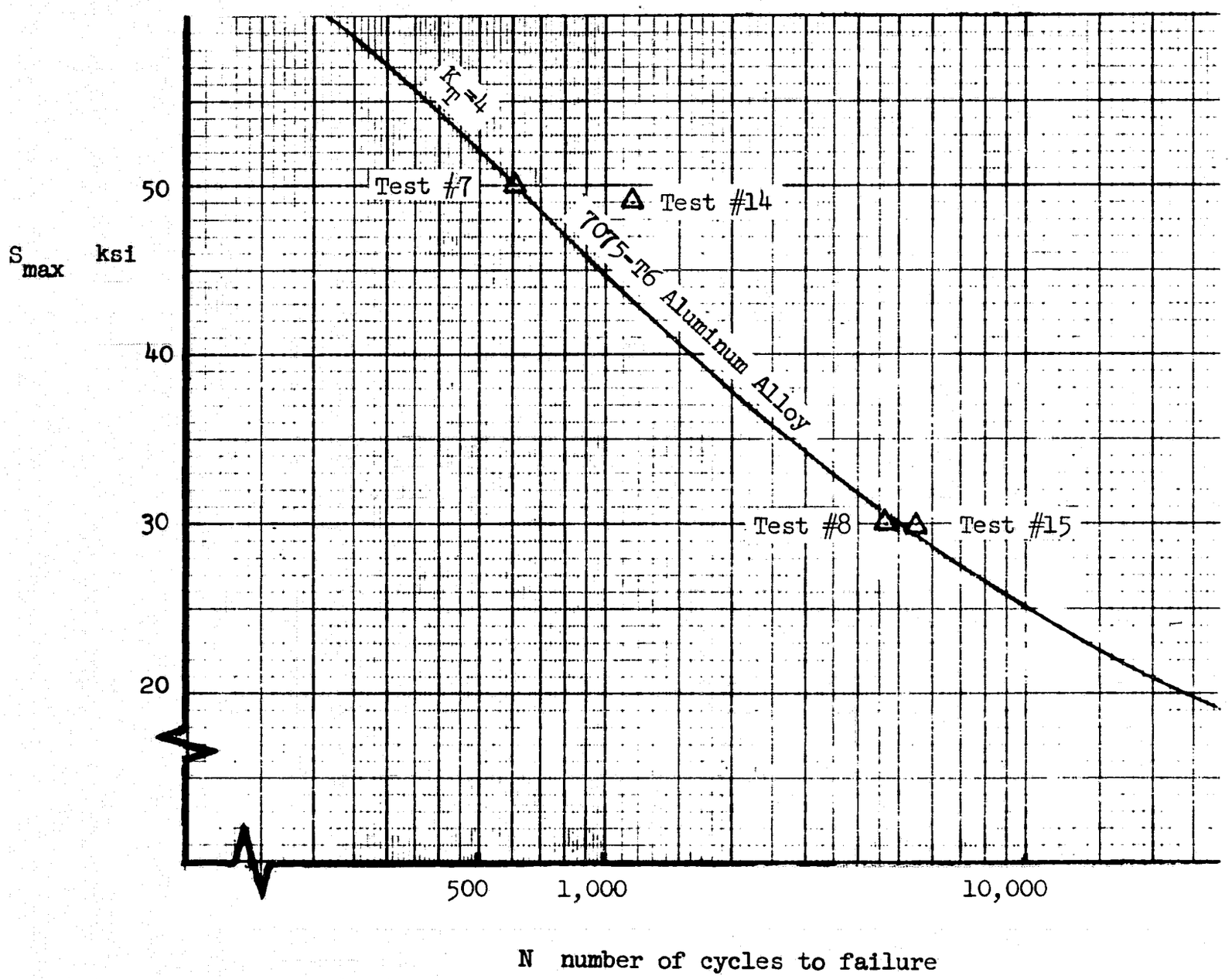

Figure 15. Fatigue test data.

Grumman

PHOTOGRAPHS

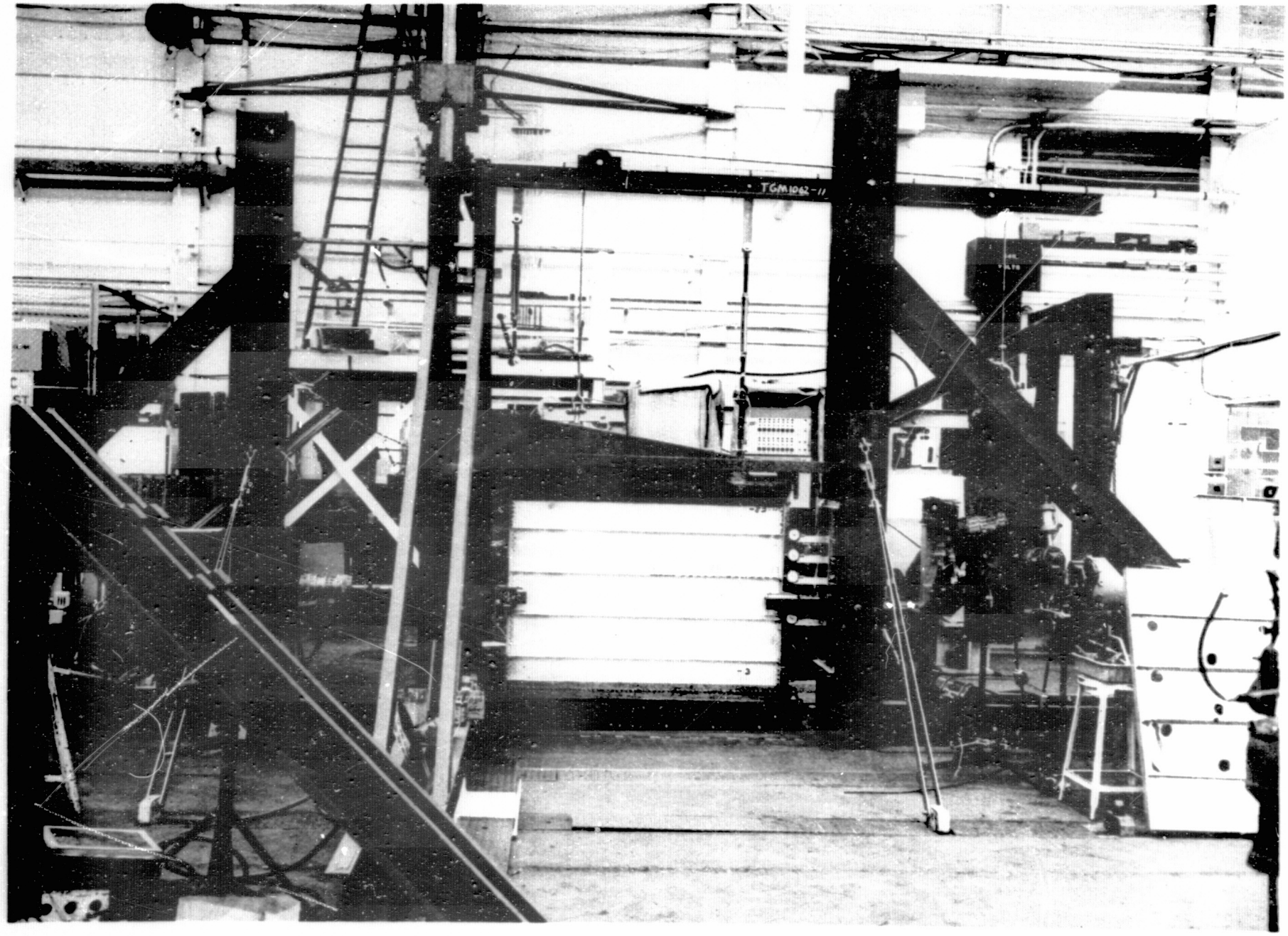

Photo 1. Overall View of Test Set-up

Grumman

Photo 2. Panel A Under 72% of Ultimate Load

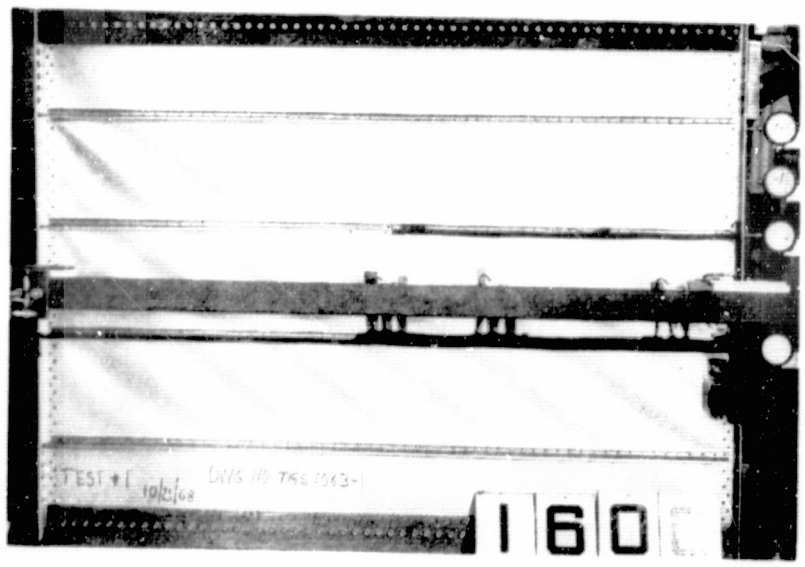

Photo 3. Panel B Under 80% of Ultimate Load

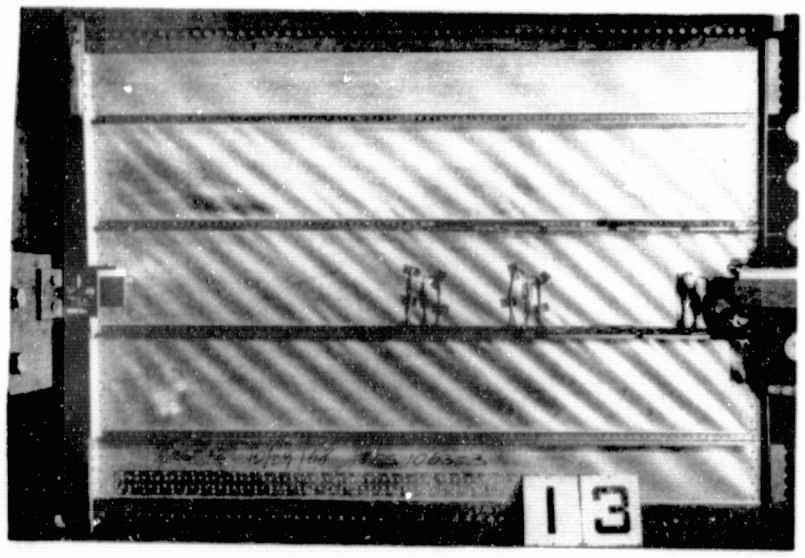

Photo 4. Panel C Under 88% of Ultimate Load

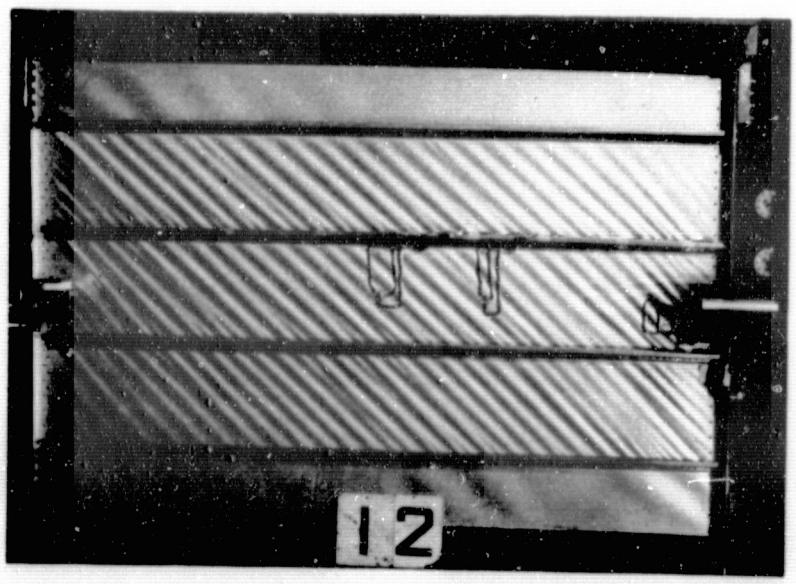

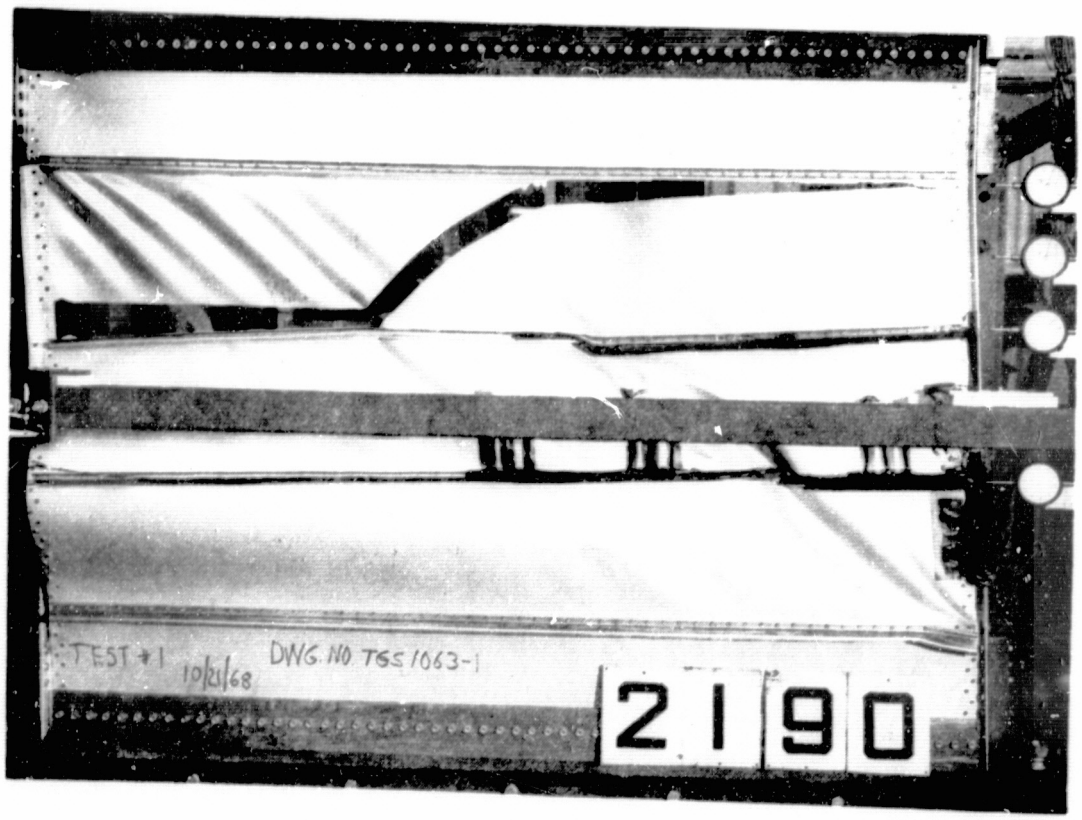

a)

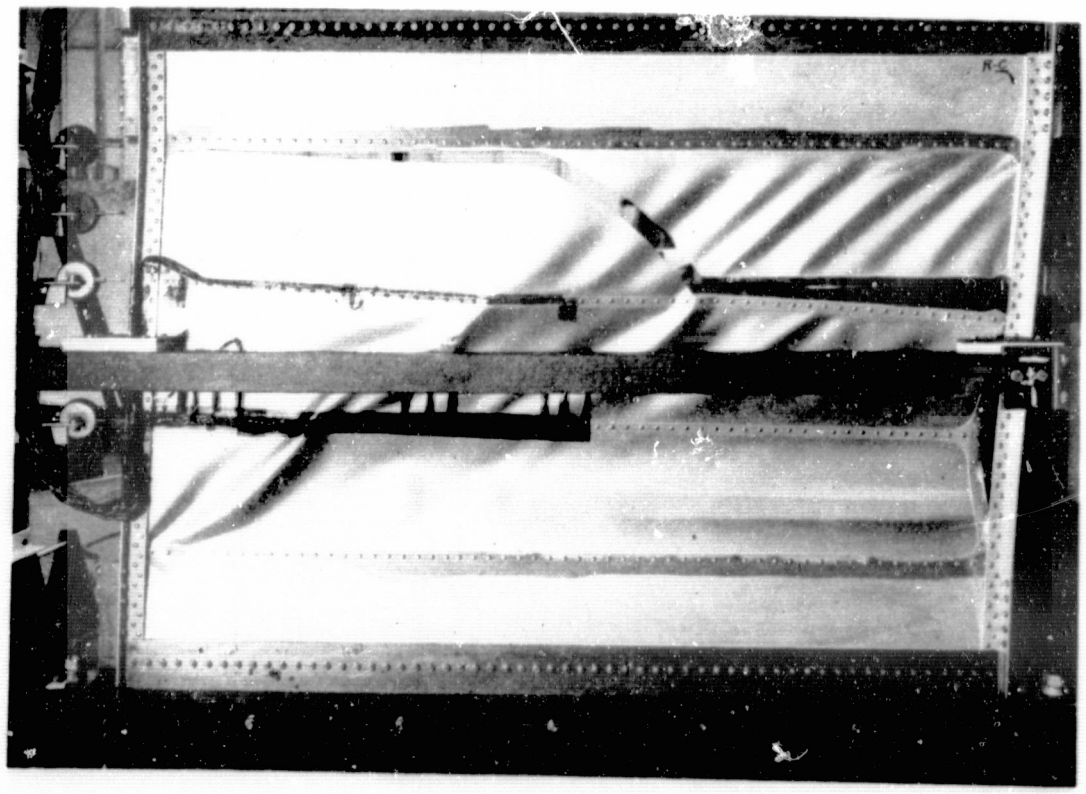

b)

Photo 5. Panel A after Collapse

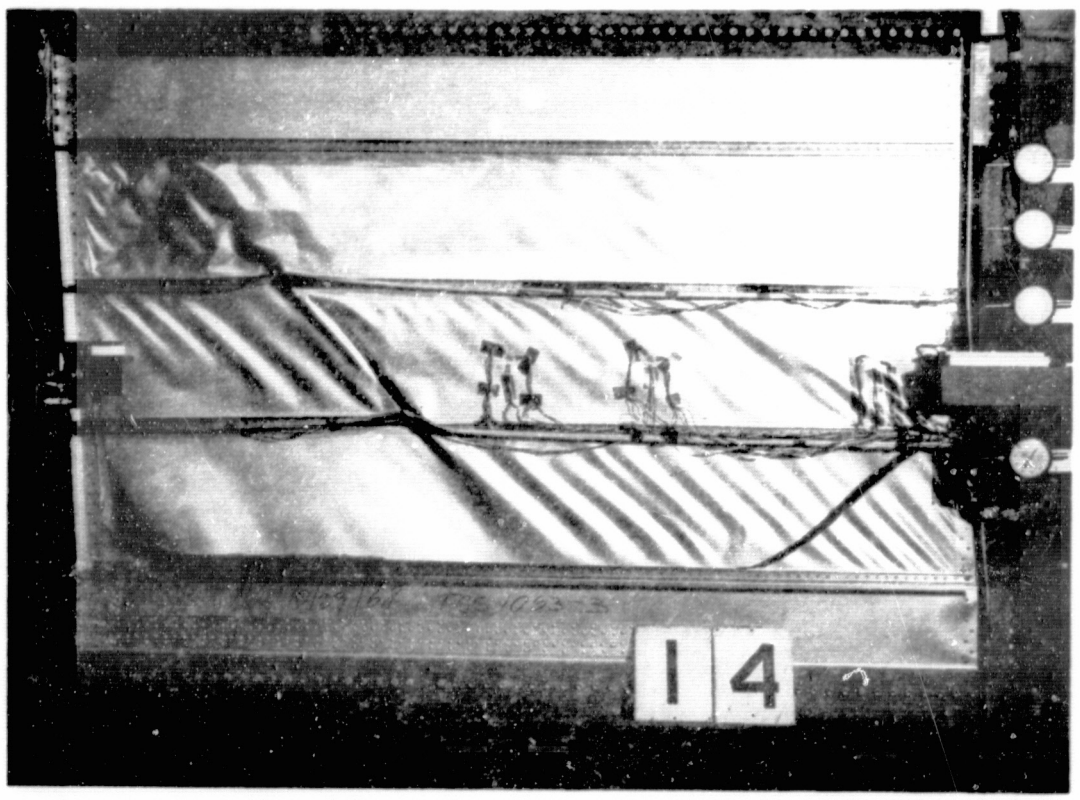

a)

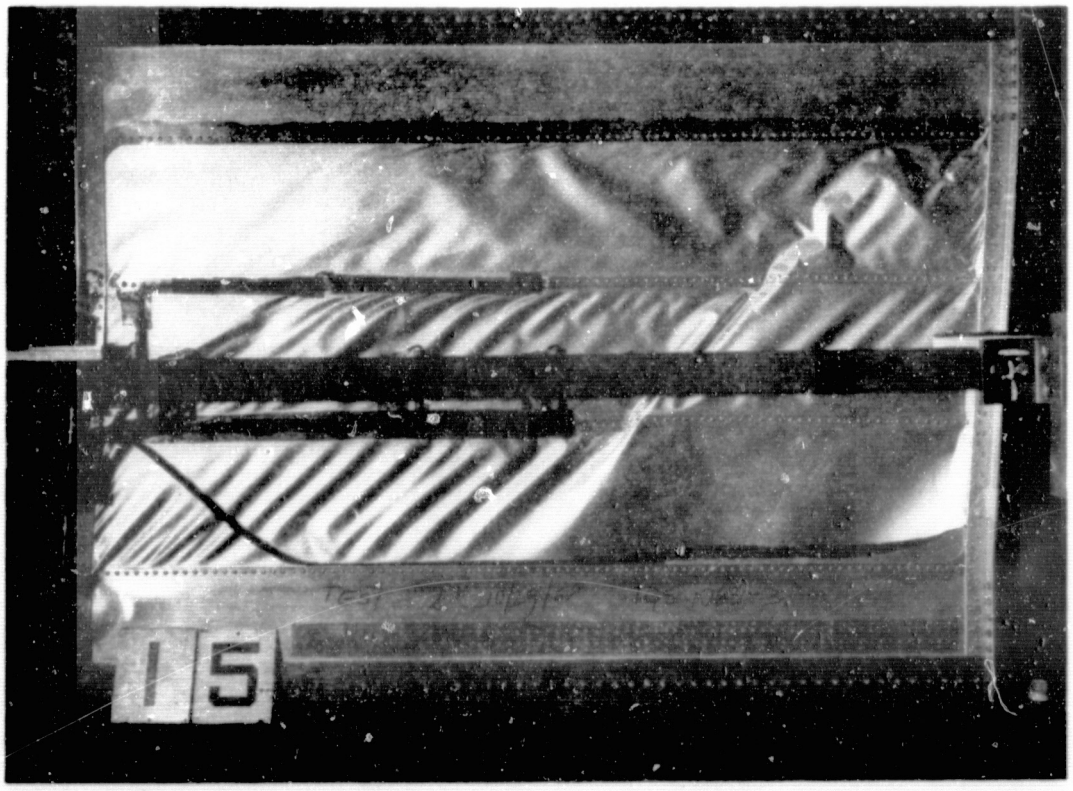

b)

Photo 6. Panel B after Collapse

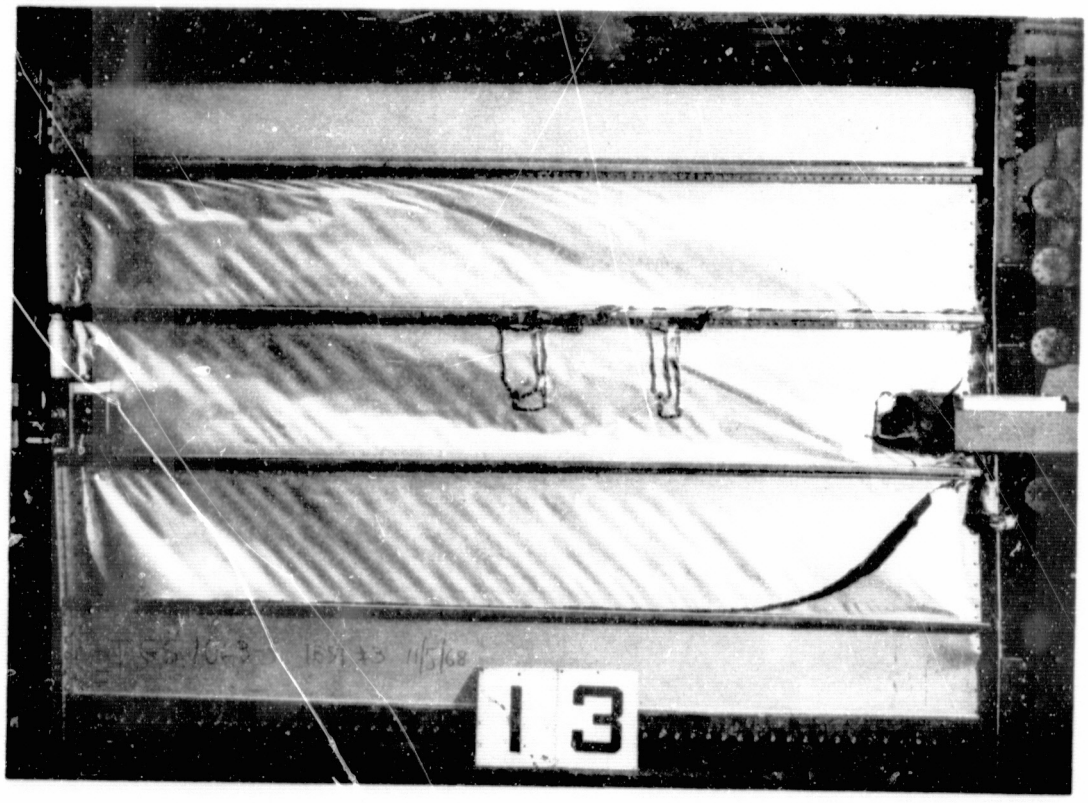

a)

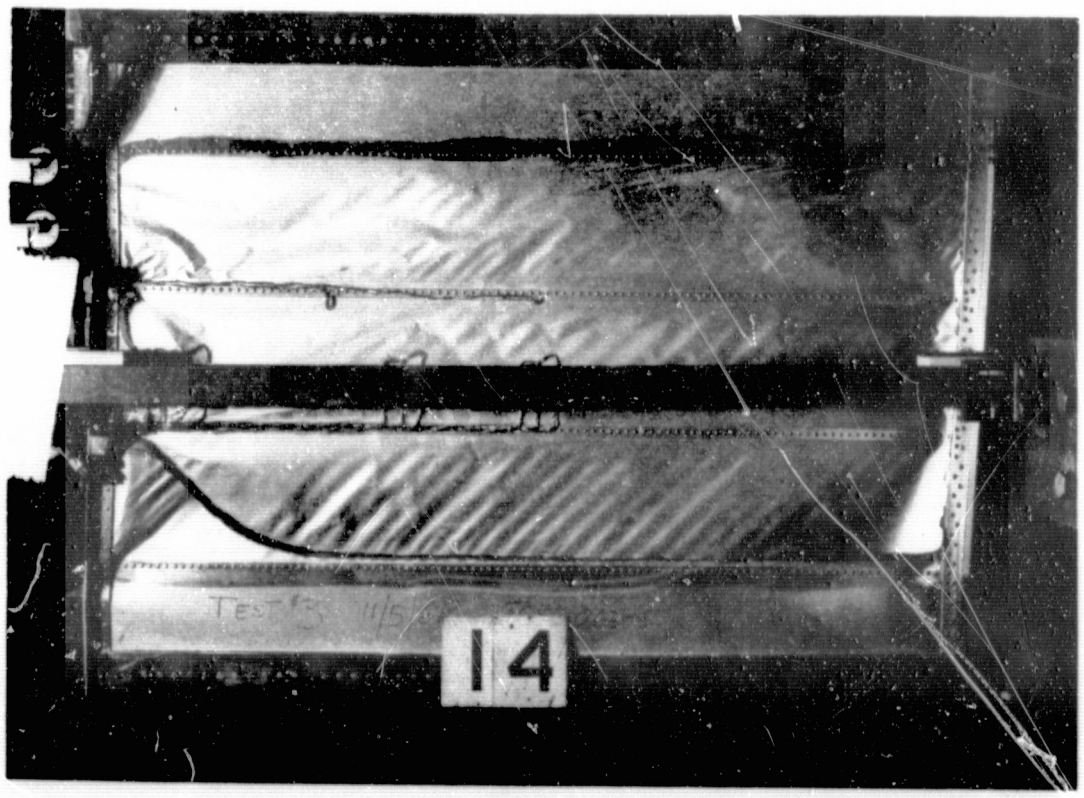

b)

Photo 7. Panel C after Collapse

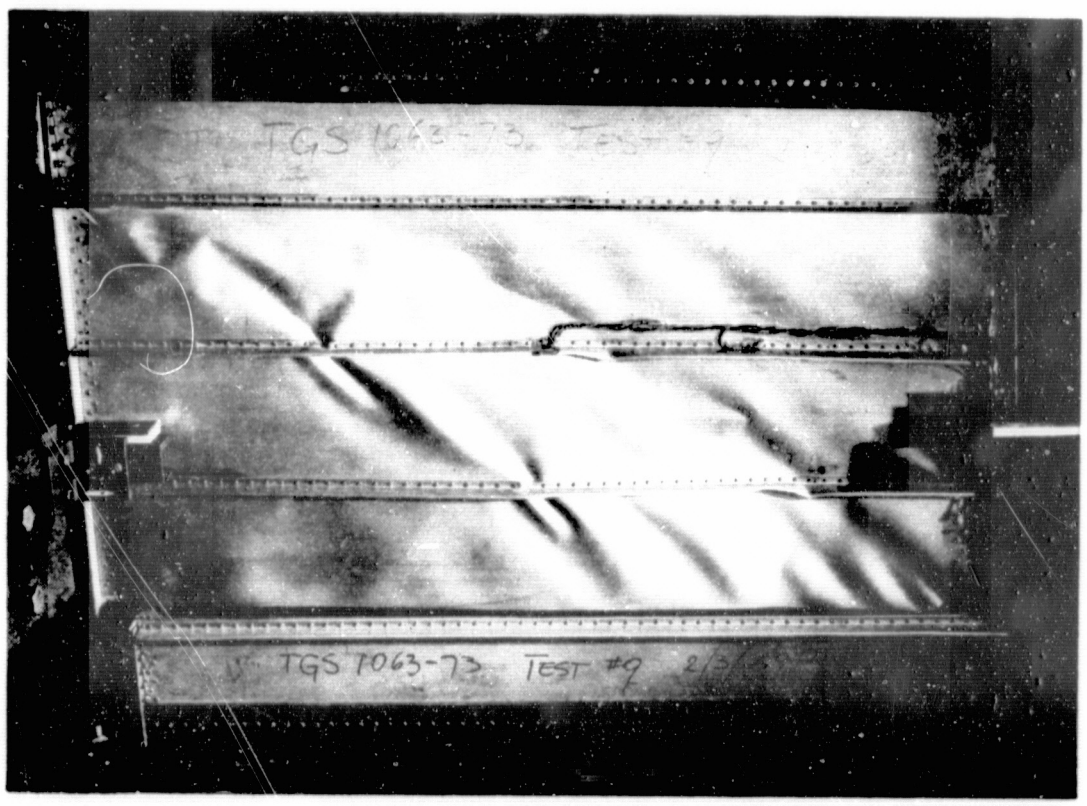

a)

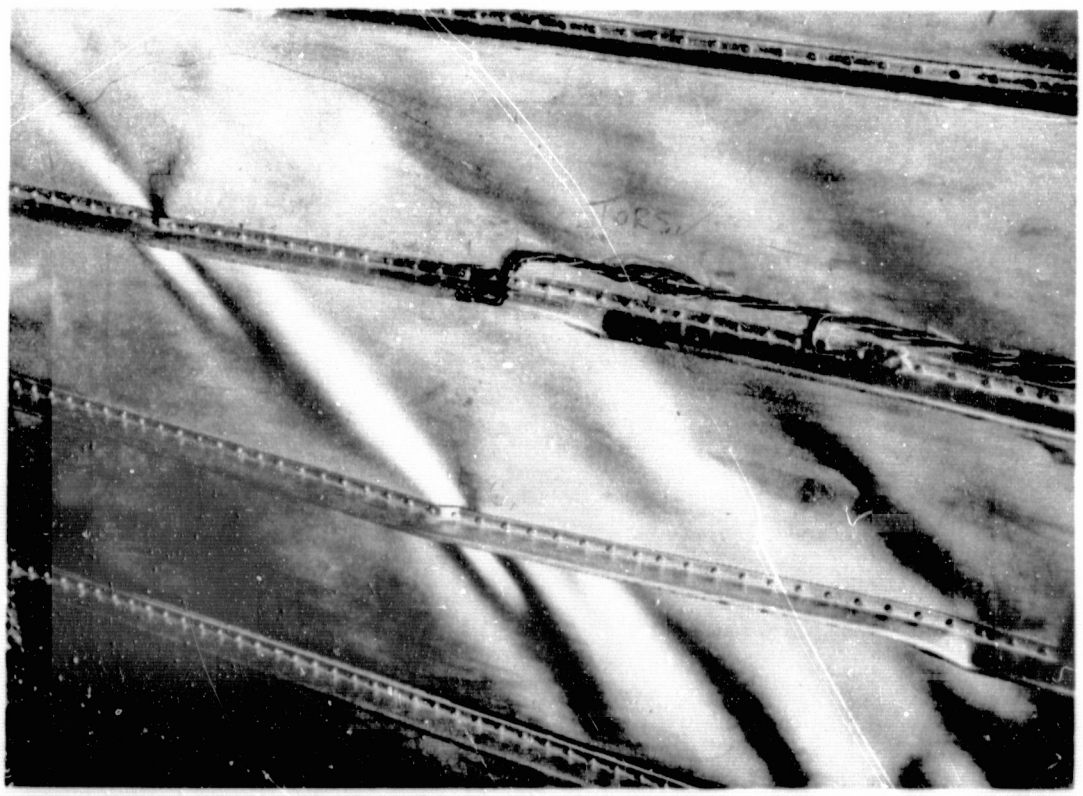

b)

Photo 8. Panel G after Collapse

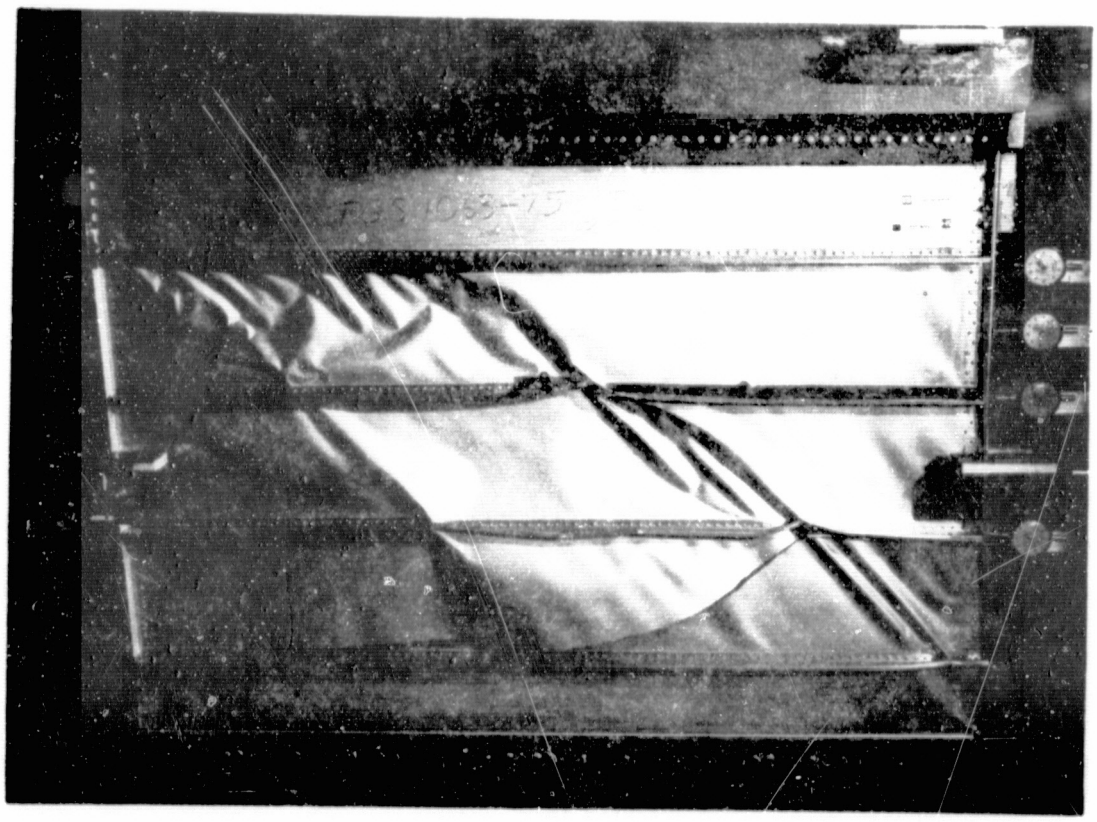

a)

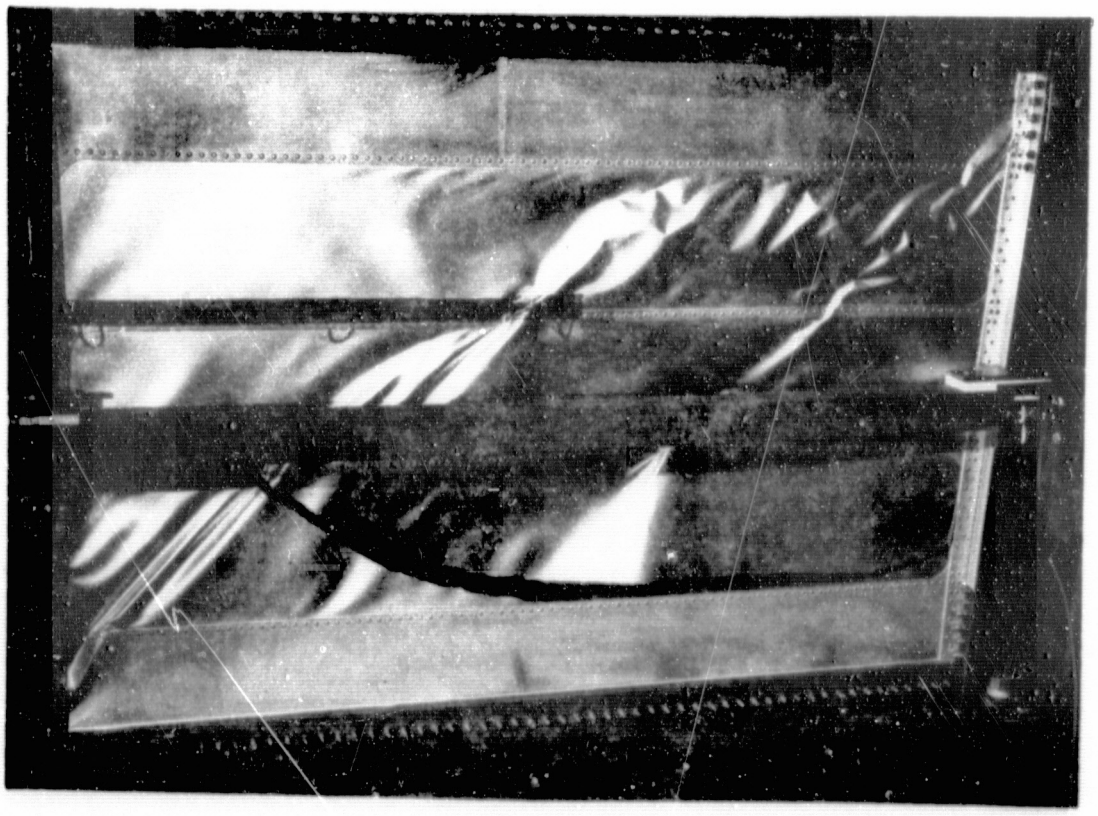

b)

Photo 9. Panel H after Collapse

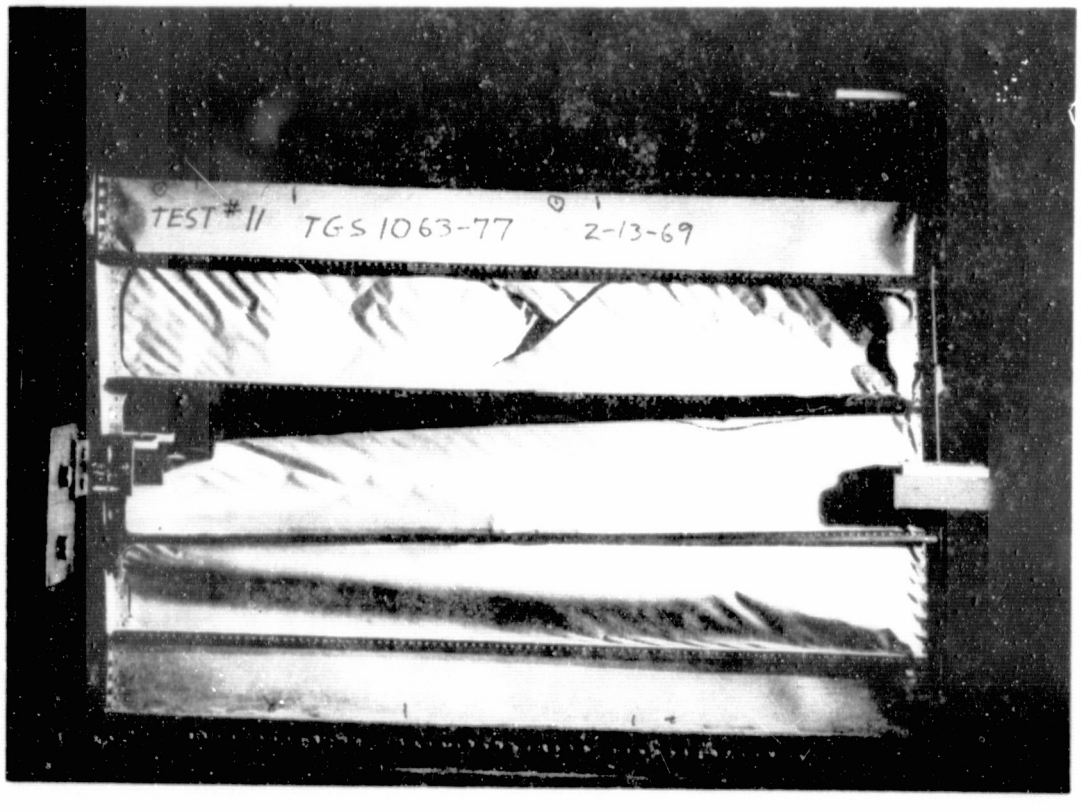

a)

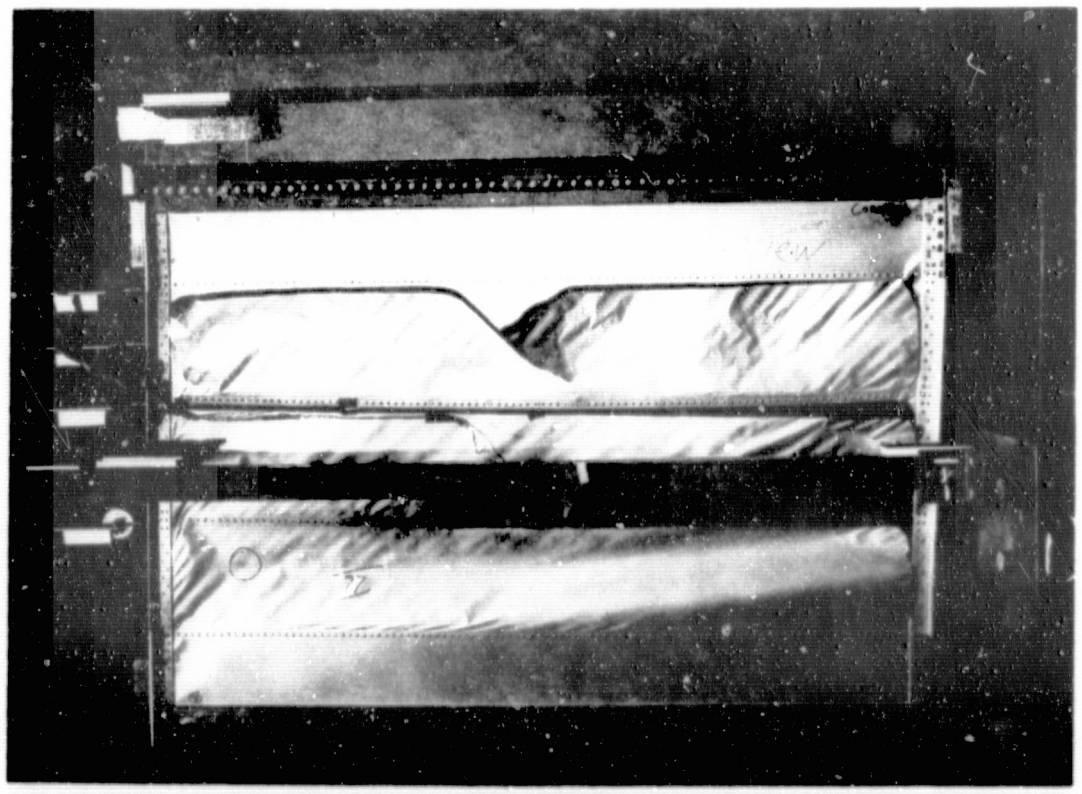

b)

Photo 10. Panel I after Collapse

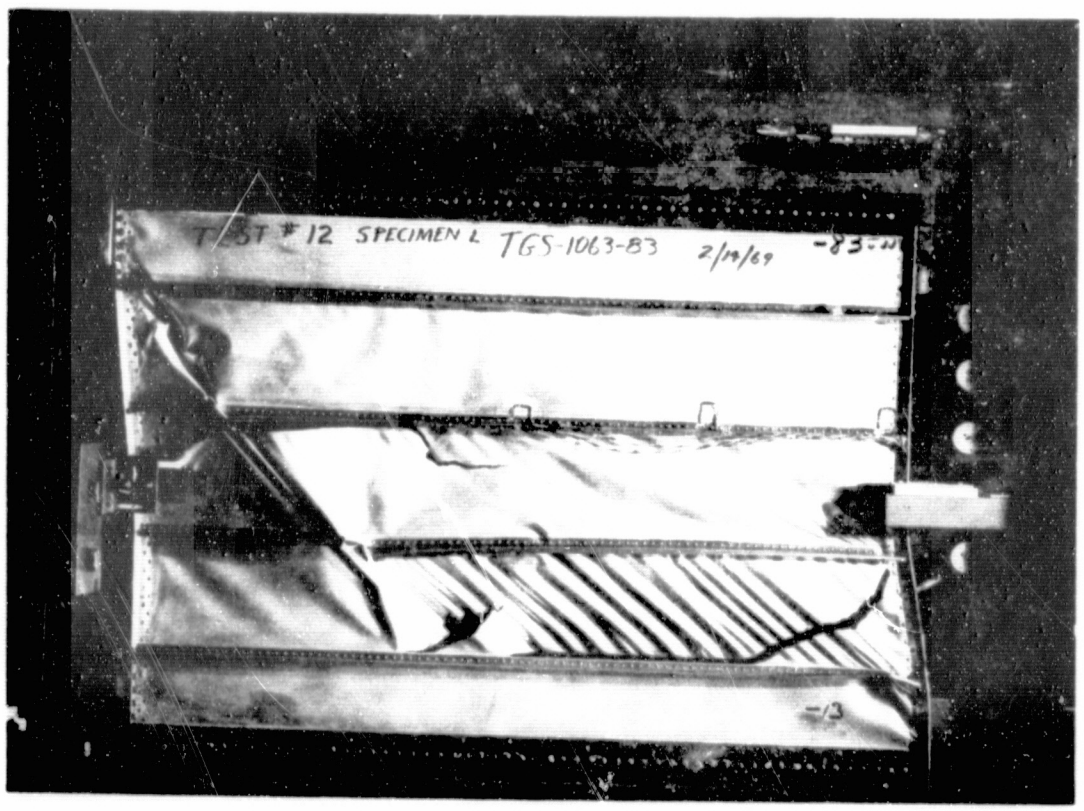

a)

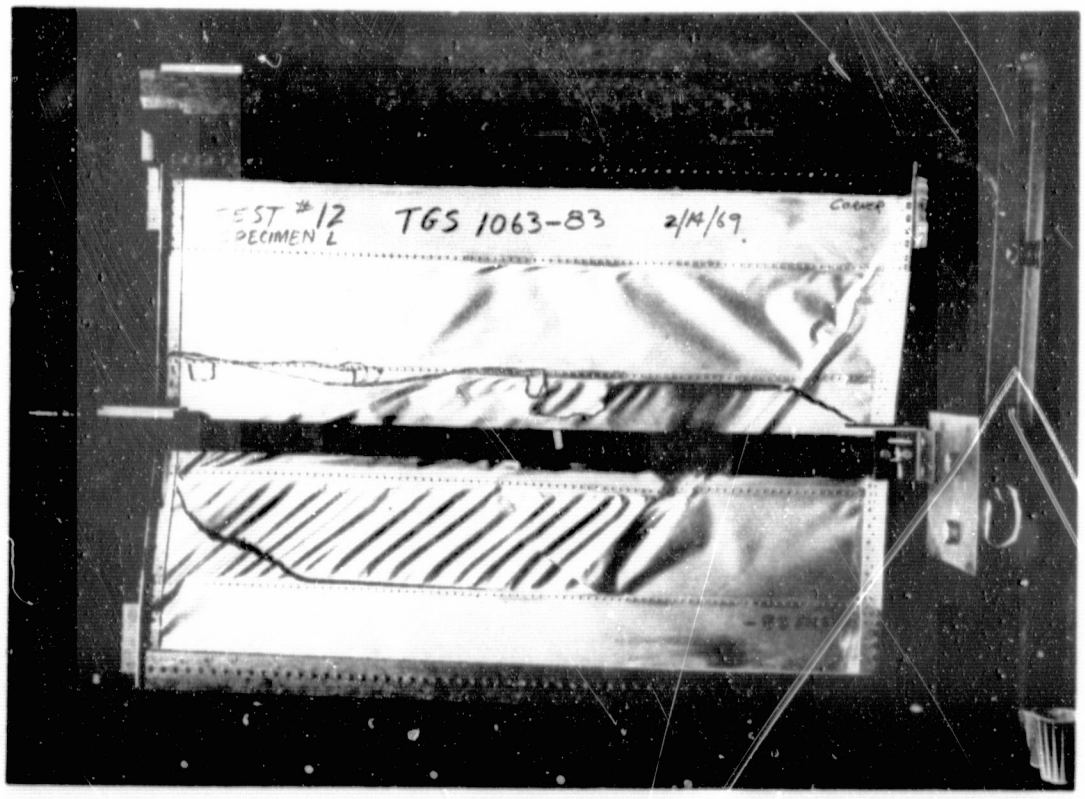

b)

Photo 11. Panel L after Collapse

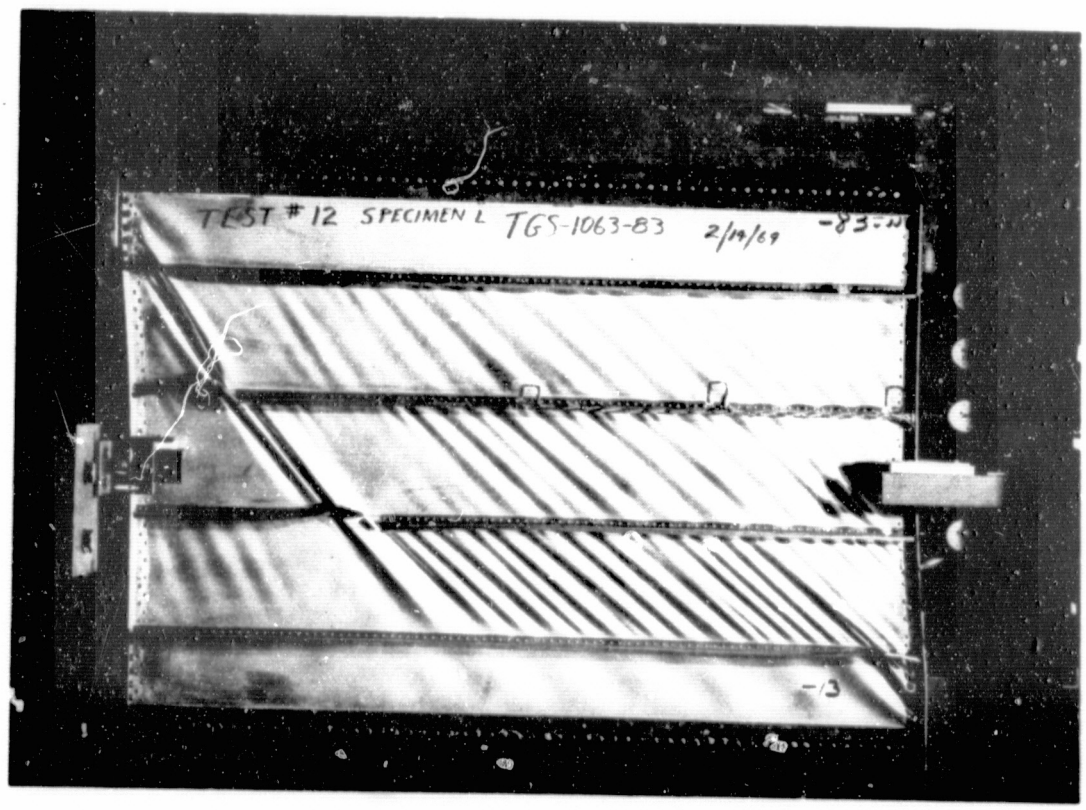

Photo 11C. Panel L after Stiffener Failure, Just Before Collapse

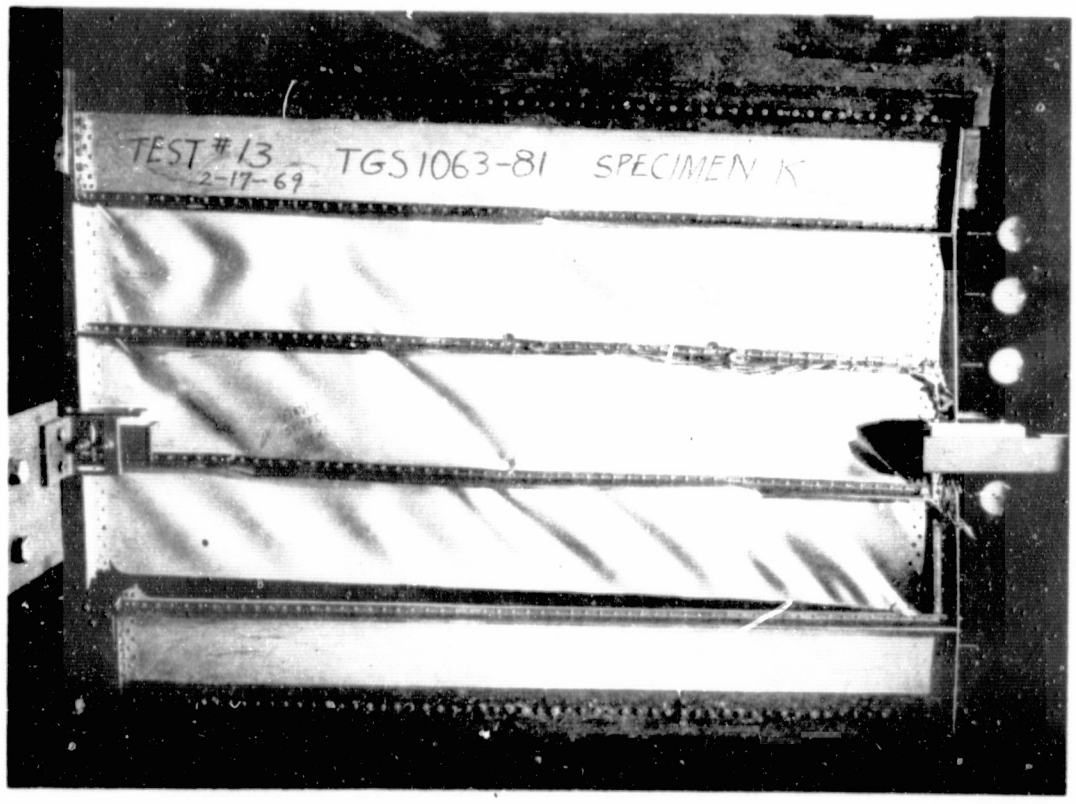

a)

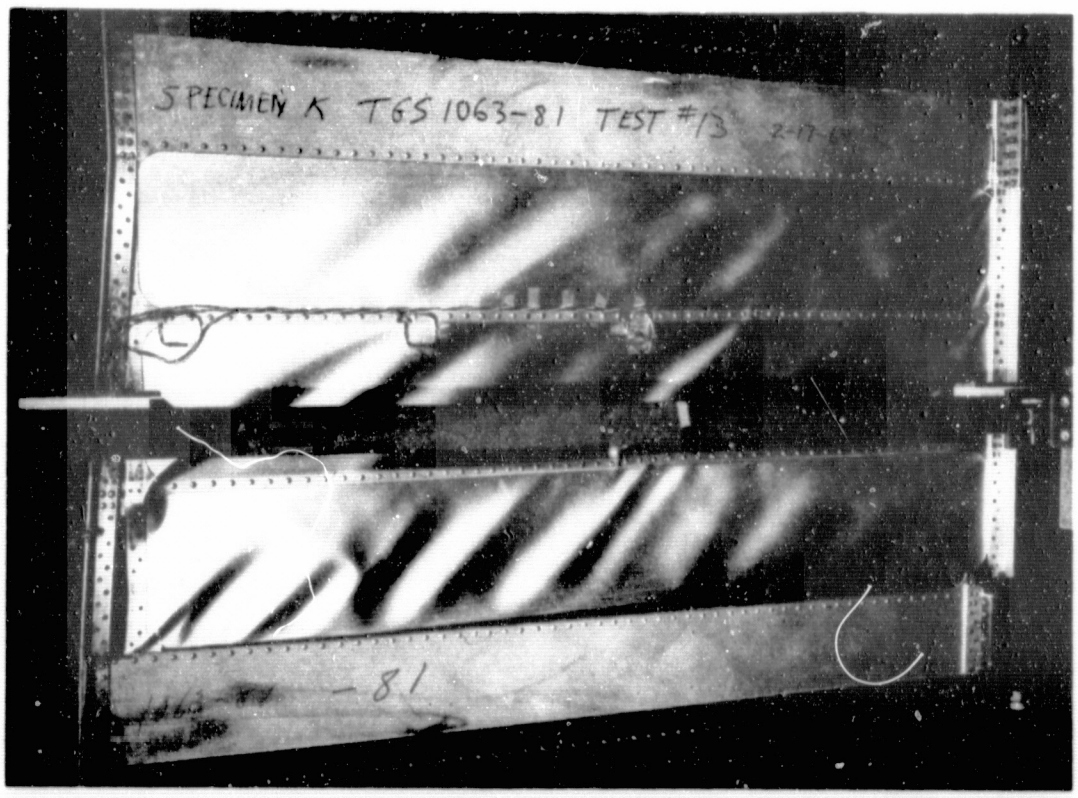

b)

Photo 12. Panel K after Collapse

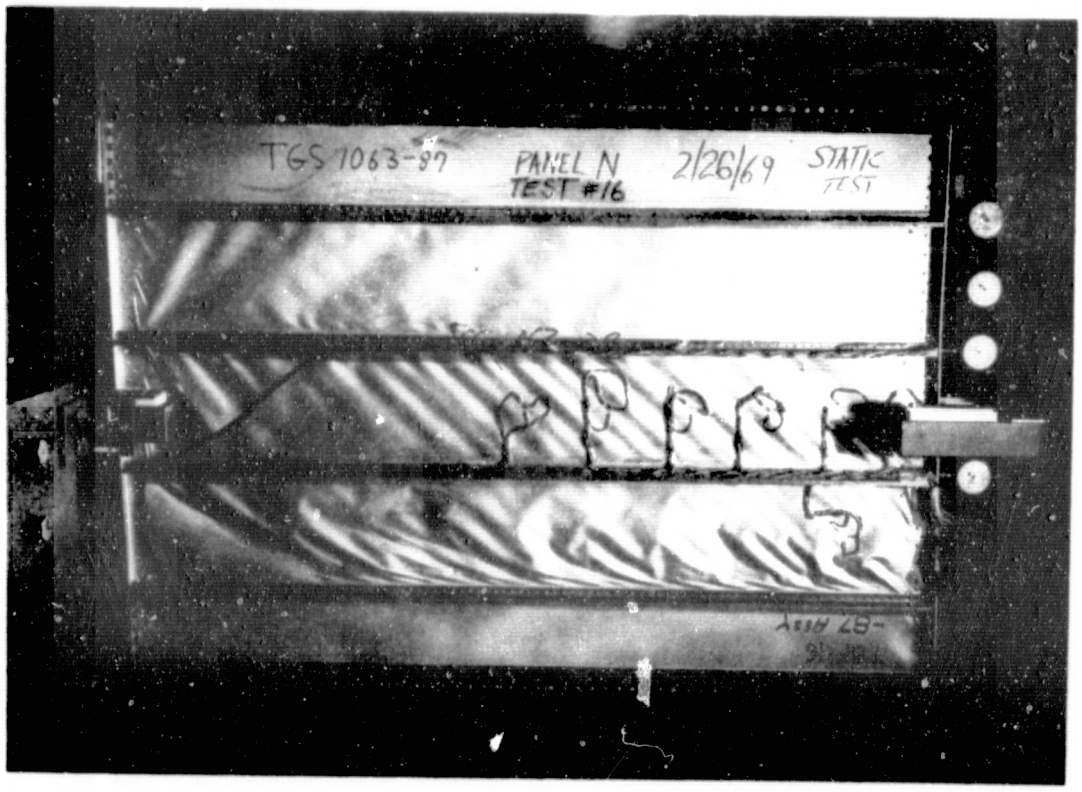

a)

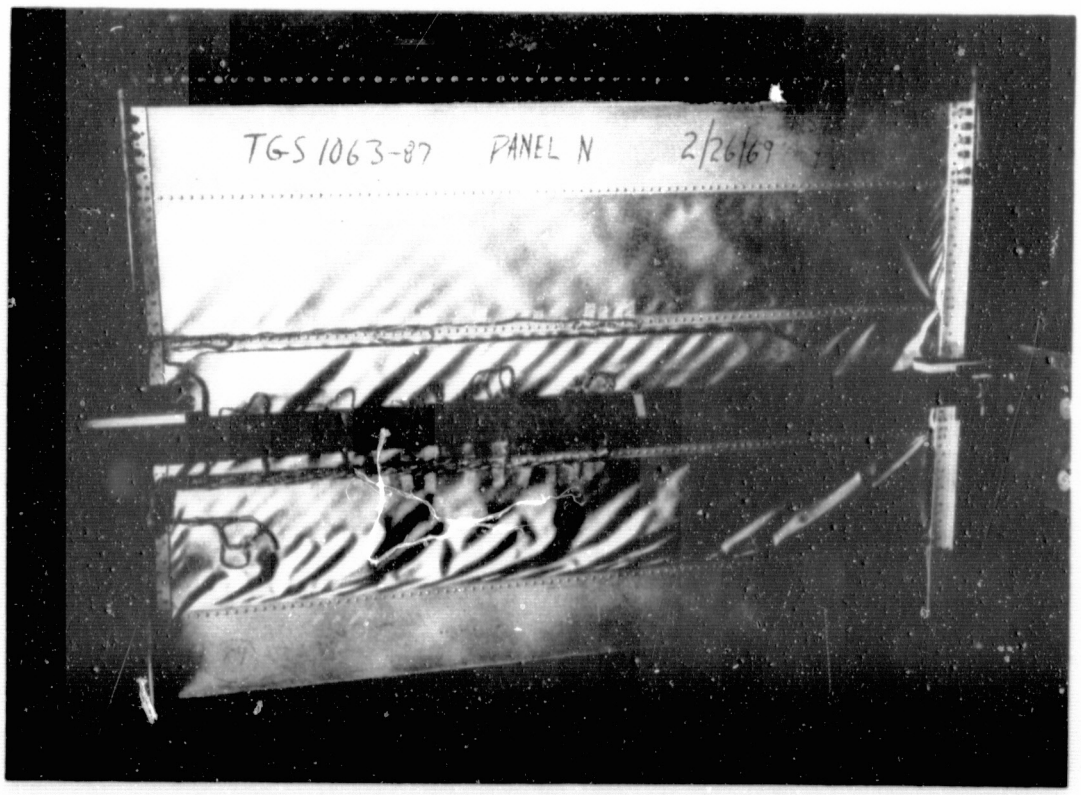

b)

Photo 13. Panel N after Collapse

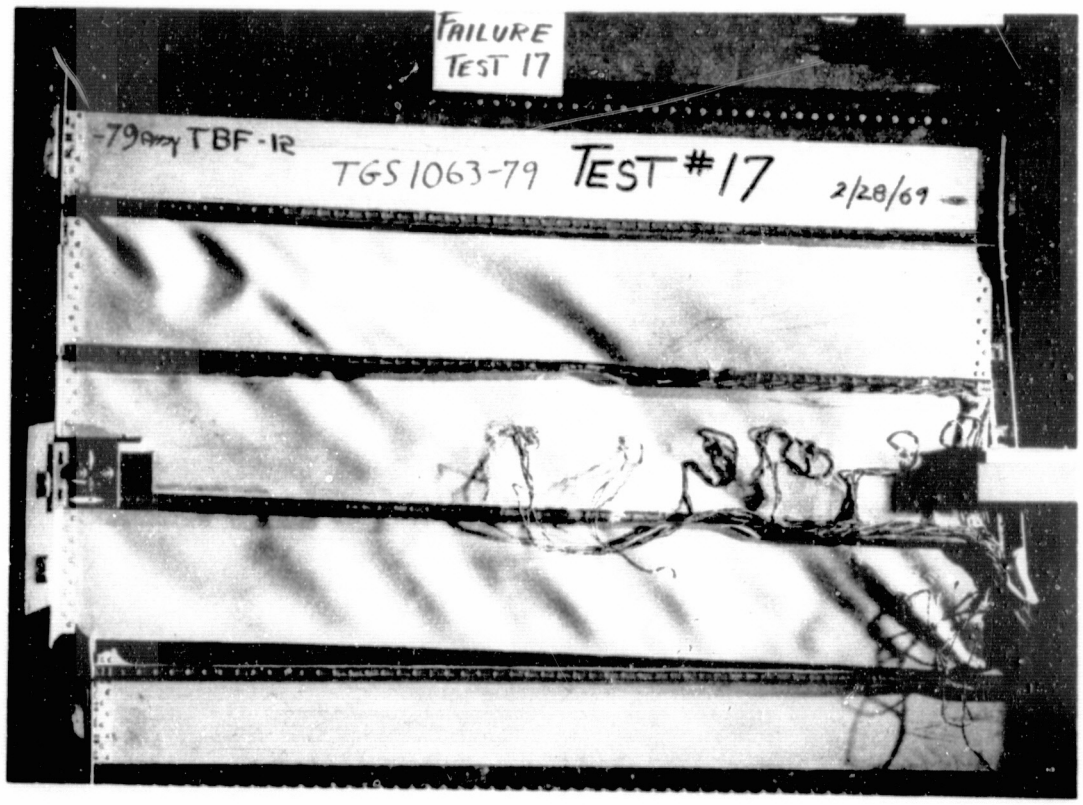

a)

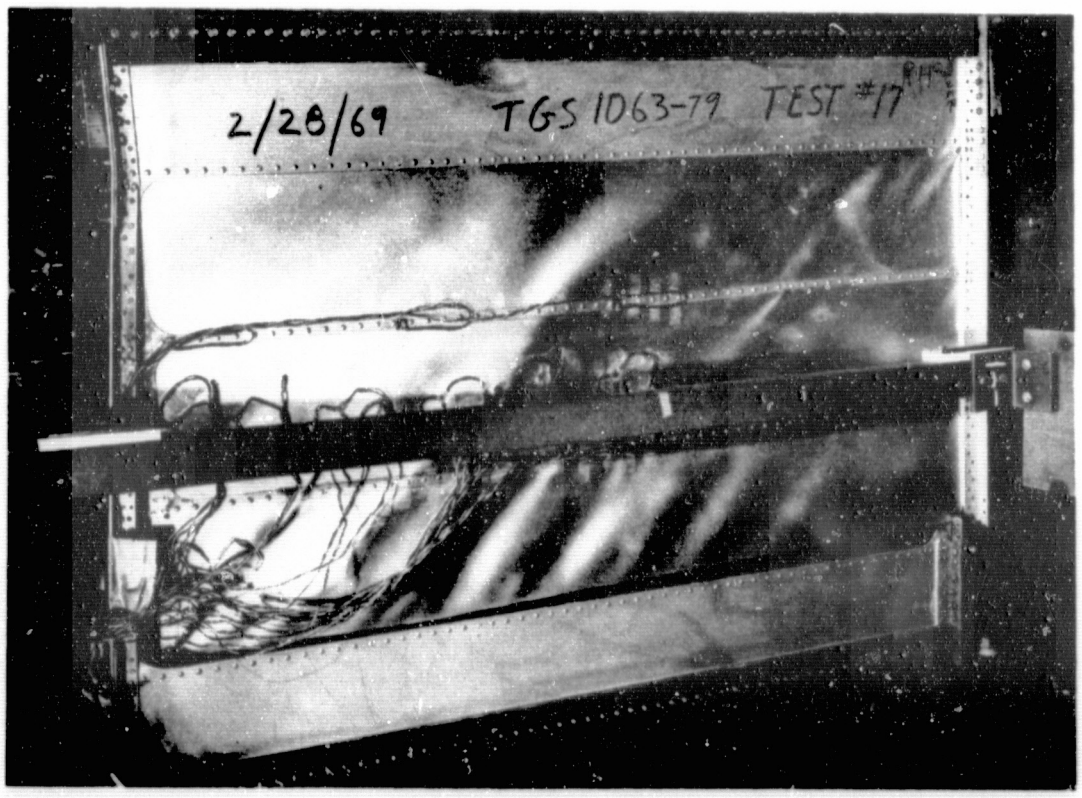

b)

Photo 14. Panel J after Collapse

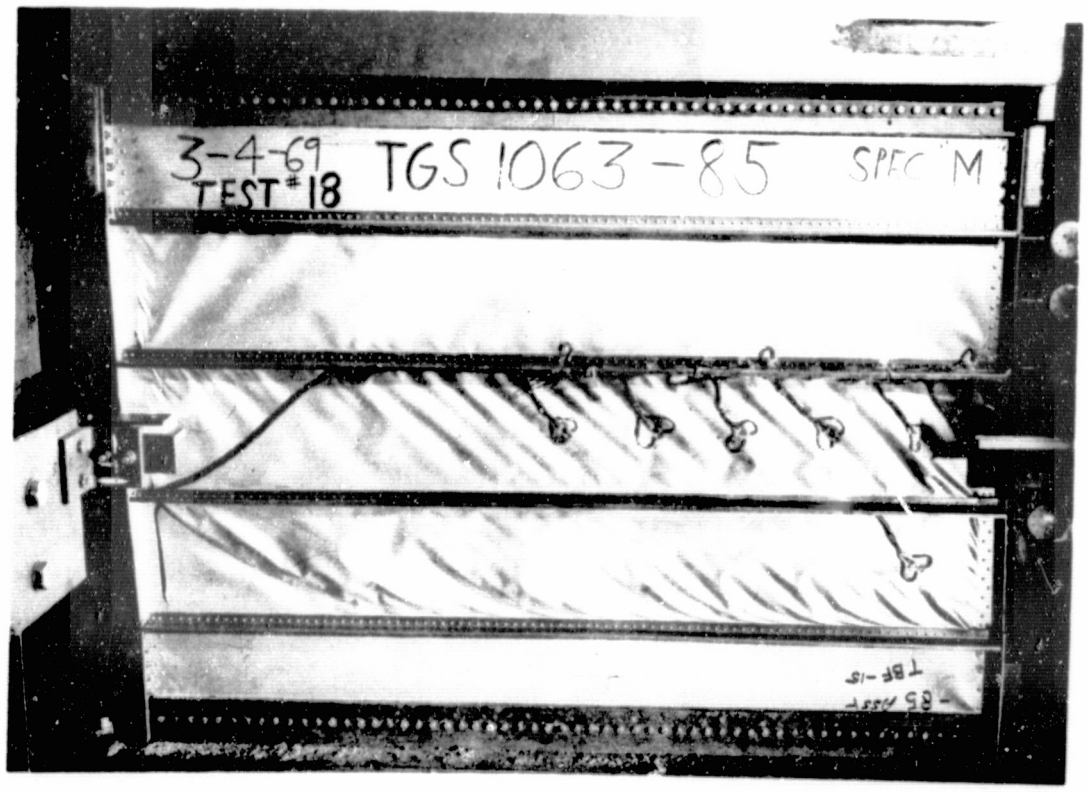

a)

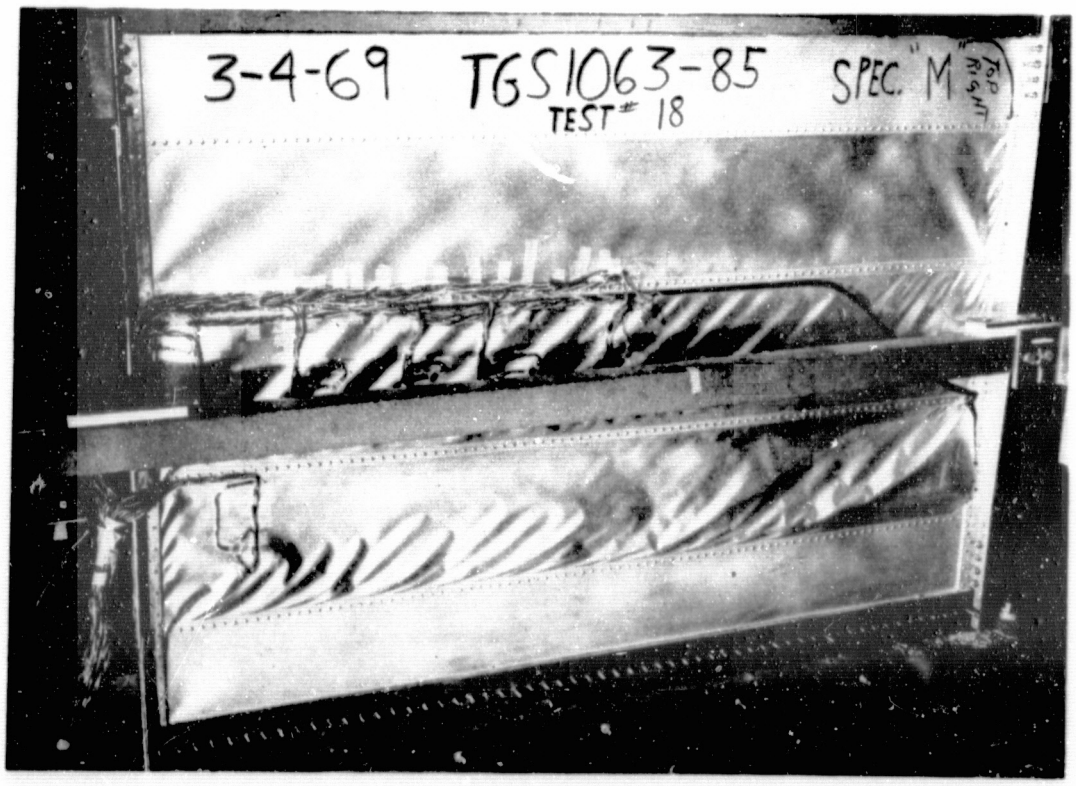

b)

Photo 15. Panel M after Collapse

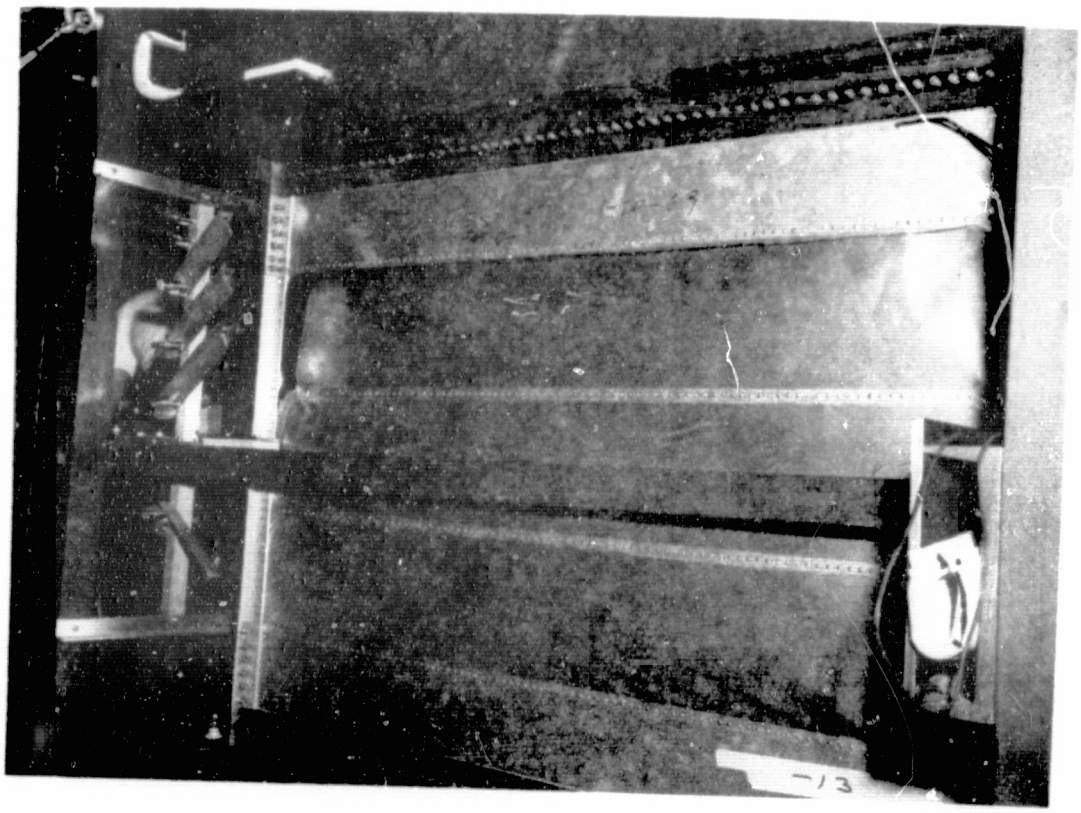

a)

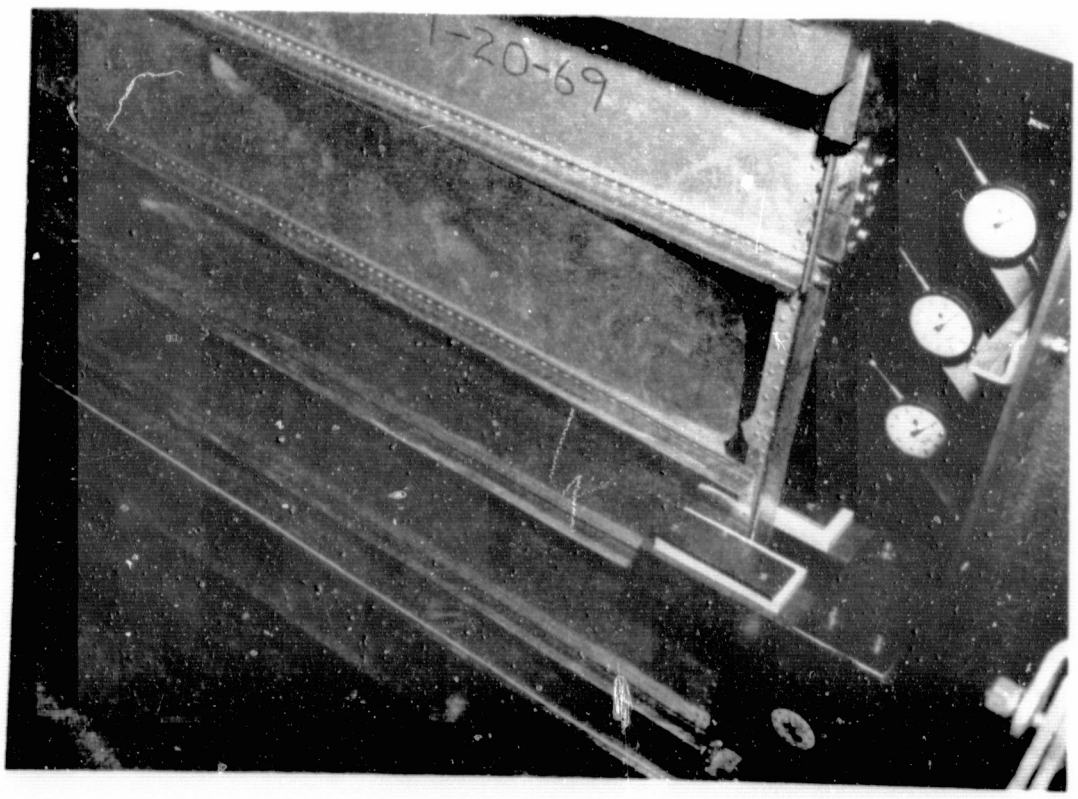

b)

Photo 16. Test #7, Panel E after Fatigue Failure

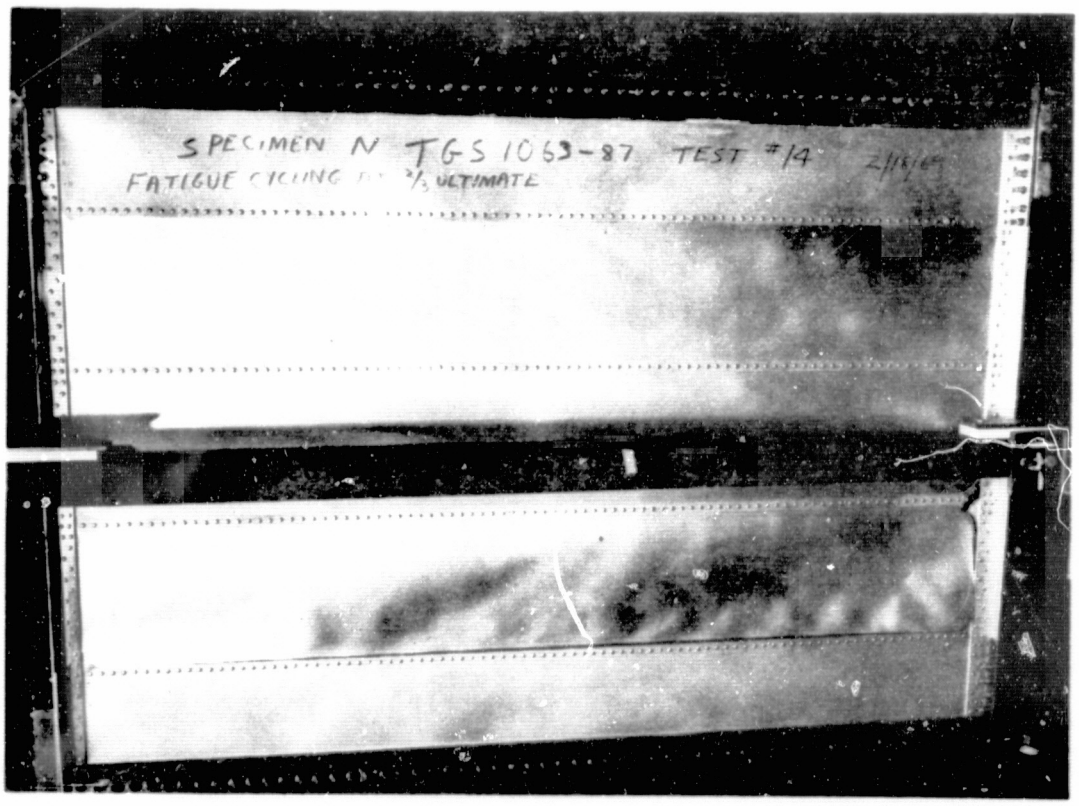

a)

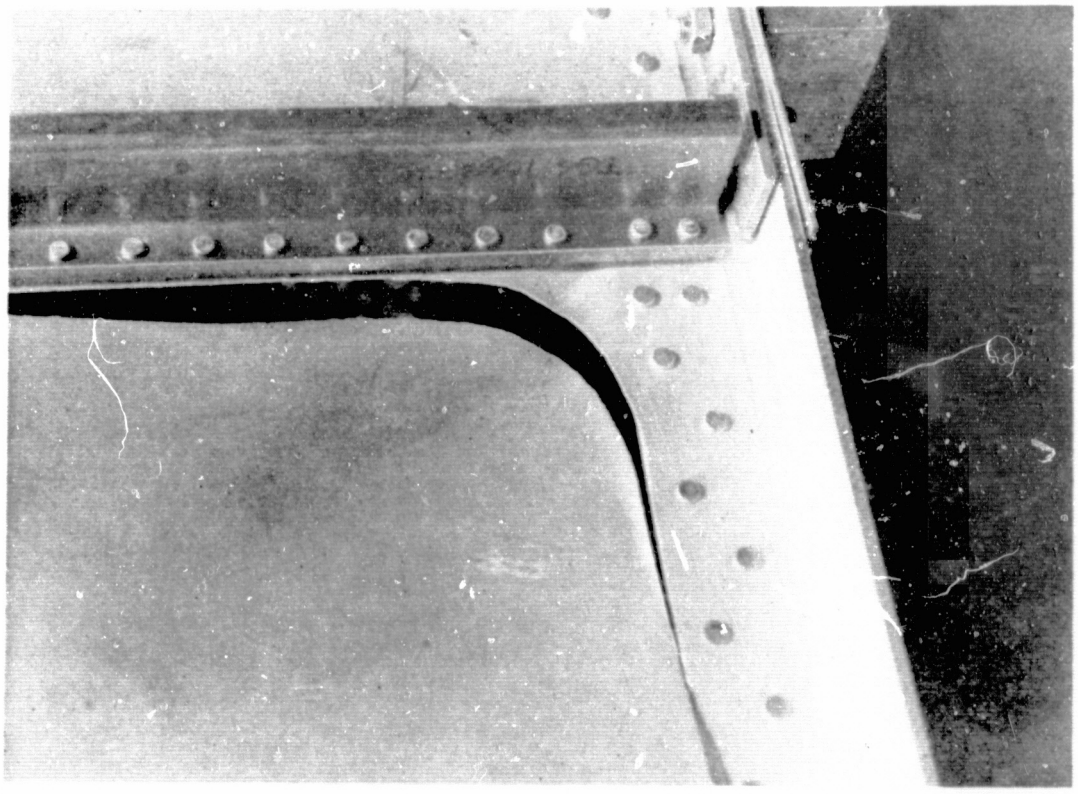

b)

Photo 17. Test #14, Panel N after Fatigue Failure.

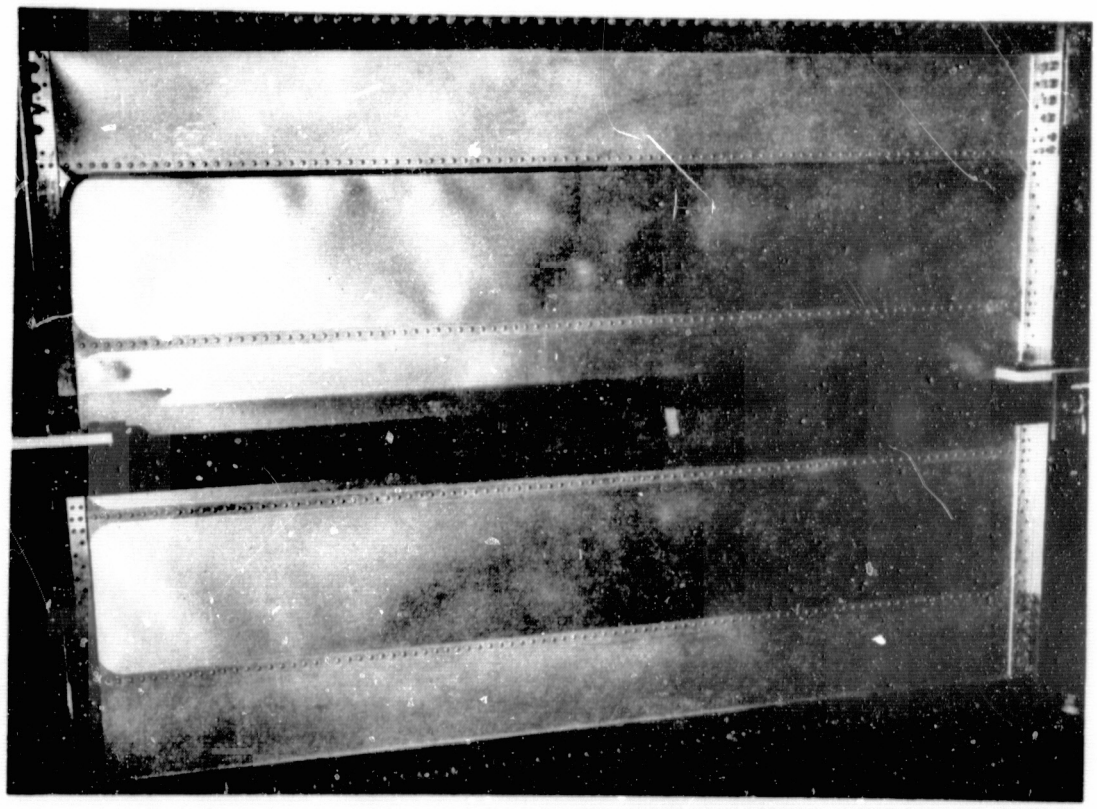

Photo 18. Test #15, Panel N after Fatigue Failure

A P P E N D I X A.

(Illustrative Analysis)

ILLUSTRATIVE ANALYSIS

Panel J, Test #17, is analyzed below as an example of the method of analysis used for comparison with test results.

INITIAL DATA.

Web properties:

$h_c = 56.0"$ $d_c = 8.4"$ $t = .028"$

$t_\ell = .063"$ $d_\ell = .75"$ $h_\ell = 1.0"$

Stiffener properties:

single stiffener $t_{st} = .082"$

$b_{pl} = .312"$ $b_{fl} = .625"$ $b_w = 1.125"$

$b_{f2} = .312"$ $b_{p2} = 0"$ $r = 0.1563"$

Flange properties:

$t_{f\ell} = .188"$ $A_{f\ell} = .715\ in^2$ $I_{f\ell} = .12\ in^4$

Material properties: 7075-T6 Aluminum alloy (bare)

$F_{ty} = 73.3$ ksi $F_{tu} = 78.85$ ksi $F_{cy} = 70.0$ ksi

$F_{su} = 48.0$ ksi $E = 10500.$ ksi $G = 3900.$ ksi

COMPUTE GEOMETRIC PROPERTIES.

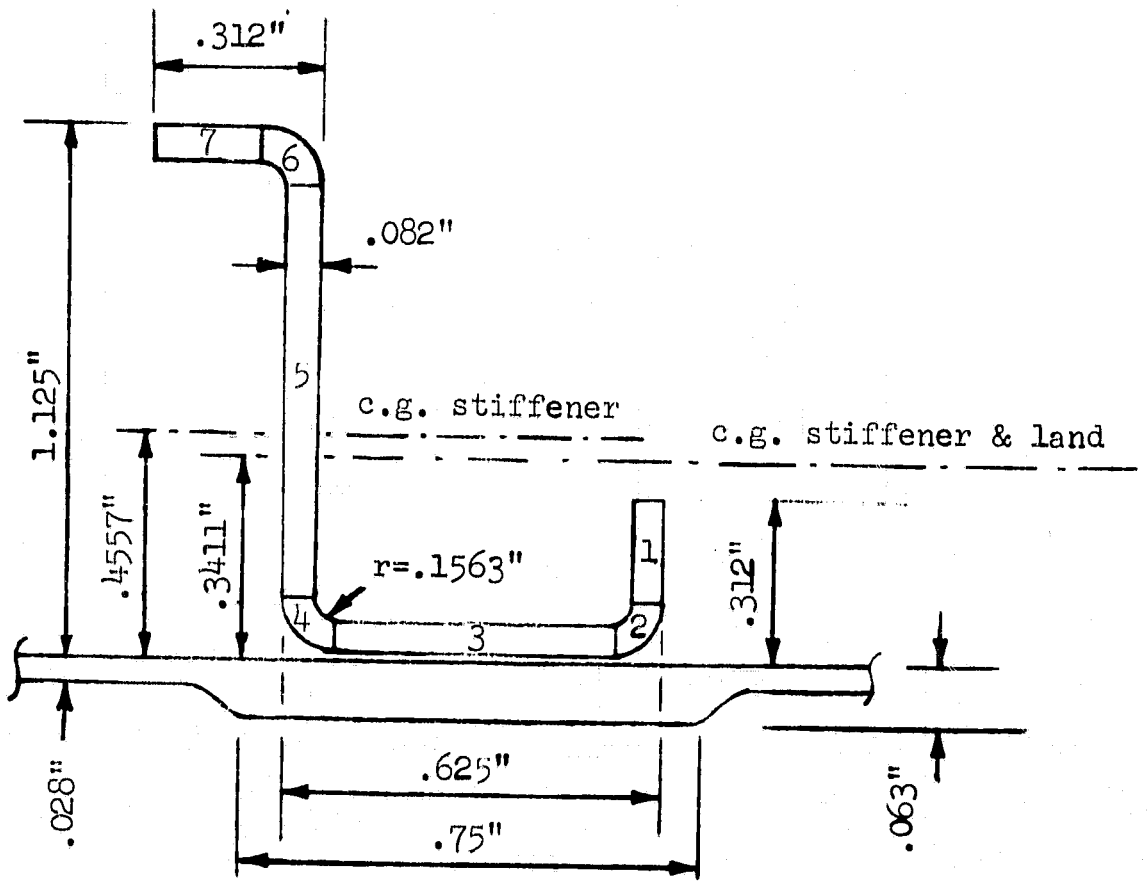

$$A_{st} = \sum_{i=1}^{7} A_i = 0.1537 \text{ in.}^2$$

$$A'_{st} = .1537 + .75(.063) = .2009 \text{ in.}^2$$

Distance from sheet face to c.g. of stiffener = .4557 in. (computation not shown).

Distance from sheet face to c.g. of stiffener - land combination = .3411 in. (computation not shown)

$$e' = .3411 \text{ in.} + .014 \text{ in.} = .3551 \text{ in.}$$

$$I_{st} = .02143 \text{ in.}^4$$

$$I'_{st} = .03006 \text{ in.}^4$$

$$\rho^2_{st} = I_{st}/A_{st} = .1395 \text{ in.}^2$$

$$(\rho'_{st})^2 = I'_{st}/A'_{st} = .1497 \text{ in.}^2$$

$$A'_{ste} = \frac{A'_{st}}{1 + (\frac{e'}{\rho'_{st}})^2} = \frac{.2009}{1 + \frac{.3551^2}{.1497}} = 0.1090 \text{ in.}^2$$

$$\frac{A'_{ste}}{d_c t} = \frac{.1090}{(8.4)(.028)} = 0.4635$$

$$\frac{A_{f\ell}}{h_c t} = \frac{.715}{(56)(.028)} = 0.4559$$

COMPUTE INITIAL BUCKLING STRESS OF WEB.

$$\frac{t_{st}}{t} = \frac{.082 \text{ in}}{.028 \text{ in}} = 2.929 \qquad \frac{t_{f\ell}}{t} \quad \frac{.188 \text{ in}}{.028 \text{ in}} = 6.714$$

From NACA TN 2661, Fig. 12 (b): (by extrapolation)

$$R_h = 1.3 \qquad R_d = 1.62$$

$$\frac{h_c}{d_c} = \frac{56.0 \text{ in}}{8.4 \text{ in}} = 6.667$$

From NACA TN 2661, Fig. 12 (a): (by extrapolation)

$$k_{ss} = 4.9$$

Using NACA TN 2661, Formula 32:

$$f_{scr} = k_{ss} \left(\frac{t}{d_c}\right)^2 \left[R_h + \frac{1}{2}(R_d - R_h)\left(\frac{d_c}{h_c}\right)^3\right] \qquad \text{(A.1)}$$

$$= 4.9(10.5 \times 10^3)\left(\frac{.028}{8.4}\right)^2 \left[1.3 + \frac{1}{2}(1.62-1.3)\left(\frac{8.4}{56}\right)^3\right]$$

$$= .753 \text{ ksi}$$

WEB STRESS.

Assume a web shear stress of 31.9 psi.*

$$\therefore \quad \frac{f_s}{f_{scr}} = \frac{31.9}{.753} = 42.3$$

From NACA TN 2661, Fig. 13:

$$k = 0.67$$

Assume an angle of diagonal-tension, α_{IDT}, of 43°.*

Then $\tan \alpha_{IDT} = .933$

From NACA TN 2661, Fig. 17:

$$C_1 = .002$$

Using NACA TN 2661, Formula 19:

$$\omega d = \sin \alpha_{IDT} \, d_c \sqrt[4]{\frac{t}{h_c(2 \times I_f)}} \qquad (A.2)$$

$$= \sin 43°(8.4) \sqrt[4]{\frac{.028}{2(.12)56}}$$

$$= 1.22$$

Then from NACA TN 2661, Fig. 18:

$$C_2 \approx 0$$

* This was arrived at after several trial solutions. Only this, the final trial, is shown here.

The maximum web shear stress is computed using Formula 33a of NACA TN 2661:

$$f_{s\ max} = f_s\ (1+k^2 C_1)(1+k\ C_2) \qquad (A.3)$$

$$= 31.9(1+.67^2 \times .002)(1+.67 \times 0)$$

$$= 31.93 \text{ ksi}$$

STRESS IN STIFFENERS.

From NACA TN 2661, Formula 30.a.(using A'_{ste} instead of A_{ste})

$$f_{st} = -\frac{k\, f_s \tan \alpha_{IDT}\ d_c t}{A'_{ste} + 0.5(1-k) d_c t} \qquad (A.4)$$

$$= -\frac{.67(31.9)(.933)(8.4)(.028)}{.1090 + .5(.33)(8.4)(.028)}$$

$$= -32.0 \text{ ksi}$$

STRESS IN FLANGES.

From NACA TN 2661, Formula 30 b:

$$f_{f\ell} = -\frac{k\ f_s\ \cot \alpha_{IDT}}{\frac{2\ A_{f\ell}}{h_c t} + 0.5\ (1-k)} \qquad (A.5)$$

$$= -\frac{.67(31.9)\cot 43^\circ}{2(.4559) + .5(.33)}$$

$$= -20.5 \text{ ksi}$$

CHECK FOR α_{IDT}.

From NACA TN 2661, Formula 30c:

$$\tan^2 \alpha_{IDT} = \frac{\varepsilon - \varepsilon_{f\ell}}{\varepsilon - \varepsilon_{st}} \qquad (A.6)$$

where

$$\varepsilon_{f\ell} = \frac{f_{f\ell}}{E} \quad \frac{-20.5}{10.5x10^3} = - .00195$$

$$\varepsilon_{st} = \frac{f_{st}}{E} = - \frac{32.0}{10.5x10^3} = - .00305$$

and from NACA TN 2661, Formula 30d:

$$\varepsilon = \frac{f_s}{E}\left[\frac{2k}{\sin 2\,\alpha_{IDT}} + (1-k)(1+\nu)\sin 2\,\alpha_{IDT}\right] \qquad (A.7)$$

$$= \frac{31.9}{10.5x10^3}\left[\frac{1.34}{\sin 86°} + (.33)(1.3)\sin 86°\right]$$

$$= .00539$$

$$\tan^2 \alpha_{IDT} = \frac{.00539 + .00195}{.00539 + .00305} = .870$$

$$\alpha_{IDT} = 43° = \text{the "assumed" } \alpha_{IDT}$$

DETERMINE MARGINS OF SAFETY.

Web:

From Figure 5, Curve B of this report, at k = 0.67

$$F_{s\ all} = 33.3 \text{ ksi}$$

$$M.S. = \frac{F_{s\ all}}{f_{s\ max}} - 1$$

$$= \frac{33.3}{31.9} - 1 = + 0.045$$

Stiffener:

(a) Local failure

From Fig. 15 of NACA TN 2661, using d/h = .15 and k = .67:

$$\frac{f_{st\ max}}{f_{st}} = 1.22$$

$$\therefore\ f_{st\ max} = 1.22\ (-31.9) = -\ 39.0\ \text{ksi}$$

$$k^{2/3}\left(\frac{t_{st}}{t}\right)^{1/3} = .67^{2/3}\left(\frac{.002}{.028}\right)^{1/3} = 1.1$$

From Fig. 6 of this report:

$$F_{fc\ all} = -\ 39.0\ \text{ksi}$$

$$M.S. = \frac{F_{fc\ all}}{f_{st\ max}} - 1$$

$$= \frac{-39.0}{-39.0} - 1 = 0$$

(b) Column failure

From NACA TN 2661, Formula 38:

$$f_{st\ avg} = \frac{f_{st}\ A'_{ste}}{A'_{st}} \qquad \text{(A.8)}$$

$$= \frac{-31.9(.1090)}{.2009} = -\ 17.4\ \text{ksi}$$

From NACA TN 2661, Sections 3.8 and 4.11 (b):

$$F_{c\ all} = -\ \pi^2 E \Big/ \left(\frac{\ell'}{\rho'_{st}}\right)^2 \qquad \text{where } \ell' = \frac{h_c}{2} = 28.0''$$

$$= \frac{-\pi^2(10.5 \times 10^3)}{28^2/.1497} = -\ 19.8\ \text{ksi}$$

$$M.S. = \frac{F_{c\ all}}{f_{st\ avg}} - 1$$

$$= \frac{-19.8}{-17.4} - 1 = +\ 0.014$$

A theoretically more accurate calculation of $f_{st\ avg}$ is:

$$f_{st\ avg} = \frac{-k\, f_s \tan\alpha_{IDT}}{\frac{A'_{st}}{d_{ct}} + 0.5(1-k)} \qquad (A.9)$$

$$= -\ 19.6 \text{ ksi}$$

which yields

$$M.S. = \frac{-19.8}{-19.6} - 1 = +\ .01$$

Following is a list of expressions for the stresses in the web derived from the "Engineering Theory of Incomplete Diagonal Tension" of NACA TN 2661.

Tension in α direction: $$f_\alpha = \frac{2\ k\ f_s}{\sin 2\ \alpha} + (1-k)\ f_s \sin 2\ \alpha \qquad (A.10)$$

Compression in $\alpha \pm 90°$ direction: $$f_{\alpha\pm 90°} = (1-k)\ f_s \sin 2\ \alpha \qquad (A.11)$$

Shear on α plane: $$f_{s\alpha} = -(1-k)\ f_s \cos 2\ \alpha \qquad (A.12)$$

Principal tension: (in β direction) $$f_1 = \frac{k\ f_s}{\sin 2\ \alpha} + f_s\sqrt{1 + k^2\left[\frac{1}{\sin^2 2\ \alpha} - 1\right]} \qquad (A.13)$$

Principal compression: (in $\beta\pm 90°$ direction) $$f_2 = \frac{k\ f_s}{\sin 2\ \alpha} - f_s\sqrt{1 + k^2\left[\frac{1}{\sin^2 2\ \alpha} - 1\right]} \qquad (A.14)$$

Principal shear: (on $\beta+45°$ plane) $$f_3 = f_s\sqrt{1 + k^2\left[\frac{1}{\sin^2 2\ \alpha} - 1\right]} \qquad (A.15)$$

where $$\tan 2\ \beta = \frac{\tan 2\ \alpha}{k} \qquad (A.16)$$

$$\alpha = \alpha_{IDT}$$

A P P E N D I X B.

(Shop Assembly Drawings.)

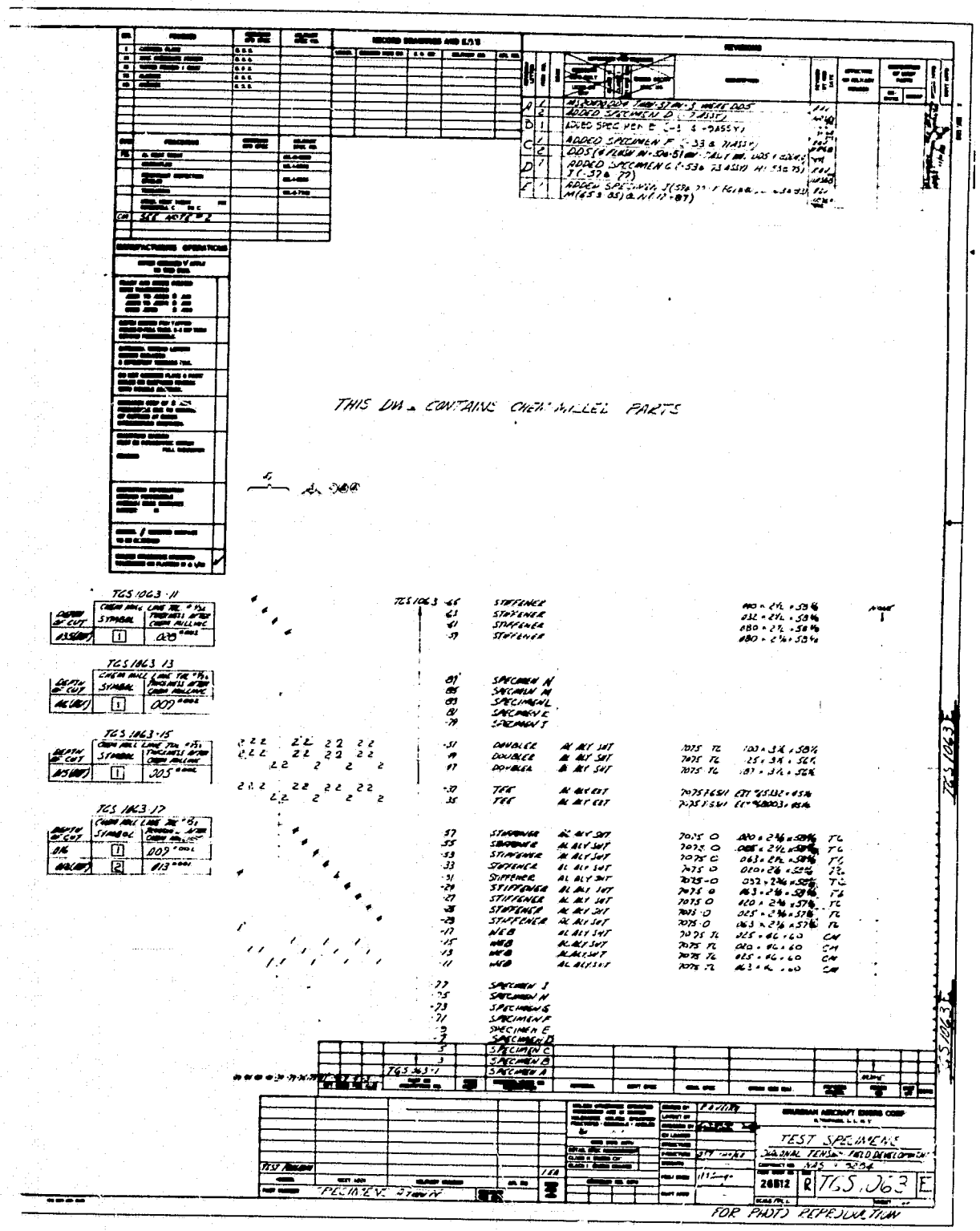

Shop assembly drawing of test specimens. 1 of 3

REPRODUCIBILITY OF THE ORIGINAL PAGE IS POOR.

Grumman

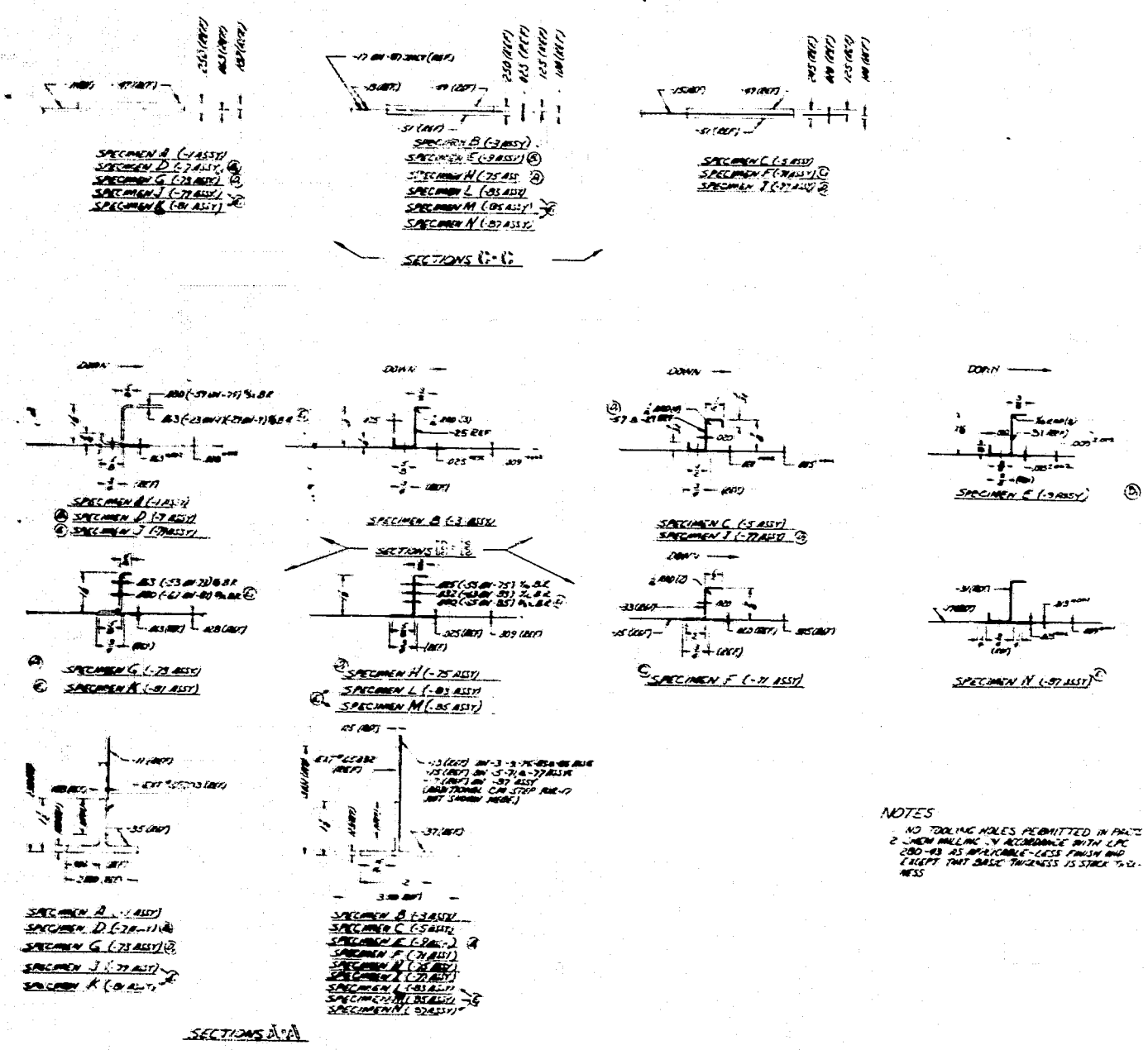

Shop assembly drawing of test specimens. 2 of 3

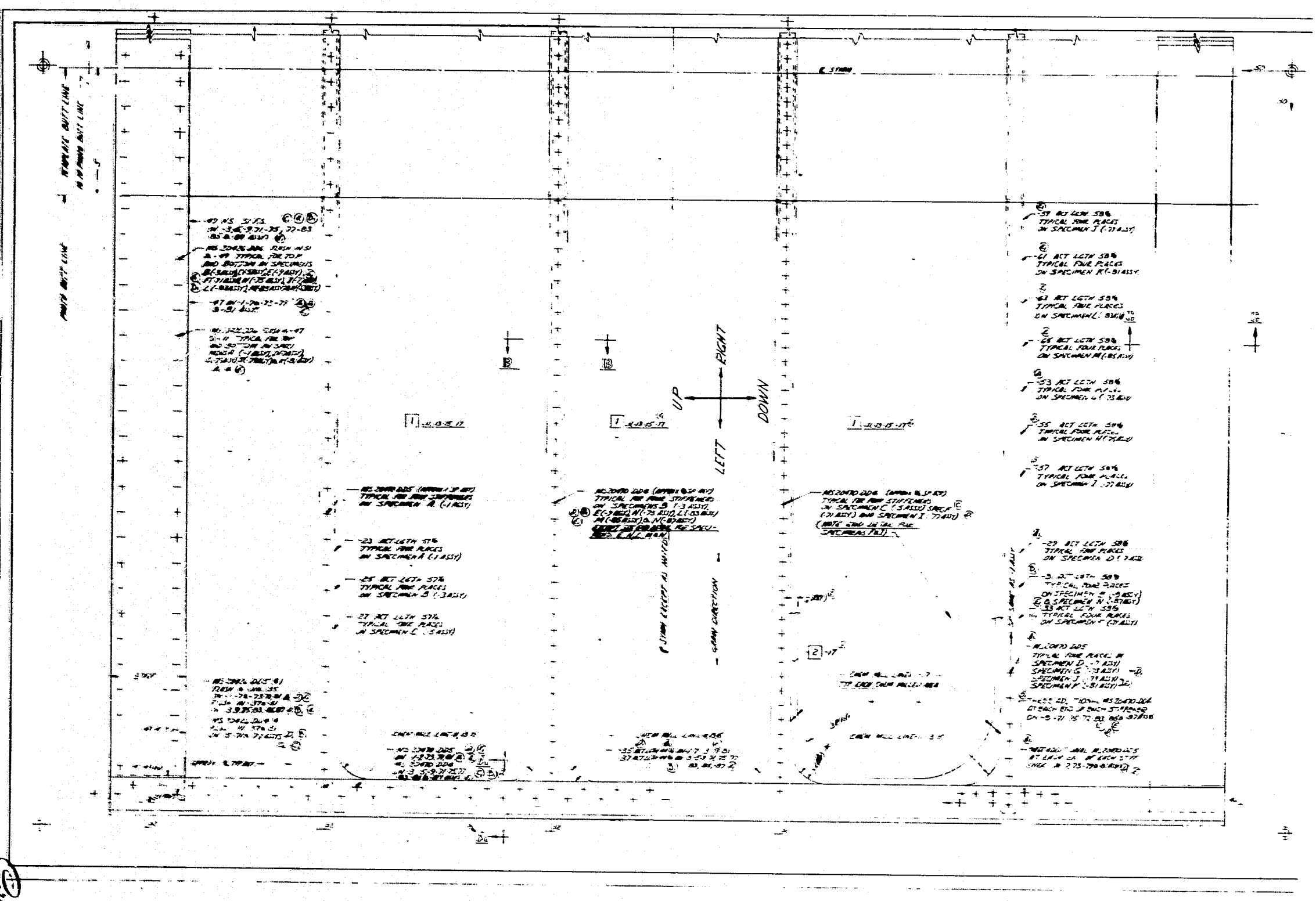

Shop assembly drawing of test specimens. 3 of 3

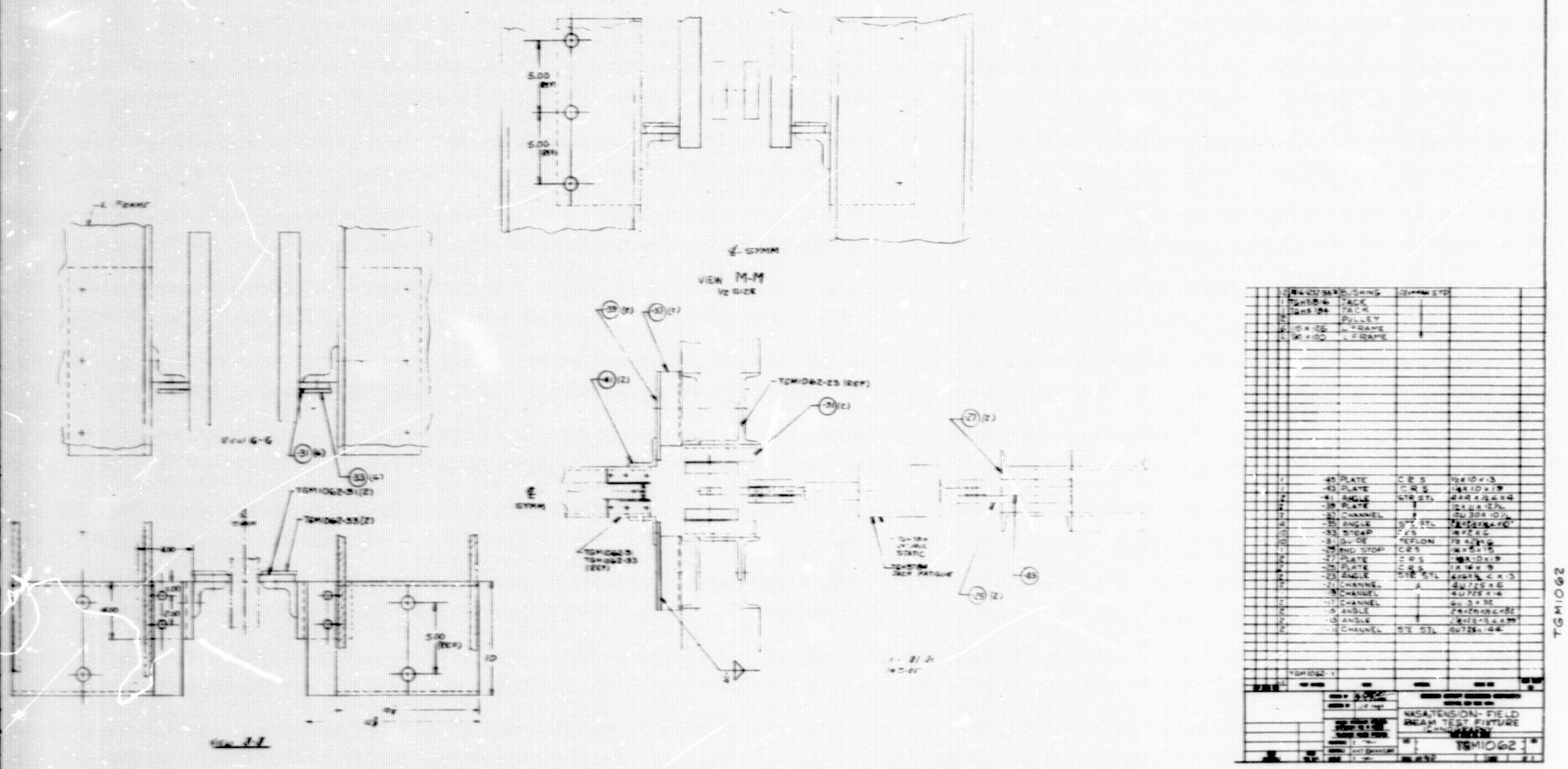

Shop assembly drawing of test fixture. 1 of 2

Grumman

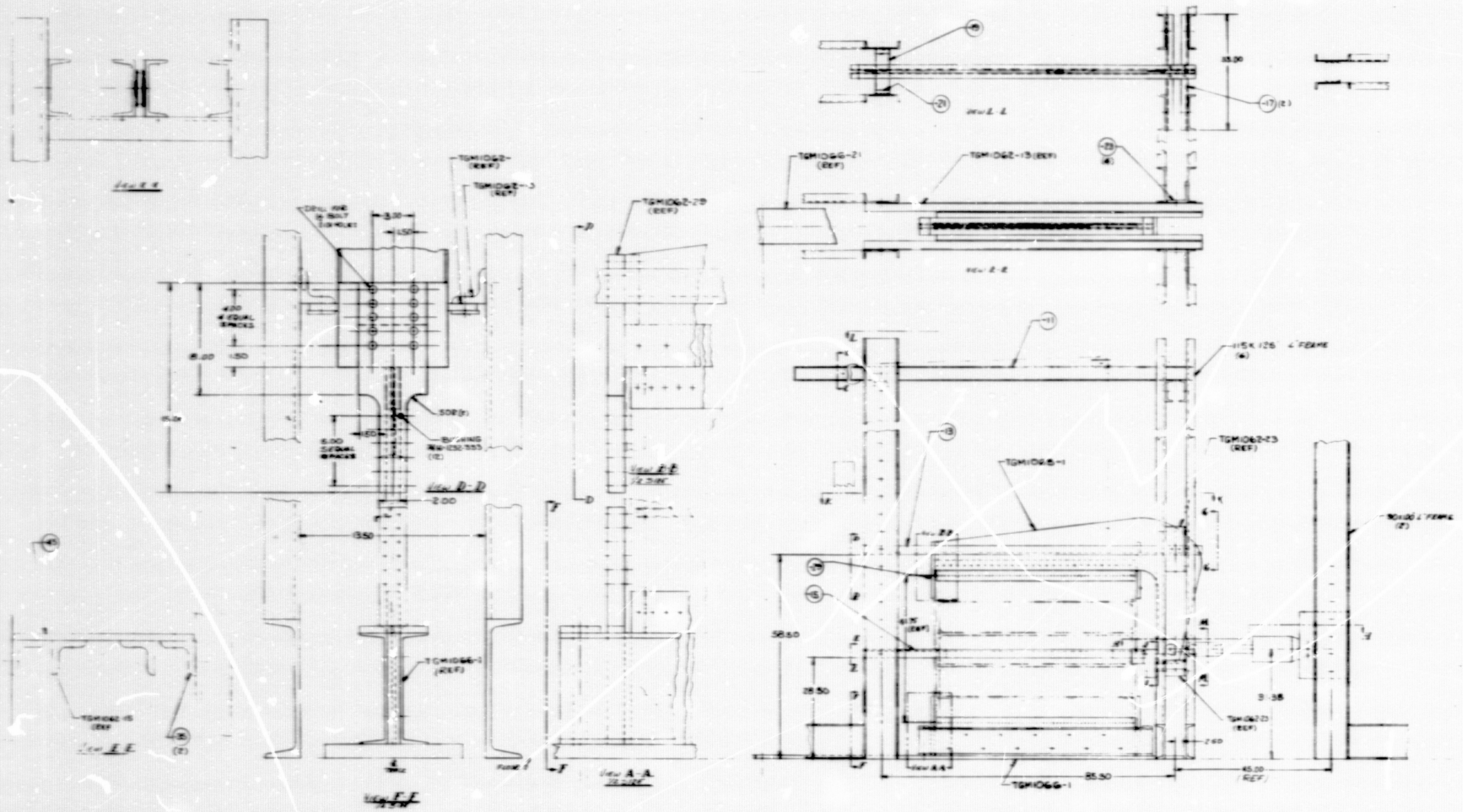

Shop assembly drawing of test fixture. 2 of 2

Grumman